

**SYNTHESIS OF SILICA NANO PARTICLES WITH
CUSTOM-MADE MORPHOLOGY FOR
CONTROLLED DRUG DELIVERY**

**A Thesis Submitted to
the Graduate School of Engineering and Sciences of
İzmir Institute of Technology
in Partial Fulfillment of the Requirements for the Degree of
MASTER of SCIENCE
in Chemical Engineering**

**by
Çağrı SİRETLİ**

**July 2012
İZMİR**

We approve the thesis of **Çağrı SİRETLİ**

Examining Committee Members:

Prof. Dr. Mehmet POLAT
Department of Chemical Engineering
İzmir Institute of Technology

Prof. Dr. Devrim BALKÖSE
Department of Chemical Engineering
İzmir Institute of Technology

Prof. Dr. Metin TANOĞLU
Department of Mechanical Engineering
İzmir Institute of Technology

9 July 2012

Prof. Dr. Mehmet POLAT
Supervisor
Department of Chemical Engineering
İzmir Institute of Technology

Prof. Dr. Mehmet POLAT
Head of the Department of
Chemical Engineering

Prof. Dr. R. Tuğrul SENGER
Dean of the Graduate School of
Engineering and Sciences

ACKNOWLEDGEMENTS

I would like to express my grateful thanks to my thesis supervisor, Prof. Dr. Mehmet Polat for his guidance, understanding, motivations and endless support during this study and preparation of this thesis.

I also would like to thank to Prof. Dr. Hürriyet Polat for her motivations and valuable help during the study.

I am grateful to Specialist Ömer Faruk Deniz at Gebze Institute of Technology in the department of Materials Science and Engineering for his valuable help in TEM analysis.

I thank to all my friends, research assistants and technicians in İzmir Institute of Technology for their helps and friendships.

I thank my family for their endless support, encouragement and help during this study.

Finally, I would like to thank to my wife, Aydan Siretli for her support, patience, encouragement, help and love.

ABSTRACT

SYNTHESIS OF SILICA NANO PARTICLES WITH CUSTOM-MADE MORPHOLOGY FOR CONTROLLED DRUG DELIVERY

The purpose was to have nanosized particles with low energy perimeters which function as non-reacting transporters for targeted delivery along with high energy sites inside the pores to achieve controlled release of specialized chemicals. Surfactants were used in combination with both base and acid catalyzed methods to achieve desired structural properties and the characterization studies such as SEM, TEM, FTIR, BET surface area, pore size, size and zeta potential measurements were conducted.

The effect of surfactants on mesoporous silica production changed depending on the type of methods. In the case of base catalysed method in alcohol, formation of stabilized emulsions with different sizes and their effect on the size and shape of silica particles was proposed. The effect of surfactants was attributed to their effect on a) the emulsification process and b) silica-silica and silica-surfactant interactions involved.

In the case of base catalysed silica production in water, however, surfactant micelles were used as templates to produce pores. The effect of surfactant type and concentration was attributed to their effect on the CMC, micelle shape and size. Rod-like (~400 nm) at high and spherical (~200 nm) particles at low concentrations were synthesized. Here the surface area of ~1000 m²/g and average pore size of ~3 nm were obtained. Carbonization of these materials were performed to obtain nanosized silica particles with low energy perimeters successfully. Acid catalysed silica production in water was similar. Rod-like (600-800 nm) and cubic (800-1000 nm) nanoparticles were produced. These particles exhibited lower surface area of ~700 m²/g and larger pore size of ~5 nm.

ÖZET

KONTROLLÜ İLAÇ SALINIMI İÇİN ÖZEL MORFOLOJİYE SAHİP SİLİKA NANO TANELERİN SENTEZLENMESİ

Amaç, kontrollü ilaç salınımında kullanmak üzere, hem hidrofilik hem de hidrofobik özelliklere sahip yapıları sentezlemektir. Asit ve baz ortamında yüzey aktif maddelerin varlığında istenen özellikte malzemeler sentezlendi ve SEM, TEM, FTIR, BET yüzey alanı, gözenek boyu, parçacık boyutu ve zeta potansiyeli ölçüm ve analizleri yapıldı.

Kullanılan metoda bağlı olarak, yüzey aktif maddeler silika oluşumunu farklı şekillerde etkiledi. Bazik ortamda ve alkol içerisinde farklı boylarda oluşan emülsiyonların, silika taneciklerin boyunu ve şeklini etkilediği öne sürüldü. Bu etkiler, hem emülsiyon oluşumuna, hem de silika taneciklerinin kendi aralarında ve yüzey aktif maddelerle olan ilişkilerine dayandırıldı.

Su ortamında bazik katalizörle sentezlenen yapılarda, yüzey aktif maddeler şablon malzeme olarak kullanıldı. Yüzey aktif madde derişimi, misel boyu ve şeklini etkilediği için farklı özellikte malzemeler sentezlendi. Yüksek konsantrasyonlarda çubuk şeklinde (~400 nm), düşük konsantrasyonlarda ise küresel (~200 nm) tanecikler sentezlendi. Bu yapılar, 1000 m²/g civarında yüzey alanına ve yaklaşık 3 nm gözenek çapına sahiptiler. Bu malzemelerin karbonla kaplanması işlemi başarıyla gerçekleştirildi. Asit katalizör yardımıyla elde edilen silika tanecikleri de benzer özellikler gösterdi. Çubuk (600-800 nm) ve kübik (800-1000 nm) yapılar elde edildi. Bu tanecikler, daha düşük yüzey alanına (~700 m²/g) ve daha büyük gözeneklere (~5 nm) sahiptiler.

TABLE OF CONTENTS

LIST OF FIGURES	xiii
LIST OF TABLES	xi
CHAPTER 1. INTRODUCTION	1
1.1. Statement of the Problem	1
1.2. Materials Used Commonly	3
1.3. The Scope of the Study	5
CHAPTER 2. SILICA AND CARBON NANOPARTICLES AND THEIR APPLICATIONS IN DRUG DELIVERY	7
2.1. Nanoparticles in Drug Delivery	7
2.1.1. The Effect of Important Characteristics in Nanoparticles	8
2.1.1.1. Particle size	8
2.1.1.2. Pore size, volume and geometry	10
2.1.1.3. Surface properties.....	12
2.2. Silica Nanoparticles in Drug Delivery	14
2.2.1. The synthesis of monodisperse silica nanoparticles	14
2.2.2. The synthesis of mesoporous silica nanoparticles	15
2.2.2.1. Micellar templates	16
2.2.2.2. Mesophases or liquid crystals	18
2.2.2.3. Formation mechanism	20
2.2.2.4. Typical ordered mesoporous silicas and commonly used surfactants in their synthesis.....	22
2.2.3. The silica particles as drug carrier	24
2.3. Mesoporous Carbon Nanoparticles in Drug Delivery.....	26
2.3.1. The synthesis of mesoporous carbon particles.....	26
CHAPTER 3. MATERIALS AND METHODS	28
3.1. Materials.....	28

3.1.1. Surfactants.....	28
3.1.2. Other Chemicals.....	30
3.2. Methods.....	31
3.2.1. Surface Tension Measurements	31
3.2.2. Size Measurements	31
3.2.3. Synthesis of Silica Nanoparticles.....	32
3.2.4. Carbon Coating of Silica Nanoparticles	35
3.2.5. Characterization Studies	36
 CHAPTER 4. RESULTS AND DISCUSSION.....	 38
4.1. The forms of surfactant molecules in water Surface tension measurements.....	 38
4.2. Shape and Size of Surfactant Micelles.....	43
4.2.1. Shape of Surfactant Micelles	43
4.2.2. Size of Surfactant Micelles	45
4.3. Synthesis of Silica Nanoparticles.....	51
4.3.1. Base Catalysed Methods	51
4.3.1.1. Synthesis of BC-I Particles	54
4.3.1.2. Synthesis of BC-2 Particles.....	68
4.3.2. Acid Catalyzed Methods.....	76
4.4. Carbon Coating of the Silica Nanoparticles.....	87
 CHAPTER 5. CONCLUSIONS	 91
 REFERENCES	 93

LIST OF FIGURES

<u>Figure</u>	<u>Page</u>
Figure 1.1. a) Concentration vs time profiles for conventional and controlled drug delivery systems, b) Release rates vs time profiles of conventional and controlled drug delivery systems	2
Figure 2.1. Adsorption isotherms	11
Figure 2.2. Main types of mesophases; Hexagonal, lamellar and cubic (Bicontinuous)	18
Figure 2.3. The phase diagram of the surfactants and mesophases with respect to temperature and weight of surfactant.....	19
Figure 2.4. Formation mechanisms of mesoporous silica	21
Figure 2.5. Cubic bicontinuous mesoporous structures.....	23
Figure 3.1. The molecular structure of pluronic triblock-copolymers.....	29
Figure 3.2. The pluronic triblock-copolymers and pluronic grid	30
Figure 3.3. The typical synthesis pathway of BC-1 particles	33
Figure 3.4. The typical synthesis pathway of AC-1 particles.....	34
Figure 3.5. The typical synthesis pathway of CBC particles.....	36
Figure 4.1. Surface tension vs concentration of selected surfactants	39
Figure 4.2. Surface tension vs concentration of selected Pluronic surfactants.....	40
Figure 4.3. Surface tension vs concentration of P-123 solutions.....	42
Figure 4.4. Surface tension vs concentration of CTAB solutions	43
Figure 4.5. Molecular lengths of the surfactants	45
Figure 4.6. (cont. from previous page) DLS measurements of the micelle solutions: a) CTAB, b) CTAC, c) SDS, and d) P-123.....	47
Figure 4.7. TEM image of P123 micelles	49
Figure 4.8. TEM image of CTAB micelles	49
Figure 4.9. TEM image of SDS micelles.....	50
Figure 4.10. TEM images of CTAC micelles.....	50
Figure 4.11. LaMer model of nucleation and particle growth	53
Figure 4.12. SEM images of BC-1 particles in the presence of TEAB	57
Figure 4.13. SEM images of BC-1 particles in the presence of CTAC.....	58
Figure 4.14. SEM images of BC-1 particles in the presence of CTAB.....	59

Figure 4.15. SEM images of BC-1 particles in the presence of SDS	60
Figure 4.16. SEM images of BC-1 particles in the presence of P-123	61
Figure 4.17. SEM images of BC-1 particles in the presence of APTS	62
Figure 4.18. SEM images of BC-1 particles including surfactants (10^{-2} M) in dispersion medium	63
Figure 4.19. Average particle size obtained from SEM images vs surfactant concentration in dispersion medium	64
Figure 4.20. SEM image of BC-1 particle synthesized in the absence surfactant.....	65
Figure 4.21. FTIR spectra of (a) BC-1 particles, (b) pure silica particles	67
Figure 4.22. Expanded FTIR spectra of (a) pure CTAB reagent, (b) BC-1 particles at high frequencies	67
Figure 4.23. Expanded FTIR spectra of (a) pure CTAB reagent, (b) BC-1 particles at low frequencies	68
Figure 4.24. SEM images of BC-2 particles including 0.01 M CTAB.....	71
Figure 4.25. SEM images of BC-2 particles synthesized at 45 °C	72
Figure 4.26. TEM images of BC-2 particles (0.05 M CTAB) with different Magnifications	74
Figure 4.27. TEM images of BC-2 particles (0.01 M CTAB) with different Magnifications.....	75
Figure 4.28. SEM images of AC particles synthesized with variable TEOS Concentrations	78
Figure 4.29. SEM images of AC particles a) AC-3-24-24 and b) AC-4-24-24.....	79
Figure 4.30. SEM images of AC particles synthesized in the presence of a) 0.0058 M CTAB and b) 0.0058 M SDS	80
Figure 4.31. SEM images of AC particles a) AC-3-24-24 b) AC-3-24-5	81
Figure 4.32. SEM images of AC particles a) AC-2-24-24 b) AC-2-24-5	82
Figure 4.33. Nitrogen Adsorption Isotherm of AC type particles	83
Figure 4.34. TEM images of AC-2-24-24 particles.....	85
Figure 4.35. TEM images of AC-1-24-24 particles.....	86
Figure 4.36. SEM images of carbonized CBC-2	87
Figure 4.37. EDX analysis of carbonized CBC-2 particles	87
Figure 4.38. TEM images of carbonized CBC-1 particles	88
Figure 4.39. SEM image of BC-2 particles on which calcium carbonate was precipitated	89

Figure 4.40. EDX analysis of BC-2 particles on which calcium carbonate was precipitated	89
Figure 4.41. TEM images of carbonized CBC-2 particles	90

LIST OF TABLES

<u>Table</u>	<u>Page</u>
Table 2.1. Main size measurement methods and their properties.....	8
Table 2.2. Packing Parameter Values and Corresponding Micelle Structures	17
Table 2.3. Surface properties and drug loading capacity of the mesoporous silica particles	25
Table 3.1. The Molecular Structures and Weights of the Ionic Surfactants Used in This Study	29
Table 3.2. Micellar Properties of CTAB.....	29
Table 3.3. Molecular formula and average molecular weights of selected Pluronics	30
Table 3.4. Classification of AC particles synthesized in this study.....	34
Table 4.1. Area of the surfactant head group (a_0), volume (V) and length (l) of the hydrophobic part, surfactant packing parameter (SPP) and micelle shape	44
Table 4.2. Micelle size measurements by different techniques	51
Table 4.3. Average particle sizes of BC-1 Particles (Additive Concentration: 10 ⁻² M) from SEM images	64
Table 4.4. Average particle sizes of BC-1 Particles at varying additive concentrations from SEM images	64
Table 4.5. Average particle sizes (nm) of BC-2 particles obtained by SEM images	73
Table 4.6. Nitrogen Sorption Measurements of BC-2 (0.05 M CTAB)	73
Table 4.7. Nitrogen Sorption Measurements of BC-2 (0.01 M CTAB)	73
Table 4.8. Average particle sizes (nm) of AC particles obtained from SEM images.....	83
Table 4.9. Nitrogen sorption measurements of the selected AC particles	84

CHAPTER 1

INTRODUCTION

1.1. Statement of the Problem

In current clinical therapy, traditional drug administration, in which drug must be administered repetitively, is still used in order to treat patients. The main reasons of this type of treatment are quick metabolism and elimination of drugs in the body. However, this may result in several negative effects (Xu et al., 2008).

The effect of a drug varies between the therapeutic and significant side effects such as toxicity. In another words, when administering a drug, there is a therapeutic concentration range determining the maximum and minimum levels between which the drug is effective. Above the maximum level, toxicity becomes significantly present in the system while below the minimum level, the drug loses its effectiveness. When using the traditional administration methods, repetitive doses are required in order to sustain the therapeutic effect of drug because a single dose may be enough to exceed the maximum effective level and drug concentration drops below the minimum effective level in a short time. The traditional administration methods cause high dosage of the drug, low efficiency and several side effects. In order to overcome these problems, controlled drug delivery systems have been developed (Babu, 2007).

Controlled drug delivery system is a formulation which provides the delivery of drugs to specific targets of the body at a controlled rate (Vallet-Regi et al., 2007). In this system a nontoxic, biocompatible material is used to load the drug and release it at a pre-determined rate while keeping the drug concentration in the therapeutic region. By use of these systems, the therapeutic drug level can be maintained for a prolonged period of time. (Figure 1.1.).

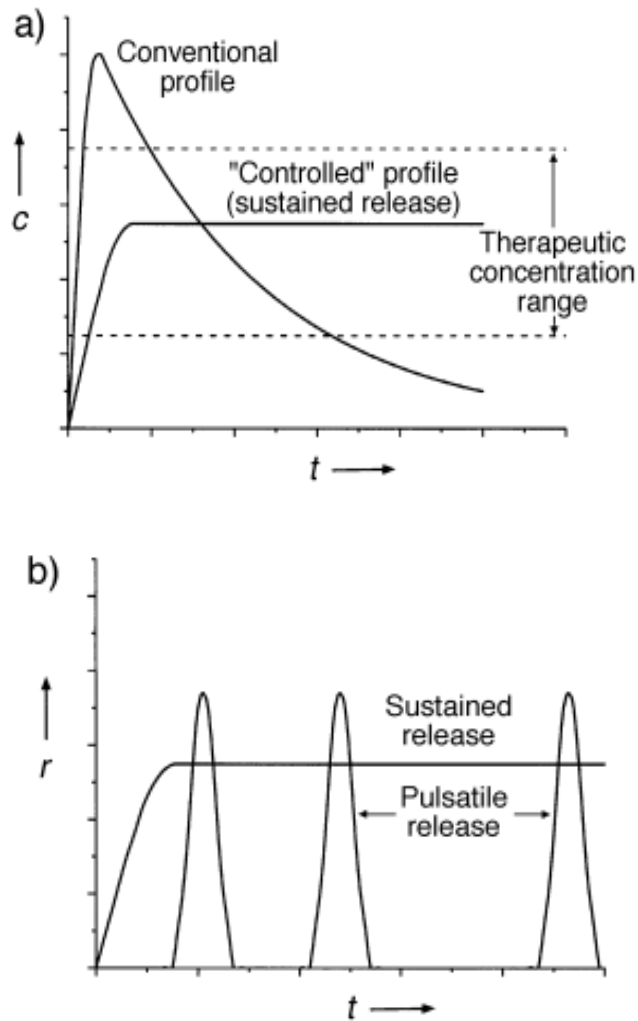


Figure 1.1. a) Concentration vs time profiles for conventional and controlled drug delivery systems b) Release rates vs time profiles of conventional and controlled drug delivery systems (Source: Santini et al., 2000)

In recent years, much of the attention of the scientists has focused on the use of nanoparticles as drug carrier. The reasons why these nanoparticles are good candidates for drug carriers are based on their important features such as their small size, having a relatively high surface area (their surface to mass ratio is larger than that of other particles), having effect on biodistribution, being capable of making drugs available for intravascular delivery, having a stabilizing effect on therapeutic agents and being able to sustain release of the drugs (Mainardes and Silva, 2004). However, there are still several limitations related to the use of the nanoparticles in drug delivery applications such as the instability in circulation and toxicity (Cho et al., 2008).

An ideal drug carrier should be inert, biocompatible, mechanically strong, capable of loading high amount of drug and releasing at a controlled rate and simple to administer and remove. As a result, the study has focused on the synthesis of nanoparticles with custom-made morphology for controlled release of hydrophilic drugs.

1.2. Materials Used Commonly

Many studies have focused on drug delivery by the aid of nanoparticles and these have been reviewed in a detailed way (Kim et al., 2010; Yokoyama, 2005). These nanocarriers can be classified into several types such as nanospheres, nanocapsules, nanotubes, nanogels and dendrimers. The biological molecules can be delivered by the dissolution within a polymeric matrix, entrapment inside lipid, encapsulation or adsorption onto the surfaces of the particles (Mishra et al., 2010).

Polymeric nanoparticles are prepared from a synthetic polymeric block and can be used to deliver drug molecules. Depending on the preparation method, polymeric nanoparticles, in which the drug is confined to a cavity surrounded by a polymeric membrane or nanospheres consisting of matrix systems where the drug is dispersed, can be obtained. Biodegradable polymers such as polylactic acid (PLA), poly(glycolic acid) (PGA), poly(lactic-co-glycolic acid) (PLGA) are usually used in these applications due to the fact that these structures can be easily hydrolyzed into monomers which can be excreted from the body through metabolic pathways. Another advantage of using these nanoparticles is that it provides the sustained release of drugs within the target site over a specific period. However, the use of these nanoparticles (especially including non-biodegradable polymers) may have several disadvantages such as the cytotoxicity of by-products and scalability (Ochekpe et al., 2009).

Polymeric micelles have been extensively used as drug carrier due to their stability in physiological solution. These nanostructures consist of both hydrophobic core and hydrophilic corona, allowing the delivery of water-insoluble drugs. While the core of micelle accommodate hydrophobic drugs, the hydrophilic part makes the micelle water soluble and allows the delivery of these type of drugs in physiological solutions. Therefore, they can increase the drug solubility and lead a prolonged

circulation time and bioavailability. However, these systems lack the well-control of the release of the entrapped molecules (Torchilin, 2007).

Liposomes are small, spherical systems which are usually synthesized from cholesterol and nontoxic phospholipids. Due to being natural, small size, hydrophobic and hydrophilic character and biocompatibility, they are frequently used as drug carriers. They can exhibit different properties affected from their size, shape, method of preparation and surface charge. Moreover, they can be present in several forms based on their size and number of layers: Small unilamellar vesicles, large unilamellar vesicles and multilamellar vesicles. They are considered to reduce the toxicity and delivering the drugs within the body for a prolonged period. However, they may have low encapsulation efficiency and causes rapid leakage of the water soluble drug molecules in the blood stream (Sahoo et al., 2003).

Solid lipid nanoparticles are the colloidal structures composed of physiological lipid, dispersed in water or aqueous surfactant solution. As a drug carrier, they are usually made up of a solid hydrophobic core containing dissolved or dispersed drug. Although these structures provide site-specific targeting, high stability, controlled drug release and good tolerability, they have insufficient drug loading and drug expulsion through storage. In order to overcome these limitations, liquid lipids with improved drug delivery characteristics may be incorporated (Ochekpe et al., 2009; Mishra et al., 2010).

Magnetic nanoparticles are also among the promising materials in biomedical applications such as drug delivery and imaging. The magnetic structure such as iron oxide or magnetite are present in the core of the particle which is coated by an inorganic or polymeric structure in order to make the particles biocompatible, stable and a support for drug molecules. The key features in the behaviour of these nanoparticles are based on their surface chemistry, size (magnetic core, size distribution) and magnetic properties. Their limitations are the relation between the drug delivery performance and the low capacity of the external magnetic field, and the accumulation of the magnetic nanoparticles with respect to the geometry of the magnetic field (Arruebo et al., 2007).

Dendrimers are highly branched macromolecules consisting of an initiator core, interior layers attached radially to the core and possessing repeating units, and exterior part. In drug delivery applications, drugs can be encapsulated in the void spaces within the dendrimer structure. The interaction of drug and dendrimer can be provided via electrostatic or covalent bonds at the terminal groups and its structure can allow the

surface functionalization, possess multivalency and ease of preparation. Both hydrophilic and hydrophobic drugs can be delivered by these nanostructures. However, these nanoparticles have several limitations related to their high cost, the challenge in the avoidance of long-term accumulation within the body and the toxicity depending on the density and nature of the charged groups at the terminal groups and their size (Arruebo et al., 2007)

Carbon based nanoparticles, especially nanotubes and porous structures, have shown promising behaviours in drug delivery applications. Carbon nanotubes are extremely small tubes which consists of either single or multi wall carbon structure. Their special structures make them good candidates to encapsulate drug molecules in their cavities. However, the toxicity of these nanocarriers has been of concern, especially when using without surface modifications. To reduce their toxicity in blood stream, the studies are in progress. In addition to the carbon nanotubes, porous carbon particles are used as drug carrier due to their good surface characteristics such as high surface area, adjustable pore sizes, and stability even in the harsh acidic stomach conditions (Xu et al., 2008; Zhua et al., 2011).

Among the ceramic based materials, silica nanoparticles have been extensively studied in drug delivery applications. Especially mesoporous silica nanoparticles are used successfully as a drug carrier due to their high surface-to-volume ratio, well-controlled pore characteristics, inertness and biocompatibility. However, the toxicity of these nanoparticles may be of concern when they are used at high dosages and exposure time (De Jong and Borm, 2008).

1.3. The Scope of the Study

The scope of the study is to synthesize mesoporous silica nanoparticles whose inner and outer surfaces show different surface characteristics by adjusting the physicochemical features of the surfactants used as template materials in the synthesis of these nanoparticles for the controlled release of hydrophilic drugs. Mesoporous silica nanoparticles (hydrophilic inner surface) with carbon coating (hydrophobic outer surface) can be used to deliver such hydrophilic drug even without being affected by the physiological environment conditions (i.e. harsh acid of the stomach fluid). Previous studies have shown that mesoporous silica nanoparticles can be used to deliver

hydrophilic drugs. By adjusting surface properties of these nanoparticles, a well-controlled release of the drug can be performed.

CHAPTER 2

SILICA AND CARBON NANOPARTICLES AND THEIR APPLICATIONS IN DRUG DELIVERY

2.1. Nanoparticles in Drug Delivery

Nanotechnology can be defined as the study and use of the materials whose size varies between 1 and 100 nm. Therefore, the products of this research area are called nanoparticles. Nanoparticles are extremely smaller than micro- and macroparticles. For example, a strand of human DNA is 2.5 nm in diameters, a sheet of paper is almost 100,000 nm thick, and the thickness of the human hair varies between 40,000 and 120,000 nm (Asiyanbola and Soboyejo, 2008).

Increasing the need of nanotechnology in biomedical applications such as drug delivery results in developments in research about formation of nanoparticles to use in medicine. In such biomedical applications, the objective of the use of nanotechnology is almost the same as that of medicine. As expected from medicine, nanotechnology in drug delivery should also provide the accurate diagnosis and well-treatment without any side effects. Therefore, a new scientific area, nanomedicine, is formed by using the relation between nanotechnology and medicine (Mishra et al., 2010).

Nanoparticles used as drug carriers, nanocarriers, show important features which make them promising in drug delivery. The size and shape of the particles, the pore size, shape and volume, the surface area and presence of functional groups on the surface determine the kinetics and efficiency of delivery. In another words, an ideal drug carrier should have suitable physico-chemical characteristics in order to have success in drug delivery (Singh et al., 2009).

2.1.1. The Effect of Important Characteristics in Nanoparticles

2.1.1.1. Particle Size

Particle size and size distribution are among the most important properties of the nanoparticles. In biological applications, the particle size of the nanocarriers influence the in vivo distribution and clearance of the drug, the toxicity of the particles and how accurate the drug is delivered. Moreover, the drug loading capacity, drug release kinetics and stability of the particles are affected by the size of these small structures (Singh et al., 2009).

First of all, the size of the nanoparticles should be determined accurately because the delivery partially depends on the particle size distribution. After that, the effect of the particle size on the delivery can be discussed.

Table 2.1. Main size measurement methods and their properties
(Source: Gaumet et al.,2008)

Method ^a	Principle	Measurement range	Limitations
LS	Light interaction	50 nm-1 μ m	Insuitable for polydisperse populations Indirect method Effect of aggregates
LLD	Light interaction	1-1000 μ m	Indirect method High amount of sample
SEM, TEM	Microscopy	50 nm-100 μ m	Time consuming Effect of sample preparation
AFM	Microscopy	10 nm-1 μ m	Sampling Subjective Setup complexity
ANUC	Centrifugation	-	Data processing
FFF	Elution	20 nm-1 μ m	Optimization requirement Handling
CE	Electrophoresis	20-500 nm	Setup complexity
PCH, SEC	Chromatography	<100 nm	Time consuming

^a LS: light scattering; LLD: laser light diffraction; SEM: scanning electron microscopy; TEM: transmission electron microscopy; AFM: atomic force microscopy; ANUC: analytical ultracentrifugation; FFF: field flow fractionation; CE: capillary electrophoresis; PCH: packed column hydrodynamic; SEC: size exclusion chromatography.

Dynamic light scattering (DLS), or photon correlation spectroscopy is one of the fastest and routine method for determining the particle size distribution and average particle size. Before the analysis, the viscosity of the medium and refractive index of the particles must be known. Its size calculation principle depends on the fact that each particle is accepted as sphere. By Brownian motion and light scattering properties, the diameter of the particles can be determined. However, the aggregation of the particles increase their size. Moreover, several important parameters such as temperature, pH of the medium and concentration may affect the results of the analysis. Therefore, this method may not give accurate results when analysing polydisperse samples.

The other commonly used size measurement technique is the scanning electron microscopy (SEM). By this method, the images with high resolution can be obtained. Especially for the particles larger than 100 nm, SEM image provides information about the size, shape and dispersity of the particles. Otherwise, SEM may not give detailed information about the particle properties due to resolution limits. Moreover, in order to obtain less-deviated data, a large number of the particles should be analysed. Therefore, this method is more subjective and time consuming (Gaumet et al., 2008)

The other techniques given in Table 2.1 have several disadvantages such as experimental difficulties and high cost. Transmission electron microscopy (TEM) requires careful sample preparation and is an expensive technique, atomic force microscopy (AFM) is more suitable for surface analysis and the other techniques are not preferred as frequently as others.

In order to eliminate the misinterpretation of the particle size effect on the delivery and analyze the size of the nanoparticles accurately, at least two measurement techniques should be performed.

Particle size also affect the toxicity of the biomaterials. Reduction in size to the nanometer scale provides high surface to volume ratio, meaning that more molecules are present on the surface and they enhance the intrinsic toxicity. Indeed, per mass, the nanoparticles usually exhibit more toxicity than larger particles of the same material (Donaldson et al., 2004). However, this topic has not been well understood and it is difficult to explain the relation between the particle size and the particle toxicity.

Drug release is also affected by the particle size of the biomaterial. Due to the high surface to volume ratio in nanoparticles, most of the drug is to be captured at the particle surface and it results in faster release than that occurs for larger particles. In the

case of large particles, more drugs can be encapsulated and a slower release can be observed (Redhead et al., 2001).

2.1.1.2. Pore Size, Volume and Geometry

Size, volume and geometry of the pores may become effective in drug delivery when the drugs are adsorbed into the pores. In such a case, these features determine whether the drug molecules can enter into the pores or not. In another words, the size, volume and shape of the pores should be appropriate for the drug molecules. Therefore, these properties must be analysed as accurately as possible.

By classifying the nanoparticles with respect to their pore sizes, three different types of materials are named : microporous (pore size < 2 nm), mesoporous (2 nm < pore size < 50 nm) and macroporous (pore size > 50 nm). The most two common techniques for determining the pore characteristics are nitrogen sorption method and mercury porosimetry.

In order to perform the gas sorption measurements, a detailed physico-chemical background related to gas adsorption theories is required. By these methods, pore sizes and volumes, type of pores and surface areas of the particles are analysed. These information can be obtained from the nitrogen sorption (both adsorption and desorption) isotherms. These isotherms are measured at 77 K (temperature of liquid nitrogen) as a result of the analysis after annealing the samples at above 100 °C under vacuum. During the measurement, small amounts of nitrogen gas are adsorbed by the sample step-by-step. Firstly, a mono layer is formed on the particle surface and then injection of more nitrogen leads to the formation of multi layers. Parallel to this formation, capillary condensation in the pores may occur. The final part of the measurement is the desorption of nitrogen molecules step-by-step until a specific relative pressure (p/p_0 , p is the pressure controlled during the analysis and p_0 is the atmospheric pressure) is reached. As a result, the adsorption/desorption isotherm giving the volume of nitrogen per mass of material as a function of p/p_0 is obtained. Figure 2.1 shows 6 types of isotherms.

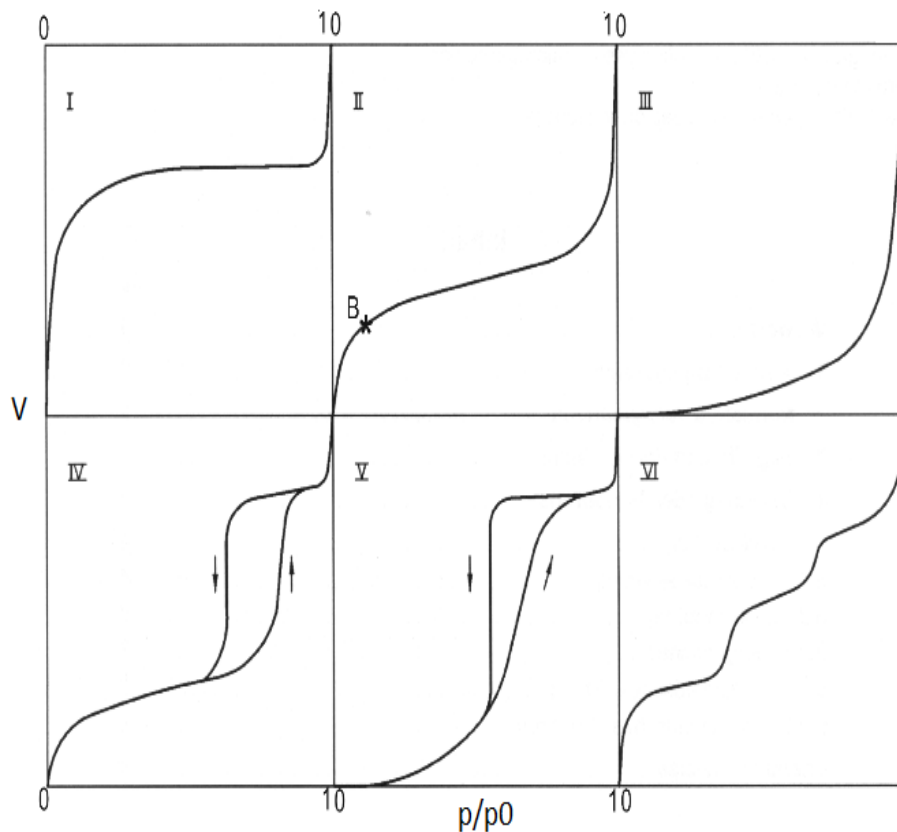


Figure 2.1. Adsorption isotherms

Type 1 explains the sorption behaviour of microporous particles. The sharp increase of the isotherm at low p/p_0 is followed by a horizontal line indicating the entire coverage of the surface with nitrogen molecules. On the other hand, type 2 isotherm indicates the multi layer adsorption of nitrogen after point B up to the $p/p_0=1$. For the particles whose pore sizes are smaller than 2 nm, total reversible sorption isotherms (desorption follows adsorption for type 1, 2 and 3) are obtained. However, in type 4 and 5 isotherms, the hysteresis formed indicate the presence of mesoporous structures (Adamson and Gast, 1997)

While gas adsorption can provide the information about the pore sizes as small as 0.3-300 nm, mercury porosimetry is appropriate for the pore diameter range of 3-200 μm . In another words, with nitrogen adsorption, the pores which are out of range of the mercury porosimetry can be characterized but the overall measurement range of the latter is wider than the other. However, the results of these methods may be similar and comparable in several cases (Westermarck, 2000). In addition to these methods, TEM images provide the most accurate data about the pore size, shape and order but it is more time consuming and expensive than other methods mentioned above.

In drug delivery applications, the pore size of the nanoparticles is preferred to be slightly larger than the size of the drug molecules in order to provide the adsorption of sufficient amount of drug into the pores (Vallet-Regi et al., 2007). Several studies proved that the reduction in the pore size results in a decrease in the release rate. Moreover, with the aid of high surface area, the loading of the drug into the nanoparticles with smaller pore size is higher than that with larger pore size (Vallet-Regi, 2009).

In addition, when the pores of the nanoparticles are filled fully with the drug molecules, the pore volume may become the governing factor in the drug loading. In another words, in the case of the large-volume drugs, the pore volume usually determines the limit of loading (Balas et al., 2008).

In several cases, not only pore size or volume affects the loading and release of the drugs but also the length of the pore channel plays an important role to determine the delivery behaviour (Marzouqa et al., 2011).

2.1.1.3. Surface Properties

According to IUPAC, surface means the boundary between two phases. In another words, the surface is the outer region of a material of undefined depth. Basically, aside from the pores, surface area, the functional groups present on the surface, zeta potential of the particles and hydrophobicity determine the main surface characteristics of the particles. Due to the fact that drug loading is mainly influenced by the adsorption behaviour of the particles, the surface becomes the ruling factor for the delivery.

Among the properties mentioned above, the surface area is one of the most effective factor determining the performance of the drug carrier. Nitrogen sorption method has been widely used in order to determine the surface area of the particles. According to the sorption isotherm obtained, langmuir or BET theories can be chosen to describe the surface area of the particles.

Langmuir theory arised from a kinetic model of adsorption in which the process is limited to the mono layer coverage. On the other hand, the BET theory originated from the introduction of the several simplifying assumptions in addition to the Langmuir theory. The assumptions for the BET theory are :

1. Multi layers are formed on the solid surface while mono layers occur in langmuir model.
2. Homogeneity on the solid particle surface providing a consistent adsorption is present.
3. Intermolecular interactions between the adsorbates do not occur.
4. The uppermost layer is in equilibrium with vapor phase
5. The heat of adsorption in the first layer corresponds to the heat of condensation of the adsorbate in the following layers.

In a real case of adsorption onto solid surfaces, these assumptions are not always valid and the absolute values of the surface areas derived from the BET model must be evaluated with caution. Nevertheless, the BET model has become a standard method to explain the sorption isotherms and gives valuable information about solid surfaces (Lu and Schüth, 2006).

The Langmuir model has been used to describe the type 1 isotherm which results from the fact that the adsorbent particle is microporous. On the other hand, type 2 and type 4 isotherms (indicating nonporous and mesoporous structures, respectively) can be explained by the BET theory (Gomez-Serrano et al., 2000).

The importance of the surface area may arise when the pore size of the particles is enough to encapsulate the drug molecules. In these cases, the higher the surface area, the higher drug loading can be achieved (Vallet-Regi et al., 2007).

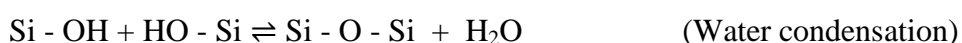
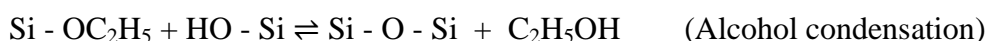
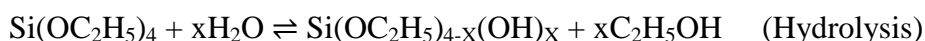
Surface functionalization has been widely used in order to increase the drug delivery performance of the carriers. According to the hydrophobicity of the drug molecules, the surface properties of the carriers can be adjusted by several modifications on the carrier surface. Moreover, the functional groups present on the surface can develop the delivery behaviour of the carriers. At the same time, not only the increase in the capacity of the drug loading but also the controlled release of the drug molecules can be achieved by using the stimuli-responsive systems which usually use the surface characteristics of the carriers and their behaviours in the specific medium conditions (Slowing et al., 2007; Vallet-Regi et al., 2007; Manzano et al., 2007; Veronese and Pasut, 2005).

2.2. Silica Nanoparticles in Drug Delivery

Silica nanoparticles have been widely used in drug delivery applications due to their significant hydrophilicity, biocompatibility and nontoxicity. Different types of these nanoparticles can be used with or without several modifications for developing the drug delivery. Monodisperse silica nanospheres, magnetic silica nanoparticles and mesoporous silica nanoparticles are the most commonly used silica-based nanoparticles.

2.2.1. The Synthesis of Monodisperse Silica Nanoparticles

The monodisperse, spherical silica nanoparticles have been commonly synthesized by the well-known Stöber method which uses the principles of the sol-gel chemistry (Stöber et al., 1968). In another words, Stöber et al. developed a synthesis based on the hydrolysis and condensation of the silicon alkoxides in a mixture of water, ethanol and ammonia. Alkoxide is used as the precursor, ethanol-water mixture as the solvent and ammonia as the base catalyst. The reactions in silica formation are given below:



Hydrolysis is the reaction in which the nucleophilic attack of the oxygen in water on the silicon atom, which leads to the formation of an intermediate state followed the shift of the hydrogen atom in water molecule to the oxygen atom of the neighboring OR-group. The hydrolysis reaction is completed by the elimination of alcohol molecule. In another words, during the hydrolysis reaction, the alkoxide group is replaced with hydroxyl group by the nucleophilic substitution (Brinker and Scherer, 1990; Turova et al., 2002).

Following the hydrolysis, the condensation reactions which include the production of siloxane bonds with the by-products such as alcohol or water occur. If the hydroxyl group of the intermediate reacts with another hydroxy group, the water condensation occurs. If the former reacts with the ethoxy group of an alkoxide molecule, the alcohol condensation occurs to form Si-O-Si bonds (Ibrahim et al., 2010).

Due to the fact that water and alkoxides are immiscible, a solvent such as alcohol which can serve as a homogenizing agent is added to the reaction medium. For a tetrafunctional silicon alkoxide such as tetraethylorthosilicate (TEOS), polar solvents are usually chosen. However, the addition of alcohols may influence the reaction conditions and promote the reverse reactions of hydrolysis and condensation which are esterification and depolymerization reactions, respectively. In the case of base-catalyzed sol-gel reactions, ammonia is the most widely used catalyst. It causes the hydrolysis to be more rapid and to complete while it helps the condensation reaction as well (Brinker and Scherer, 1990).

2.2.2. The Synthesis of Mesoporous Silica Nanoparticles

The synthesis of mesoporous materials has been in progress in recent years. The pathway followed in the synthesis of mesoporous silica particles is: 1) The formation of mesophases, liquid-crystalline phase of the micellar aggregates, determined by the surfactant concentration, hydrophobic chain length, the charge of the headgroup, temperature and pH value of the solution, 2) The presence of hydrolysable and condensable silica precursor, 3) The interaction between the inorganic silica species and micellar mesophases which are used as the structure-directing agents and inclusion of these agents without phase separation and 4) The removal of the surfactants by extraction or calcination after the polymerization is complete and the formation of the final mesoporous silica particles.

The use of template materials allows the formation of mesoporous structures. Among the hard and soft template methods, the latter are used in the synthesis of mesoporous silica materials. Soft templating can be defined as the process in which organic molecules act as a mold and then a framework is built around it. These templates, including cationic, anionic, nonionic surfactants and mixed surfactant systems are called “soft” due to their fluid characteristics. The micelles which are the surfactant aggregates are used as the soft-template in the mesoporous silica synthesis. The understanding of the micellar behaviour in the synthesis of mesoporous silica structures is very important.

2.2.2.1. Micellar Templates

Micelles are important in the mesoporous silica synthesis in that their size and shape have effect on the pore size and order of the particles. Their sizes and shapes are varied by the surfactant characteristics and its thermodynamic interactions with the surrounding solution.

Surfactant molecules are formed by the fact that two different structures with different properties are present in their skeleton: a polar head group and nonpolar chain. The existence of these two parts makes the surfactant molecule amphiphilic which means a structure possessing both hydrophilic and hydrophobic parts. The hydrophobic part is usually a long-chain hydrocarbon structure while the hydrophilic head group is ionic or highly polar. According to their hydrophilic head group, they can be classified into four main types: anionic, cationic, nonionic and zwitterionic. The anionic surfactants have hydrophilic parts with negative charged while the cationic surfactants have positive charged group. On the other hand, the surface-active portion in the nonionic surfactants have no ionic charge while zwitterionic surfactants possess both positive and negative charged head groups (Rosen, 2004).

The orientation of the surfactant molecules leads the formation of micelles. The hydrophobic chains are self-assembled in such a way that they form a liquid core which is separated from the surrounding solution by the presence of hydrophilic head groups. The energy of micelle formation depends on the fact that free energy obtained by reducing the interaction of the nonpolar chains to water decreases. The presence of surfactant molecules which do not take part in micelle formation provides less conformations available to the surrounding water molecules by interrupting the network of hydrogen bonds between the water molecules. As a result, entropy proportional to area of water-nonpolar chain interface decreases by the dissolution of a surfactant. When the surfactant in concentration reaches above the critical micellar concentration (cmc), at which micelles start to form, the interaction between the nonpolar chains and water is drastically reduced.

Micelles can possess different shapes affected by their several properties. The major types of micelles are 1) small, spherical structures, 2) cylindrical, rodlike structures, 3) large, lamellar structures, and 4) vesicles. Changes in temperature, surfactant concentration, presence of additives in the solution and structural groups in

the surfactant may affect the shape, size and aggregation number of the micelle which is the number of surfactant molecules forming a micelle (Winsor, 1968).

According to the theory developed by Israelachvili et al. (1976), the micellar structure can be defined by the geometric approach. The volume (V) of the hydrophobic groups in the micellar core, the length (l) of the nonpolar chain in the core and the cross-sectional area (a_0) occupied by the polar head group at micelle-water interface are the parameters which are used to calculate the packing parameter, determining the shape of the micelle. This value varies between 0 and 1/3 for spherical micelles, 1/3 and 1/2 for cylindrical micelles and 1/2 and 1 for lamellar micelles (Table 2.2) (Schüth et al., 2002).

Table 2.2. Packing Parameter Values and Corresponding Micelle Structures

Value of $V/l \cdot a_0$	Shape of micelle
0-1/3	Spherical in aqueous media
1/3-1/2	Cylindrical, rodlike in aqueous media
1/2-1	Lamellar in aqueous media
>1	Reversed micelles in nonpolar media

Volume of the hydrophobic groups in the micellar core can be calculated via $V = 27.4 + 26.9n \text{ \AA}^3$, where n is the number of carbon atoms of the chain present in the core and accepted as almost the total number of carbon atoms in the nonpolar chain. On the other hand, the length of the hydrophobic chain present in the core can be determined by the approach $l \leq 1.5 + 1.265n \text{ \AA}$. In the case of saturated, straight chains, this value is almost 80% of the fully extended chain (Tanford, 1980). The value of a_0 is affected by not only the structure of the hydrophilic head group but also medium conditions such as the presence of additives and electrolyte, temperature and pH. It increases in the presence of medium-chain alcohols. In the case of ionic surfactants, a_0 decreases while the amount of electrolyte in the solution increases because of the compression of the electrical double layer. Moreover, the increase in the surfactant concentration reduces a_0 due to the increase in the counterion concentration in the solution. When a_0 value decreases by this way, the spherical shape of the micelle turns into cylindrical. In another words, when a_0 decreases, the size of micelle increases as well. In addition, some ionic surfactants form long, wormlike structures in the presence of electrolyte due

to the decreasing repulsion between the ionic head groups. For nonionic POE surfactants, the increase in temperature may change the shape of the micelle if the dehydration of POE chain increases with the increasing temperature.

2.2.2.2. Mesophases or Liquid Crystals

When the number of surfactants increases or there is sufficient number of micelles, these micelles start to pack together in geometric arrangements with respect to their shapes and the repulsion between them grow. At a given concentration, entropy is overcome by the repulsion forces and micelles self-organize in an ordered arrangement, and a mesophase or liquid crystal is formed. These structures possess the ordered molecular arrangement observed in solid crystals but they have the liquid mobility.

Typical mesophases are shown in Figure 2.2. Cylindrical micelles can grow and pack together to form hexagonal phases while lamellar micelles can extend and form lamellar mesophases. With increasing surfactant concentration, several cylindrical micelles become branched and interconnected, and then form bicontinuous cubic mesophases (Rosen, 2004)

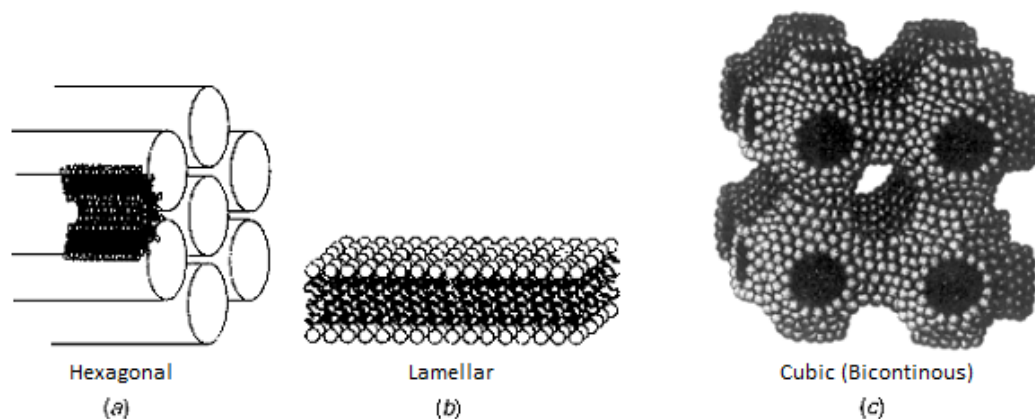


Figure 2.2. Main types of mesophases; Hexagonal, lamellar and cubic (Bicontinuous)

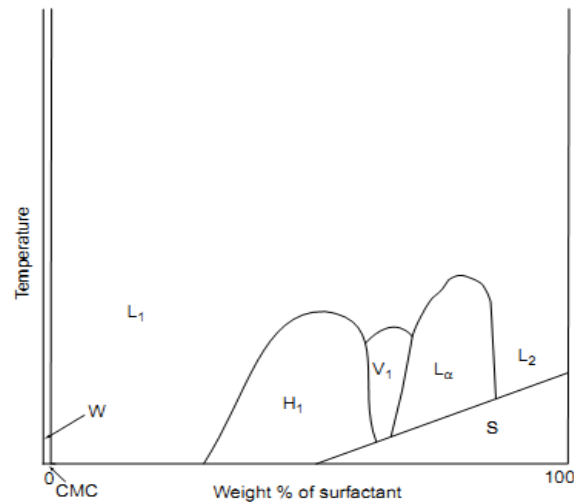


Figure 2.3. The phase diagram of the surfactants and mesophases with respect to temperature and weight of surfactant. H₁: Hexagonal, V₁: Bicontinuous cubic, L_x: Lamellar, W: nonmicellar solution, L₁: Micellar solution, L₂: Reversed micellar solution, S: Solid surfactant

In Figure 2.3., the phase diagram of the surfactants is shown. In many surfactant systems, the mesophases which vary with the increasing surfactant concentration are : Micellar, hexagonal, cubic and lamellar. Above c.m.c., in the region of L₁, the surfactants are present as micelles in the solution. When the surfactant concentration increases, the cylindrical rods form a hexagonal ordered mesophase and the region H₁ starts. At high surfactant concentrations, the stability limit of cylindrical rods is reached and lamellar structures are formed, leading the formation of lamellar mesophases (L_x). Between the hexagonal phase and micellar solution, a cubic phase can be observed (V₁). In fact, Fontell (1990) showed that between the micellar solution and hexagonal phase, another cubic phase, which may be arised from the array of the aggregation of short rod-like structures, is observed. The L₂ phase, which is the reversed micellar region, is formed at very high surfactant concentration. The effect of the temperature is generally significant for surfactants whose solubility is directly proportional to the temperature. When the temperature is high enough, the mesophases are transformed to micellar solutions. In addition, at high concentration of surfactant and low temperature region, the solid surfactants may precipitate (Rosen, 2004).

2.2.2.3. Formation Mechanism

Mobil's scientists first proposed the mesophase template mechanism for the synthesis of mesoporous silica particles (Beck et al., 1994). At the present, two main formation mechanisms can explain the formation of silica particles by the micelle templating method: "true liquid-crystal template mechanism" and "cooperative liquid-crystal template mechanism" (Figure 2.4.). In the true liquid-crystal template mechanism, a mesophase forms and then the silicate species are impregnated into the spaces between the micelles present in the pre-existing mesophase. This mechanism is based on the use of high concentration of the surfactants as templates in order to create liquid-crystal mesophases. The condensation of the silica precursor takes place around the surfactants and after this process, the final mesoporous product is obtained by removing the organic species by either calcination or extraction (Feng et al., 2000).

In the cooperative liquid-crystal template mechanism, the silicate precursors promote the formation of the mesophases. This mechanism explains the templated mesoporous silica synthesis arising from the interactions between the surfactants and inorganic species present in the solutions such as silicates and formation of inorganic-organic composites. With the effect of Coulomb forces, positively charged groups of surfactants interact with silicate polyanions. At the interface, the silicate species start to cooperatively polymerize and cross-link, and then causes the change in the charge density of inorganic layers. Therefore, the cooperative arrangements of surfactants and the charge density between organic and inorganic species in the solution affect each other and the compositions of organic-inorganic structures become different to some degree. The assembly process is governed by the matching of the charge density at the inorganic-organic interfaces. By this method, the mesophase may form below the surfactant concentration required to create the micellar mesophase only.

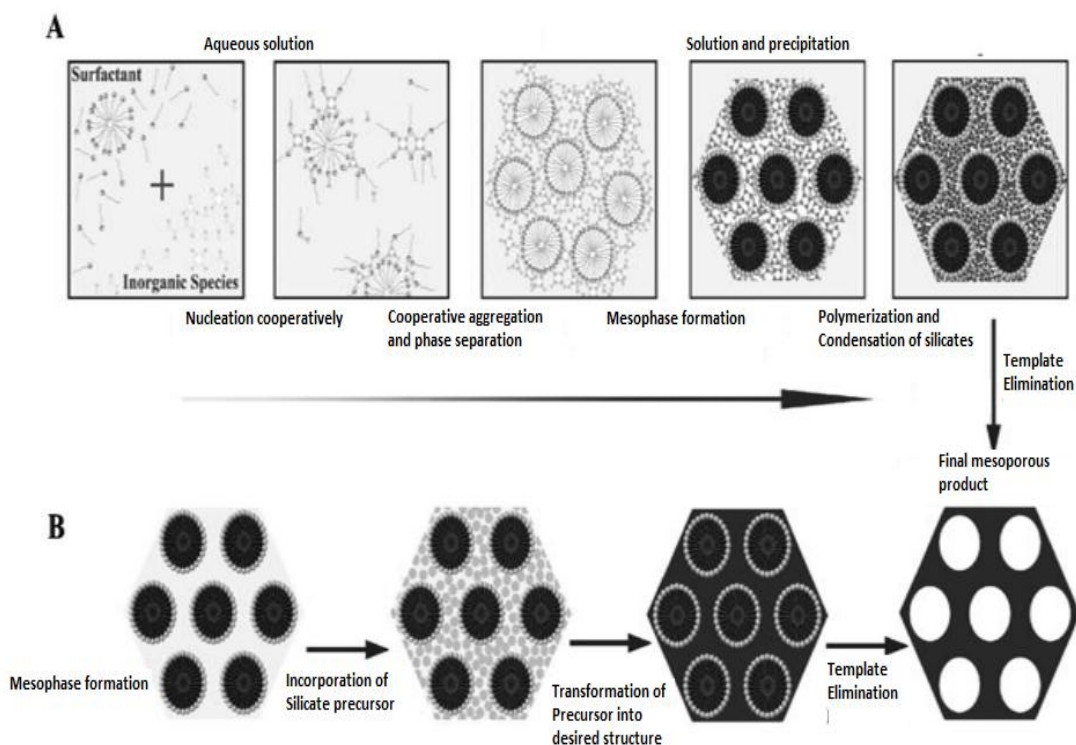


Figure 2.4. Formation mechanisms of mesoporous silica. A) Cooperative liquid-crystal template mechanism and B) true liquid crystal templating mechanism (Source: Wan and Zhao, 2007).

Huo et al. (1994) suggested to explain the interactions between the surfactants and inorganic species. They found that if the reaction occurs under basic conditions, the silica species are present as anions, deprotonated silanol groups (Si-O^-), and the surfactants must have positive charge in order to provide the interactions between both structures. This pathway is defined as S^+T . On the other hand, the reaction may take place under acidic conditions below pH 2, which is the isoelectric point of Si-OH bearing species. In this case, the silica species are positively charged (protonated silanol groups, Si-OH_2^+) and a mediator ion, X^- (usually a halide) must be added in order to ensure the interaction with cationic surfactants. This pathway is termed as $\text{S}^+\text{X}^-\text{T}$. Under basic conditions, it is also possible to work with negatively charged surfactants but a positively charged mediator ion, M^+ must be added in order to keep the interaction with the negatively charged silica species. The pathway is defined as $\text{S}^-\text{M}^+\text{T}$. In addition, the reaction may take place under acidic media in which the negatively charged surfactants are used as the structure directing agents. Its pathway can be termed as S^-T . These interactions are based on the electrostatic forces while the attractive interactions can be ensured by the hydrogen bonds in the case of using nonionic surfactants. At low pH, the

formation of silica-nonionic surfactant mesophase can be proposed by the pathway, $(S^0H^+)(X^-I^+)$ (Zhao et al., 1999). In very acidic conditions, the oxygen molecules of poly(ethylene oxide) headgroups can form oxonium ions and behave like cationic headgroups. At higher pH, the formation of silica-nonionic surfactant mesophases has been reported as following the S^{0I^0} pathway. In the absence of strong electrostatic interactions, the ordered silica-nonionic surfactant mesophases can be formed by the effect of hydrogen bonds and entropy (Kim et al., 2000).

2.2.2.4. Typical Ordered Mesoporous Silicas and Commonly Used Surfactants in Their Synthesis

With respect to their pore arrangements and lattice characteristics, mesoporous silica structures can be mainly classified as 2-D hexagonal, 3-D cubic bicontinuous, and 3-D cage-like cubic. Among these materials, the 2-D hexagonal structures have been widely synthesized and used in many applications. The first micelle-templated mesoporous silica structure was synthesized by Mobil researchers in 1992 by using alkyltrimethylammonium surfactants as the micellar templates. This structure was called “Mobil Crystalline Material” (MCM-41) (Beck et al., 1992).

MCM-41 is one of the most simple mesoporous silica particles and can be synthesized in a wide range of basis conditions (pH=9-13, optimum 11.5). In the synthesis of these structures, cationic surfactants, such as long-chain alkyl ammonium ($C_nH_{2n+1}N(CH_3)_3^+X^-$, $n=8-22$, $X=Br,Cl$), are commonly used. Among them, hexadecyltrimethylammonium bromide (CTAB, $n=16$) is the most often used cationic surfactant.

MCM-41 has a hexagonal mesopore arrangement whose pore size varies between 2 and 5 nm. The nitrogen adsorption/desorption isotherms do not show any hysteresis loop. Its pore wall thickness is estimated nearly 1 nm and BET surface area is about 1000 m^2/g . Moreover, its specific pore volume is about 1 cm^3/g . Moreover, micropores are not detected in the silica pore walls.

Another important hexagonally ordered mesoporous silica material is “Santa Barbara Amorphous”(SBA-15). Compared to the synthesis of MCM-41, SBA-15 is synthesized by using nonionic triblock copolymer surfactants as templates under acidic conditions. The most suitable template is pluronic P-123 (Zhao et al., 1998). It belongs to pluronic family which are triblock copolymers consisting of poly(ethylene oxide) and

poly(propylene oxide) blocks. There are several pluronic members whose ethylene oxide and propylene oxide percentages vary, which are shown in the pluronic grid.

If P-123 is used as the structure-directing agent in the mesoporous silica synthesis, the pore size and the specific pore volume of the particles are larger than that of MCM-41 type particles. The pore size varies between 5-20 nm while the pore wall thickness is around 2-5 nm, which is thicker than that of MCM-41. Therefore, SBA-15 exhibits higher thermal and hydrothermal stability than MCM-41. On the other hand, its surface area is not as high as that of MCM-41. Another important property of SBA-15 is that there are plenty of micropores and these micropores connect the mesoporous channels (Yang and Sayari, 2005).

Among the 3-D cubic bicontinuous mesoporous silica particles, the synthesis of MCM-48 was reported first. It has cubic symmetry and 3-D bicontinuous mesochannels. The schematic view of these type structures is shown in Figure 2.5. In addition to MCM-48, KIT-6 and FDU-5 are the other samples of 3-D cubic bicontinuous silica structures.

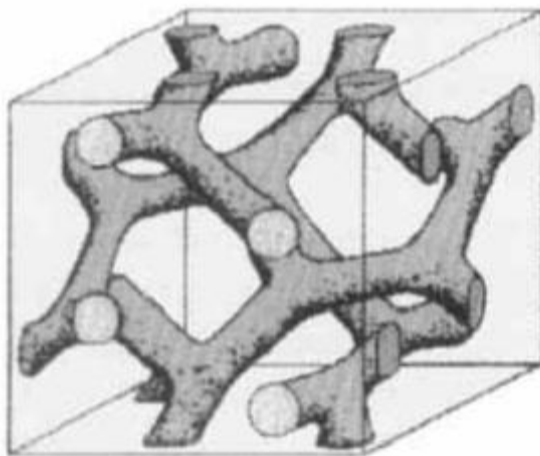


Figure 2.5. Cubic bicontinuous mesoporous structures (MCM-48, KIT-6 and FDU-5)

The mesostructure observed in the particles mentioned above is called minimum surface gyroid (G-surface). The cubic bicontinuous mesostructure is formed as a result of dividing the space into identical but separate 3-D mesopore channels by the minimum surface. These two mesochannel sets are arranged with a highly symmetrical structure (Zhao et al., 1998).

Mesoporous silica FDU-5 was reported the first cubic bicontinuous mesostructure synthesized under acidic conditions (Liu et al., 2002). Alternatively, KIT-6 is also synthesized under acidic conditions in the presence of P-123 and n-butanol (Kleitz et al., 2003). In addition to these particles, other triblock copolymers or surfactant mixtures can be used to synthesize cubic bicontinuous mesostructures with large pore size and micropore channels inside the pore walls.

2.2.3. The Silica Particles as Drug Carrier

In 2001, MCM-41 was proposed as a drug carrier for the first time and then mesoporous silica particles became promising drug carriers due to several important features: 1) An ordered pore arrangement, being uniform in size and providing controlled drug loading and release, 2) A high pore volume causing adsorption of the required amount of drug into the particle, 3) A high specific surface area, increasing the amount of drug adsorbed, and 4) the functional groups on the particle surface which allow the functionalization of the particle and better drug delivery (Vallet-Regi et al., 2001; Vallet-Regi et al., 2007). Several studies used these structures without any modifications and the results obtained are shown in Table 2.3.

Vallet-Regi and her colleagues (2007) tested MCM-41 type materials with different pore sizes and investigated the effect of both the pore size and the drug loading method on the drug release. In the range of the lower limits of the mesopore size, the release rate of the determined drug decreases with decreasing pore size (Horcajada et al. 2004). On the other hand, functionalization of the mesoporous particle surface influences the drug loading and release performance, varying with respect to the drug solubility (Zeng et al., 2005; Horcajada et al., 2006; Munoz et al., 2003).

A few studies focusing on MCM-48 have provided information about the ease of the molecular accessibility and fast molecular transport due to their bicontinuous mesoporous channels. Likewise the studies with MCM-41, MCM-48 exhibited good drug delivery characteristic and the release rate is reduced due to the change in pore size and surface functionality (Izquierdo-Barba et al., 2005).

SBA-15 has been also reported in several studies as a promising drug carrier due to the silanol groups on its surface and large pore sizes ensuring delivery of the large biomolecules. While hydrophilic pore walls of the SBA-15 provides good drug delivery

performance, the surface functionalization needs to be carried out in order to make the delivery of the hydrophobic drugs from the particle better (Doadrio et al., 2006; Song et al., 2006).

Table 2.3. Surface properties and drug loading capacity of the mesoporous silica particles

Particle	S_{BET} (m^2/g)	Pore diameter (nm)	Drug	Loading (wt%)	Reference
MCM-41	1157	3.6	Ibuprofen	34	Vallet-Regi et al. (2001)
SBA-15	787	6.1	Gentamicin	20	Doadrio et al. (2004)
MCM-41	1210	2.6	Ibuprofen	36	Zhu et al. (2005)
MCM-41	1200	3.3	Ibuprofen	41	Andersson et al. (2004)
MCM-41	-	3.8	Erythromycin	29	Doadrio et al. (2006)
SBA-15	787	8.8	Erythromycin	34	Doadrio et al. (2006)
SBA-15	787	4.9	Amoxicillin	24	Vallet-Regi et al. (2004)
SBA-15	910	9.37	Captopril	23	Qu et al. (2006)
MCM-41	1211	2.79	Captopril	34	Qu et al. (2006)
MCM-48	1166	3.6	Ibuprofen	29	Izquierdo-Barba et al. (2005)
MCM-48	1166	3.6	Erythromycin	28	Izquierdo-Barba et al. (2005)

2.3. Mesoporous Carbon Nanoparticles in Drug Delivery

Until today, mesoporous carbon has been widely used in several applications such as catalytic, electrochemical, separation, gas storage, transport and adsorption processes (Gokulakrishnan et al., 2011; Huang et al., 2011; Vix-Guterl et al., 2005; Cooper et al., 2004). High surface area, large pore volume, inert nature and low toxicity of these nanostructures make them good candidates for being drug carriers (Zhao et al., 2012).

2.3.1. The Synthesis of Mesoporous Carbon Particles

There are several methods to synthesize mesoporous carbon materials such as a) activation by physical or physical/chemical methods (Hu et al., 2000; Kyotani, 2000), b) carbonization of carbon precursors composed of one thermosetting and one thermally unstable component (Ozaki et al., 1997; Kowalewski et al., 2002), c) activation of carbon precursors with metal or organometallic compounds (Tamai et al., 1996; Oya et al., 1995), d) carbonization of aerogels (Tamon et al., 1999; Pekala et al., 1989), e) replication synthesis by using hard template materials (Knox et al., 1983) and f) self-assembly using soft templates (Liang et al., 2004; Tanaka et al., 2005). Among these methods, “e” and “f” are more commonly used than the other methods due to their well-controlled surface characteristics (Liang et al., 2008).

In the case of the hard-template synthesis, a presynthesized organic or inorganic material as hard template is used (Lu and Schüth, 2006). These templates serve as a mold in order to replicate the mesoporous carbon while no significant chemical interactions occur between them and carbon precursors. As a result of this replication process, a porous carbon structure is shaped with respect to the template material. This method performed by Knox and his colleagues in early 1980s included 1) the synthesis of porous silica gel, 2) impregnation of the silica template with carbon precursor, 3) cross-linking and carbonization of the carbon precursor and 4) removal of the silica template. The final step leads to the formation of pores in the corresponding carbon materials. Knox's group used a phenol-hexamine mixture as the carbon source and obtained a rigid mesoporous carbon. This type of materials was later called “Hypercarb” and used in liquid chromatographic separations (Knox et al., 1986).

The developments in the synthesis of mesoporous carbon materials has been proceeding simultaneously with the developments in mesoporous structures possessing highly ordered porous structure, uniform pore sizes etc. by using ionic or nonionic surfactants as structure-directing agents (Beck et al.,1992; Zhao et al., 1998; Zhao et al., 1998; Tanev and Pinnavaia, 1995). In 1999, Ryoo and his colleagues reported the synthesis of the first self-supported ordered mesoporous carbon, named as CMK-1, by using the ordered aluminosilicate MCM-48 as the hard template (Ryoo et al., 1999). They impregnated aluminosilicate MCM-48 template with solutions of sucrose and sulfuric acid as the carbon source and acid catalyst during carbonization at temperatures of up to 800-1100 °C, respectively. Finally, silica template was removed by solvent extraction.

The use of hexagonally ordered mesoporous silica particles, SBA-15, leads to the formation of CMK-3 (Jun et al., 2000). CMK-3 is composed of several carbon nanorods which are arranged in a hexagonal order and connected to each other. A similar structure to SBA-15, MSU-H, which is synthesized under neutral conditions instead of acidic, was used as template in the synthesis of C-MSU-H (Kim and Pinnavaia, 2000). Another significant advancement in the synthesis of mesoporous carbon particles resulted in the formation of CMK-5, containing hexagonally ordered array of amorphous carbon nanopipes (Kruk et al., 2003). Alumina is incorporated onto the SBA-15 surface to introduce acidic groups which serve as catalyst in the polymerization of furfuryl alcohol onto the pore walls. Chemical vapor deposition (CVD) of mesoporous silica particles also leads to the formation of several types mesoporous carbon materials (Kaneda et al., 2002; Vix-Guterl et al., 2002). In addition to these studies, direct carbonization of pluronic type triblock copolymer (e.g., P123) was also examined. By the sulfuric acid treatment, SBA-15 including P123 in their pores was carbonized and then silica template was removed to form mesoporous carbon structures (Kim et al., 2004).

CHAPTER 3

MATERIALS AND METHODS

3.1. Materials

3.1.1. Surfactants

Both ionic and nonionic surfactants were used in the present study. The ionic surfactants were hexadecyltrimethylammonium bromide (CTAB) (Sigma, 98%) sodium dodecyl sulfate (SDS) (Sigma, 99%) and hexadecyltrimethylammonium chloride (CTAC) (Merck, 50% solution in 2-propanol/water 3:2) while the nonionic surfactants were pluronic type triblock copolymers (P-123, P-104, F-127, F-68 and L-64) (BASF). These surfactants were used as soft templates or additives in the synthesis of mesoporous silica nanoparticles. The common features of the ionic surfactants with their chemical structures are given in Table 3.1. and micellar properties of CTAB is shown in Table 3.2. The chemical structure of the pluronic triblock copolymers and the pluronic grid which classifies the pluronic copolymers with respect to their hydrophilic and hydrophobic groups are shown in Figure 3.1 and Figure 3.2, respectively, while the chemical formulas and molecular weights of the selected pluronic surfactants are displayed in Table 3.3.

Table 3.1. The Molecular Structures and Weights of the Ionic Surfactants Used in This Study

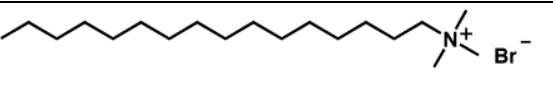
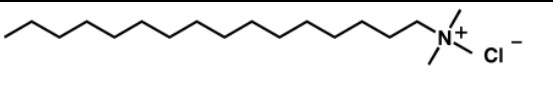
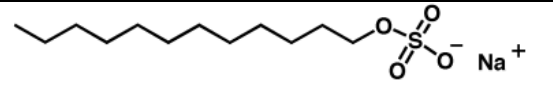
Commercial name	Molecular structure	Molecular weight (g/mol)
Hexadecyltrimethyl ammonium bromide		364.5
Hexadecyltrimethyl ammonium chloride		320.0
Sodium dodecyl sulfate		288.4

Table 3.2. Micellar Properties of CTAB

Molecular weight (g/mol)	364.45
Critical micelle concentration (c.m.c.) (M) (25 °C)	0.0009-0.001
Aggregation number	60-100
Mean area per molecule (Å ²)	50
Molecular length (in theory) (nm)	2.2
Micelle size (nm) *	6-8
Molecular volume (Å ³ /molecule) (in theory)	460
Micellar volume (Å ³ /molecule) (in theory)	41200

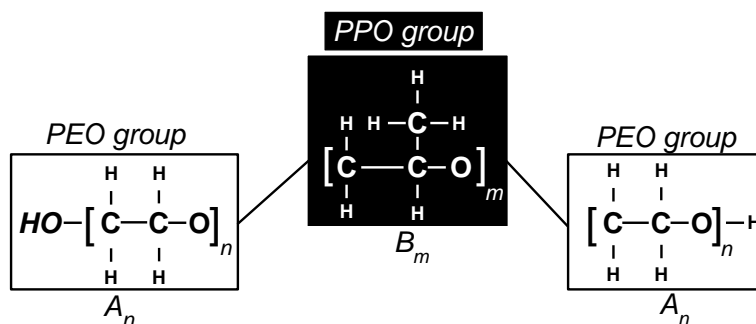


Figure 3.1. The molecular structure of pluronic triblock-copolymers (A_n : # of EO groups, B_m : # of PO groups)

Table 3.3. Molecular formula and average molecular weights of selected Pluronics

Commercial name	Chemical formula	Molecular weight (g/mol)
Pluronic L-64	PEO ₁₃ PPO ₃₀ PEO ₁₃	2900
Pluronic F-68	PEO ₇₅ PPO ₃₀ PEO ₇₅	8400
Pluronic P-104	PEO ₂₇ PPO ₆₁ PEO ₂₇	5900
Pluronic P-123	PEO ₂₀ PPO ₇₀ PEO ₂₀	5800
Pluronic F-127	PEO ₉₈ PPO ₆₇ PEO ₉₈	12600

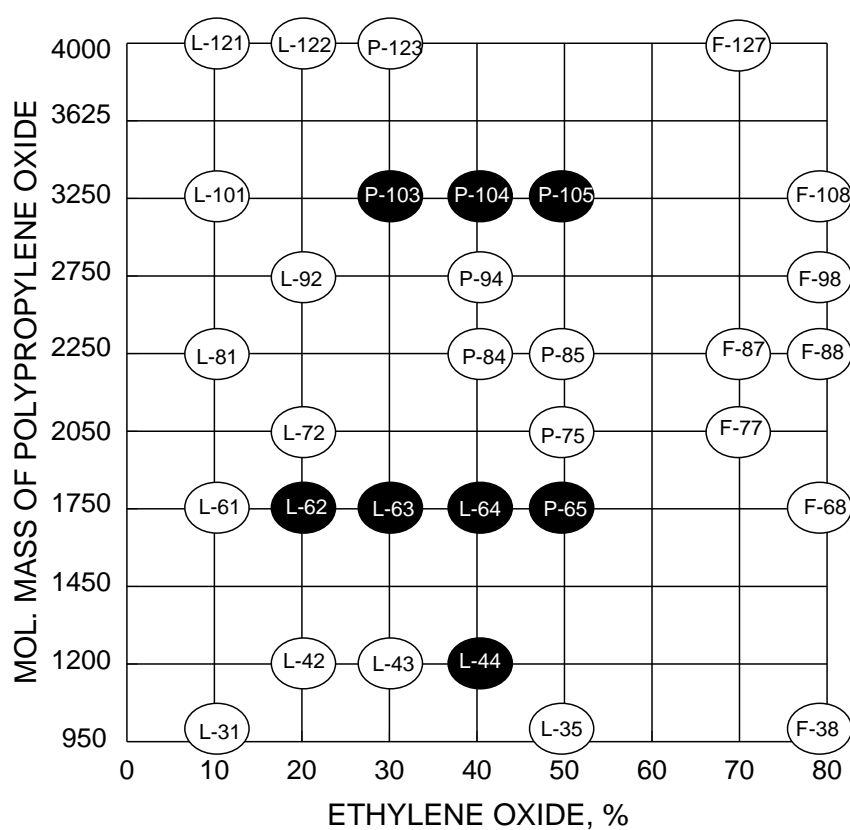


Figure 3.2. The pluronic triblock-copolymers and pluronic grid

3.1.2. Other Chemicals

Tetraethyl orthosilicate (TEOS) (Merck, 98%) were used as silica source. Ethanol (Merck, absolute) and Methanol (Merck, ACS) were used as solvents. Ammonium hydroxide (Merck, 28%) was served as a basic catalyst and Hydrochloric

acid (HCl) (Sigma-Aldrich, 37%) provided the acidic medium in the synthesis of silica nanoparticles under basic and acidic conditions, respectively. Glycerol (Riedel, 87%), Potassium chloride (KCl) (Sigma-Aldrich, ACS), Tetraethylammonium bromide (TEAB) (Aldrich, 98%) and 3-Aminopropyltriethoxy silane (APTS) (Sigma, 99%) were used as additives in the synthesis of silica nanoparticles. Sodium carbonate (Na_2CO_3) (Merck, anhydrous) and Calcium chloride (CaCl_2) (Merck, anhydrous) were used as the reactants in calcium carbonate formation. Sucrose (Merck) was used as carbon source and Sulfuric acid (H_2SO_4) (Sigma-Aldrich, 95-97%) was used as carbonization catalyst. In all experiments, Ultrapure water (18.2 M Ω) was used.

3.2. Methods

3.2.1. Surface Tension Measurements

The surface tension of aqueous surfactant solutions were measured with a Krüss K10 ST model device by using the ring type surface tension method. All glassware for the measurements was entirely cleaned with 5% aqueous nitric acid solution and rinsed with distilled water. The measurements were carried out at the concentrations varying between as low as 10^{-7} M and as high as 10^{-1} M. For the analysis, a fixed amount of surfactant solutions (30-35 ml) was taken in each case and the measurements started with the sample of lowest concentration. Between the measurements, the ring and the beaker containing the surfactant solutions were rinsed with distilled water, then the ring was burned in a flame. Then, all samples were mixed and after a two-minute wait to provide stability, the samples were analyzed. The surface tension values presented in this study was the average value of at least two measurements.

3.2.2. Size Measurements

The surfactant solutions of 0.01 M were prepared by dissolving the surfactants in aqueous solutions to form micellar structures. Size of these micelles was measured by using Malvern Zetasizer Nano ZS at 25 °C.

3.2.3. Synthesis of Silica Nanoparticles

The synthesis of silica nanoparticles is based on the idea of acid and base catalyzed sol-gel reactions. To create the pores with a specific order on the surface of these nanostructures, the surfactants were used as soft-template molecules. In this study, the final particles synthesized with base and acid catalyzed reactions were named as BC and AC, respectively.

In the case of base catalyzed sol-gel reactions, the main target was to form monodisperse, spherical and mesoporous silica nanoparticles. To perform this, two different synthesis pathways were followed: a) A modified sol-gel synthesis, b) Templated mesoporous silica (MCM-41) synthesis. In this study, the modified sol-gel particles were called BC-1 and MCM-41 particles were called BC-2. In the first case, a typical sol-gel synthesis includes these steps : 1) The surfactants (their concentrations vary but above c.m.c. in all cases) were dissolved in 50 ml ethanol/methanol mixtures (1:1 v/v). 2) After dissolving, 5 ml NH₄OH (28%) was added to the solution. 3) After stirring for 5 min, 2 ml TEOS was added dropwisely with a plastic syringe under stirring. 4) The stirring was performed for 24 h at a constant temperature (38 °C) in Gerhardt Thermoshake model shaker. 5) After 24 h, the solutions containing silica nanoparticles were centrifuged by Eppendorf Centrifuge 5804, washed with ultrapure water and ethanol several times. Then the solid particles were taken and then were dried in DHG-9140A drying oven at 90 °C. Finally, the dried nanoparticles were calcined at 550 °C for 5 h under air. As a result, monodisperse, spherical silica nanoparticles were obtained.

In a typical synthesis of BC-2, a cationic surfactant, CTAB (0.05 M, 0.01 or 0.001 M), was dissolved in 60 ml water. After the surfactant was dissolved in aqueous medium, 4 ml NH₄OH was added and the stirring continued for 5 min. At the end of 5 min, 5 ml TEOS was added dropwisely into the solution under stirring. The mixture was kept in shaker at 25 °C (In other cases, 35 and 45 °C were also tried.) for 24 h. Then, the steps in the synthesis of BC-1 particles were repeated for BC-2. At the end of the synthesis, almost monodisperse, spherical or rod-like mesoporous silica nanoparticles were formed. The synthesis pathway is illustrated in Figure 3.3.

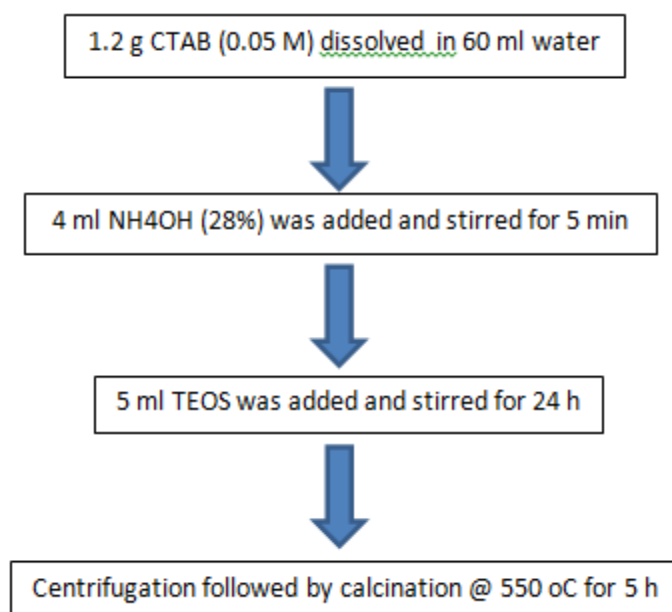


Figure 3.3. The typical synthesis pathway of BC-2 particles

The templated mesoporous silica nanoparticles in acidic conditions were synthesized by using pluronic P-123 micelles as template structures. The particles synthesized by this way were called AC. In this case, P-123 (5.8×10^{-3} M) was dissolved in 30 ml 2 M HCl solution. After dissolved, different amounts of TEOS in each case (0.01 and 0.0075 mol) was added dropwisely into the P-123 solution under stirring and the mixture was stirred at 38 °C for 24 h in shaker. At the end of this period, the synthesized silica particles were hydrothermally aged at 100 °C for 24 h, followed by the centrifugation and then washed with water and ethanol. The calcination prodecure was the same as BC-2 synthesis. The other conditions applied in this synthesis were : 1) The presence of co-surfactant and additive (CTAB and SDS (5.8×10^{-3} M) as cosurfactants, KCL (0.1 M) as a salt and glycerol (1 g) as an additive), 2) After TEOS addition, stirring of the mixture for 5 or 10 min and then keeping at the same temperature without stirring, 3) The change in the reaction time from 24 h to 6 and 3 h in each case and 4) Particle synthesis without hydrothermal treatment. The synthesis pathway is shown in Figure 3.4.

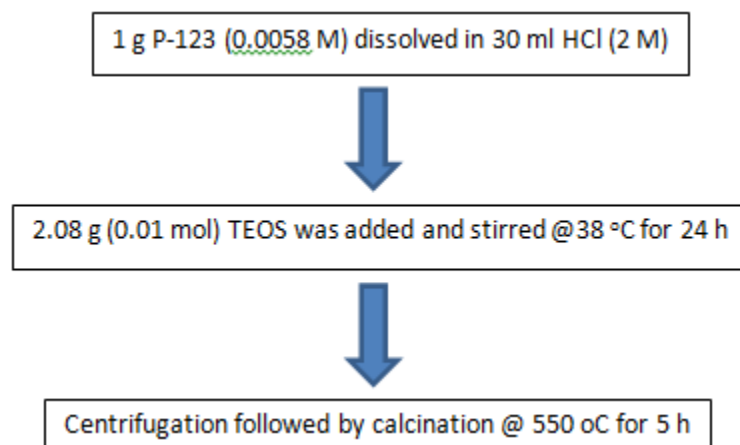


Figure 3.4. The typical synthesis pathway of AC-1 particles

AC particles were labelled with respect to their synthesis conditions as shown in Table 3.4. The classification of these particles were based on the amount of the additives added into the surfactant solution (before TEOS addition).

Table 3.4. Classification of AC particles synthesized in this study

Sample	Additives used in the synthesis	
AC-n (n:1-4)	n = 1	0.01 mol TEOS
	n = 2	0.0075 mol TEOS
	n = 3	0.01 mol TEOS + 1 g glycerol
	n = 4	0.01 mol TEOS + 0.1 M KCl
	Reaction and stirring time periods	
AC-n-RT	RT = 3	Reaction time : 3 h
	RT = 6	Reaction time : 6 h
	RT = 24	Reaction time : 24 h
AC-n-RT-ST	ST = 5	Stirring time : 5 min
	ST = 24	Stirring time : 24 h
AC*	Particle formation without hydrothermal treatment	

3.2.4. Carbon Coating of Silica Nanoparticles

Before the carbon coating step, calcium carbonate nanostructures covered the surface of the calcined BC-2 nanoparticles in order to protect the pores from the carbon formation. In a typical synthesis, 0.5 mmol calcium chloride (CaCl_2) was dissolved in 10 ml water and then 0.1 g calcined silica was added into the solution. Aqueous sodium carbonate (Na_2CO_3) (0.5 mmol) solution was added dropwise by using ATTO AC-2110 model peristaltic pump at a rate of 2 ml/min. Then, the mixture was stirred on IKA C-MAG HS7 model magnetic stirrer for 2 h at room temperature. The formed silica/ CaCO_3 composites were separated from turbid suspensions by centrifugation (4500 rpm, 10 min), washed with water and ethanol several times, finally dried in the oven.

Carbonization step was carried out for both calcined silica nanoparticles and silica/ CaCO_3 nanoparticles. The nanoparticles were impregnated with aqueous sucrose solution containing sulfuric acid. In a typical synthesis, 0.2 g nanoparticles was added to a solution obtained by dissolving 0.25 g sucrose and 0.028 g sulfuric acid in 1 g water. This mixture was heated in the drying oven for 6 h at 100 °C, and subsequently the temperature was increased to 160 °C and the sample was kept for another 6 h. During this treatment, the sample turned black or dark brown. The nanoparticles which were partially carbonized were treated again by following the same steps after the addition of 0.16 g sucrose, 0.0045 g sulfuric acid in 1 ml water. The carbonization was completed by pyrolysis in Protherm tubular oven at 900 °C for 2 h under nitrogen flow. The carbonized BC-2 particles without CaCO_3 precipitation were named as CBC-1 and the carbonized BC-2 particles containing CaCO_3 on their surface before the carbonization were named as CBC-2. CBC-2 particles were then treated with 2 M HCl solution overnight to remove CaCO_3 from the pores of BC particles. The synthesis pathway is shown in Figure 3.5.

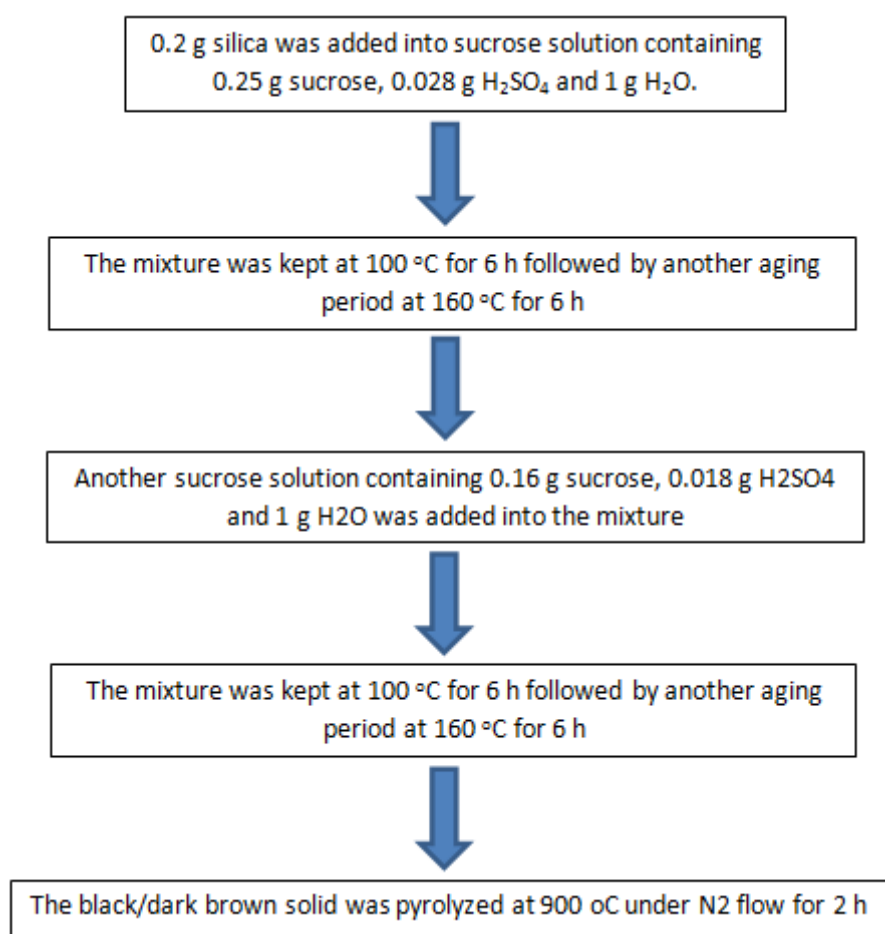


Figure 3.5. The typical synthesis pathway of CBC particles

3.2.5. Characterization Studies

Characterization of the surfactants and nanoparticles was carried out by using SEM/EDX analysis, BET analysis, TEM analysis and FTIR.

SEM/EDX characterization was performed by using a Quanta 250FEG type instrument. In SEM analysis, the reflected electron beam is limited by a raster across the surface of the sample and the image is created by counting backscattered electrons. Prior to the analysis, the nanoparticles were dispersed in water and then the sample was taken from these suspensions for SEM analysis. The sample was dropped onto the metallic SEM stub. The images of the nanoparticles were recorded at different magnifications.

During BET analysis, all samples were analyzed by Micromeritics ASAP 2010 volumetric adsorption device to investigate the surface characteristics of the nanoparticles (average pore diameter, specific pore volume and specific surface area). Before analyses, all samples were degassed at 200 °C for a day. Nitrogen was used at 77 K for the determination of surface area and mesopore properties as recommended by IUPAC. In this system, the sample is exposed to a controlled gas environment and volume of adsorbed and desorbed gas is measured as function of relative pressure at constant temperature. As a result, a sorption isotherm which is the plot volume versus p/p_0 , where p is the absolute pressure and p_0 is the saturation vapor pressure.

TEM analysis was performed by Tecnai G² F20 S-TWIN. In a TEM device, the electrons are emitted from a filament and accelerated by a high voltage and this results in the focalization of resulting electron beams onto the sample by electromagnetic fields. The electrons which are diffracted are detected on a photographic film or fluorescent screen. In this analysis, solid silica nanoparticles were dispersed in ethanol/water solution (1:1 v/v) by using an ultrasonic probe. The samples taken from the prepared suspensions were dropped onto the carbon coated copper grids and the grids were kept in a drying oven at 60 °C for 1 h.

The FTIR spectra of the particles were obtained by using Shimadzu FTIR spectrophotometer (8400S). The pellets for samples were prepared for the analysis. First, certain amount of silica particle was mixed with KBr (3mg sample in 150 mg KBr-silica sample). Then, the samples were kept at 100 °C overnight, followed by grinding in a mortar and pressing.

CHAPTER 4

RESULTS AND DISCUSSION

4.1. The Forms of Surfactant Molecules in Water : Surface Tension Measurements

The role of surfactants in the synthesis of mesoporous silica particles is very important. The forms of surfactant molecules in solutions vary significantly with their concentrations. In order to determine their forms in aqueous systems, surface tension measurements were performed as a function of surfactant concentration under several conditions and the results were discussed in the following paragraphs.

The surface tension values of aqueous surfactant solutions at 25 °C were plotted as a function of their concentrations and shown in Figure 4.1. Typically, the increasing surfactant concentration reduces the surface tension of aqueous surfactant solutions, causing an increase in surfactant activity under constant coverage of liquid/vapor interface. Then, the surface tension reaches a constant value, c.m.c., which does not vary with a further increase in surfactant concentration. In this study, the surface tension curve with respect to the concentration usually tends to follow the same way: At low concentrations below 10^{-4} M, the surface tension values almost remain constant in the region of 66-70 mN/m which can be defined as the region I. As the surfactant concentration in water decreases, the surface tension approaches the value of distilled water (~ 72 mN/m at 25 °C). The increase in surfactant concentration leads to the region II where the single surfactant molecules in the region I start to accumulate at the interface. In this region, a decrease in surfactant concentration with a constant slope is observed and indicates the monolayer coverage of the surface. It is a dynamic phenomena; The rate of surfactant molecules exchange between bulk solution and the surface increases as the concentration increases. For nonionic surfactant P-123, the concentration range in which the measurements were performed hide the region I and the possible another inflection point on the surface tension curve below 10^{-6} M. As shown, between 10^{-6} and almost 10^{-2} M surfactant concentration, there is a big difference between the surface tension values of ionic and nonionic surfactants. After leaving the region II behind, the surface tension starts to remain constant after a critical

point while the surfactant concentration increases. At this point, critical micelle concentration, the surfactants form the micelles. The c.m.c. values obtained by the surface tension measurements are about 10^{-3} M, 5×10^{-5} M, 10^{-2} M and 10^{-3} M for CTAB, P-123, SDS and CTAC, respectively. All values agree with the ones reported in literature (Szymczyk and Janczuk, 2007; Tofani et al., 2004; Mukerjee and Mysels, 1971; Sahu et al., 2006).

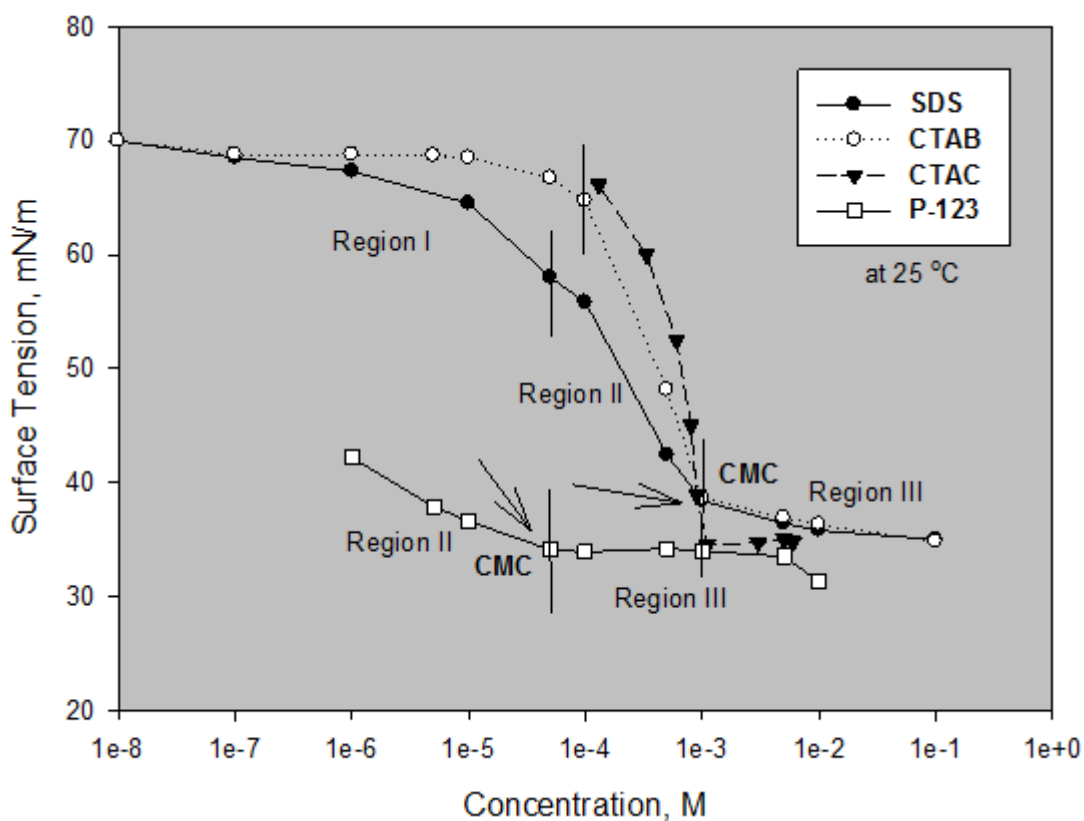


Figure 4.1. Surface tension vs concentration of selected surfactants

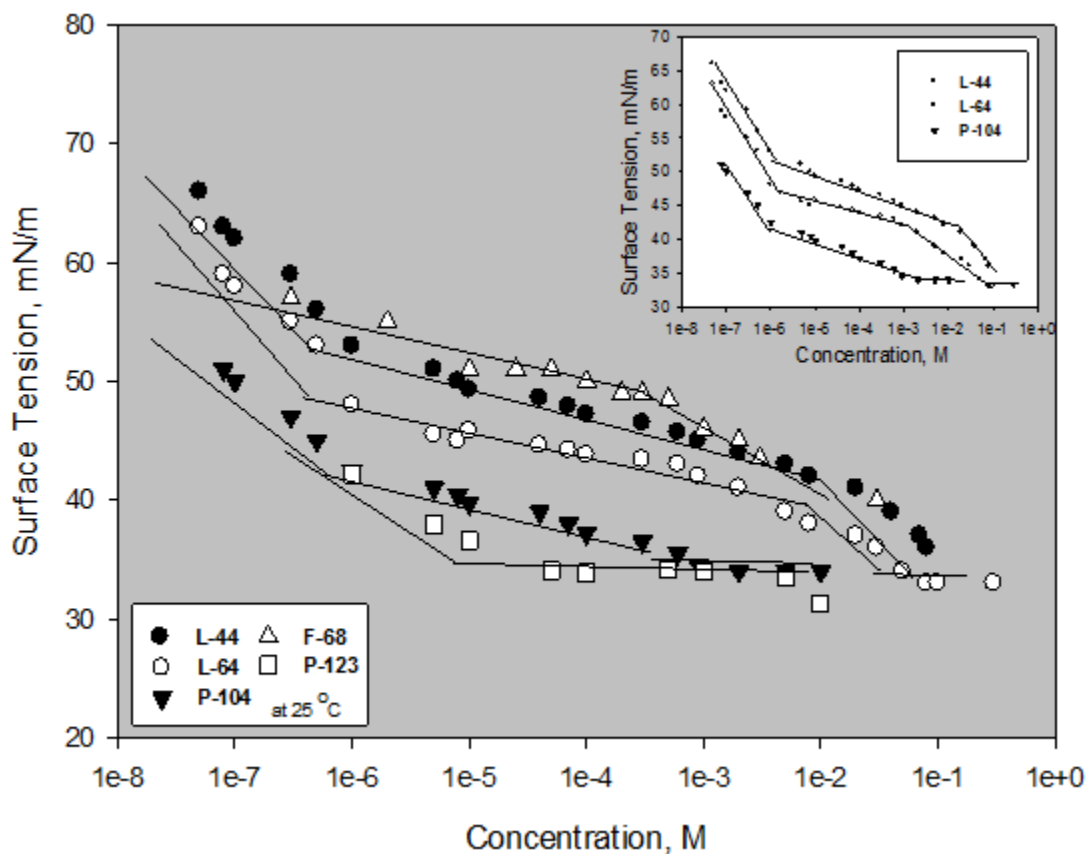


Figure 4.2. Surface tension vs concentration of selected Pluronic surfactants

The surface tension curves for other pluronic surfactants than P-123 were also obtained and shown in Figure 4.2. Unlike the ionic surfactants, the selected nonionic surfactants exhibited a different behaviour under constant conditions. As mentioned in the case of P-123, these type of surfactants have two inflection points before c.m.c. The first break point may be due to the fact that these surfactants are not well-defined samples and have a broad molecular weight distribution. At this point, only the highly surface active component starts to aggregate (Hecht and Hoffmann, 1994). The first break may be attributed to reconfiguration of single surfactant molecules at the surface. This idea is related to the monolayer coverage at the interface, followed by accumulation of more surfactant molecules at the interface to produce a more compact layer. The surface tension continues to decrease in this region until the second break is reached where all components form micelles (Alexandridis et al., 1994).

P-104 had a c.m.c. of about 10^{-3} M and this value is close to the reported value (5×10^{-4} M) (Alexandridis et al., 1994). In the case of L-64, two inflection points on the surface tension versus concentration plot can be well observed. Its experimental c.m.c.

value found in this study was almost 5×10^{-2} M, which is close to the reported value (3.5×10^{-2} M) (Kozlov et al., 2000). On the other hand, for the remaining nonionic surfactants, a definite c.m.c. point was not observed in the concentration range up to 10^{-1} M. In another words, the selected concentrations and temperature of the surfactant solutions for surface tension measurements did not reach the c.m.c. F-68 is highly hydrophilic due to the high percentage of EO segments in its structure and may have a c.m.c. higher than 10^{-1} M because its micellization requires higher temperatures (Figure 3.2.). This situation can be explained by the fact that at high temperatures water becomes a poorer solvent for both hydrophilic and hydrophobic components of the polymers. Entropy is the main driving force of the micellization process and the free energy of micellization is mainly a function of the hydrophobic PO blocks in surfactant. In the case of L-44 which has the same EO percentage as that in L-64 and P-104, no c.m.c. is observed under the studied conditions, likewise F-68. According to the studies, when the percentage of PEO segment in polymeric surfactant is constant, an increase in the number of PPO blocks reduces c.m.c. of the surfactant. Thus, it was expected that c.m.c. would vary with the order of $P-104 < L-64 < L-44$.

In fact, the determination of the critical micelle concentration is a difficult task for the nonionic surfactants. For the same surfactant under the same conditions, the c.m.c. values may vary by 1-3 orders of magnitude from one method to another. Such a difference depends on the surface tension measurement technique, the presence of impurities arising from the surfactant production and the chemical ingredients of the surfactants used.

The surfactants may behave differently if the medium conditions vary. The change in the temperature and solvent, the presence of an additive such as salt or another surfactant affect the behaviour of the surfactants in solution.

In Figure 4.3, the surface tension curves of P-123 solutions prepared at different solvents and temperatures are shown. At 25 °C, c.m.c. of P-123 was found almost 5×10^{-5} M and 1.5×10^{-4} M (Gonzalez-Lopez et al., 2010) in water and HCl, respectively. The increase in c.m.c. in the presence of HCl may be contributed by the enhancement of the interaction between the alkyl group and the protonated water molecules. Hence, the dehydration process of pluronic surfactant becomes more difficult and leads to the increase of c.m.c. (Yang et al., 2006). Furthermore, to observe the temperature dependence on c.m.c., the surface tension measurements of P-123 aqueous solution were performed at 30 °C, as well. As expected, the critical micelle concentration has

decreased almost with the order of 1 in magnitude as temperature has increased. This effect can be explained by the fact that the increase of temperature may cause the dehydration of the polyoxyethylene group, varying the hydrophobic-hydrophilic balance toward the hydrophobicity (Kabanov et al., 1995).

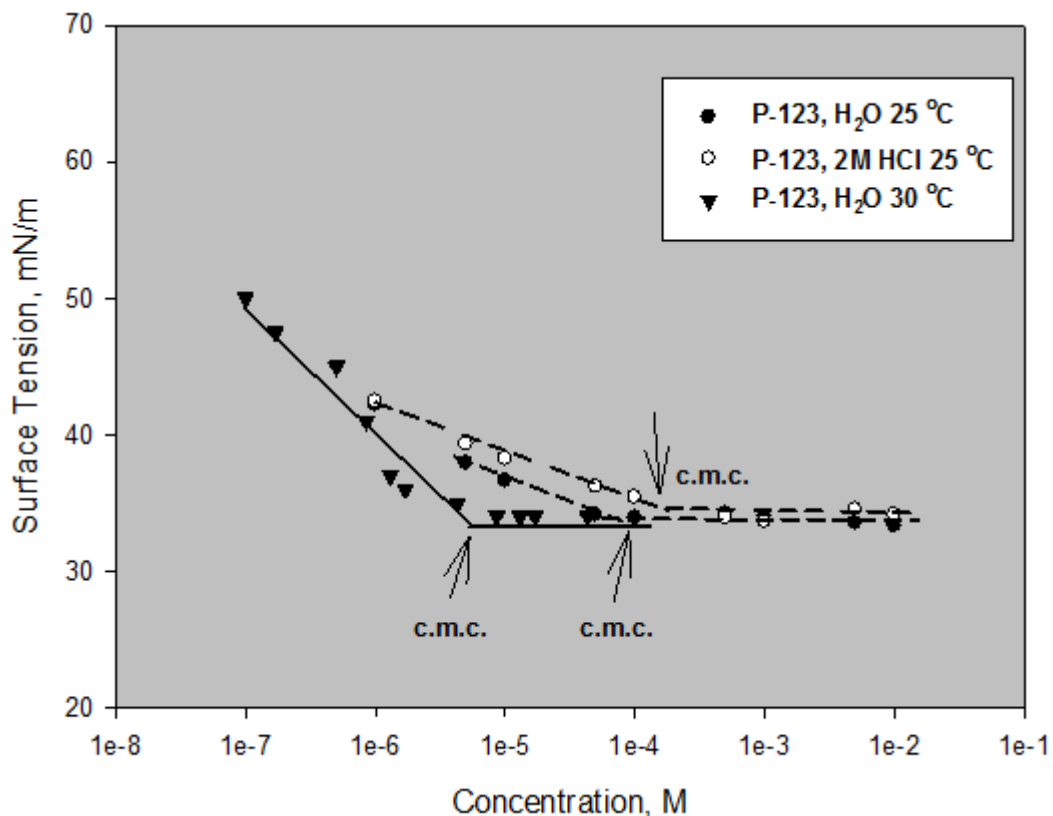


Figure 4.3. Surface tension vs concentration of P-123 solutions

As shown in Figure 4.4., ionic surfactants are not significantly affected by change in temperature. On the other hand, the solvent which forms the solution medium is important in interfacial behaviours of the surfactants. In a study by Anderson et al. (1998) it was reported that the presence of methanol changes the micellization behaviour of CTAB. They found that the increasing concentration of methanol causes an increase in c.m.c. of CTAB in aqueous solution. The effect of dipole of the surfactant decreases due to the low dielectric constant of methanol. Thus, the entropy of mixing of surfactant becomes larger than the entropy of mixing micelles. When the methanol percentage in aqueous solution reached 60 wt%, the c.m.c. of CTAB became $\sim 5.5 \times 10^{-2}$ M, which is higher than c.m.c. in pure water at the same temperature. Tunçay and

Göktürk (1997) investigated the effect of the presence of ethanol on micellization of CTAB. The results revealed that at low concentrations, c.m.c. of CTAB increased as the ethanol percentage in solution increased. However, at ethanol percentages above 15 % by volume, the presence of alcohol was totally inhibitory.

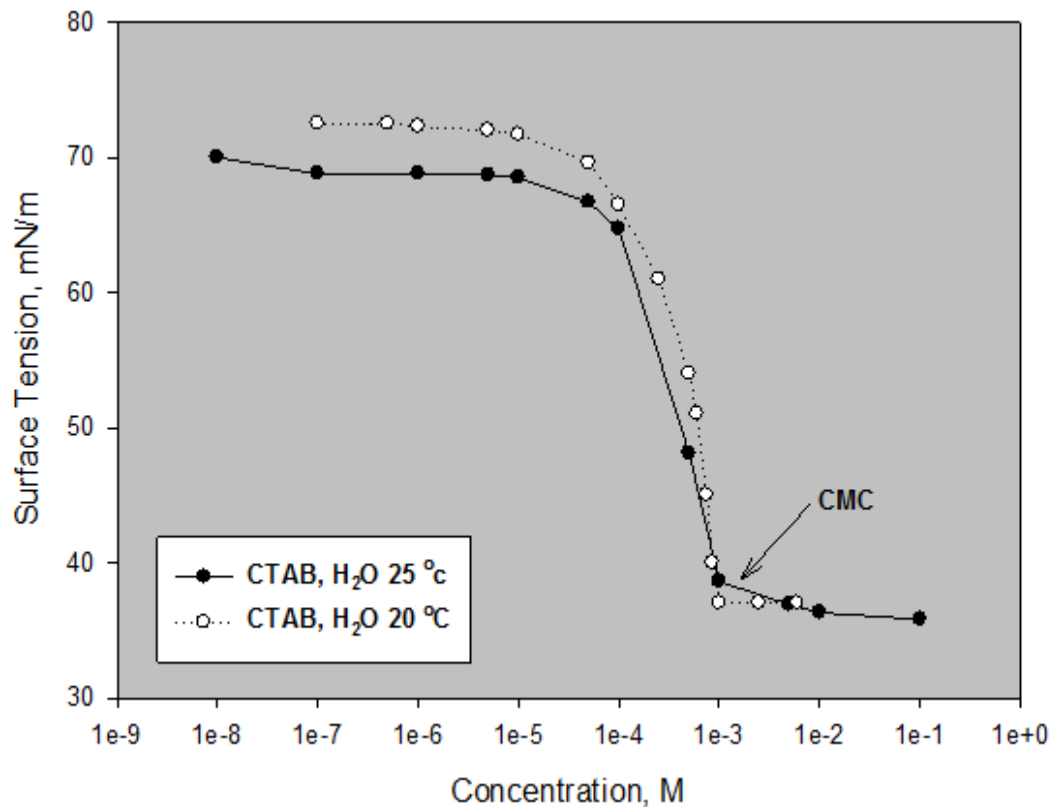


Figure 4.4. Surface tension vs concentration of CTAB solutions

4.2. Shape and Size of Surfactant Micelles

4.2.1. Shape of Surfactant Micelles

It is well known that the major types of micelles are a) relatively small spherical structures (aggregation number < 100), b) cylindrical, rodlike micelles, c) large, lamellar micelles, and d) vesicles. In the case of ionic micelles, the region of aqueous medium-micelle interface contains the ionic head groups, the Stern layer of the electrical double layer with the counterions and water. The remaining counterions are present in the Gouy-Chapman portion of the double layer which extends into the

solution. For the nonionic pluronic surfactants, the outer region contains no counterions but includes coils of hydrated PEO chains.

The critical packing parameter depending on the volume of the hydrophobic part of the surfactant, the cross-sectional area of the hydrophilic head group and the length of the hydrophobic segment can be used to determine the shape of the micelle. In the case of P123, spherical micelles are formed at room temperature due to high hydration ability of PEO segments (Sakai et al., 2011). However, the packing parameter is affected significantly by the electrolyte content, temperature, pH change, and the presence of additives in the system. In the presence of salt, a reduction in the hydration of PEO segment occurs, the effective volume of the hydrophilic part and a_0 significantly decrease, causing the increase in the critical packing parameter. As a result, the transition from spheres to rodlike micelles occurs.

This phenomena is valid for the ionic surfactants, as well. Although the micelles of the common surfactants are usually spherical above their c.m.c., their size and shape can be easily altered by the changes in experimental conditions. The presence of counterions in aqueous medium may suppress the micellar charge and lower the surface area per surfactant molecule by reducing the electrostatic repulsion between the head groups of the surfactant. Therefore, the transition from spherical to wormlike micelles is promoted. Moreover, the change in aggregation number resulting from the varying temperature or surfactant concentration may be attributed to explain the micellar behaviour in solutions.

Table 4.1. Area of the surfactant head group (a_0), volume (V) and length (l) of the hydrophobic part, surfactant packing parameter (SPP) and micelle shape (Source: Macakova et al., 2007; Nomura et al., 2000; Jian et al., 2009)

Surfactant	a_0 (nm ²)	l (nm)	V (nm ³)	SPP	Micelle shape
CTAB	0.650	2.174	0.458	0.324	spherical
CTAC	0.627	2.174	0.458	0.336	spherical
SDS	0.663	1.668	0.350	0.316	spherical

As shown in Table 4.1., ionic surfactants form spherical micelles above c.m.c. at moderate concentrations ($\sim 10^{-3}$ - 10^{-2} M). The SPP values were calculated by using the

theory developed by Israelachvili et al. (1976). To find the volume and the length of the hydrocarbon chain, the number of carbon atoms were taken as 16, 16 and 12 for CTAB, CTAC and SDS, respectively. As the surfactant concentration increases, the micelle transition from spherical to cylindrical or ellipsoidal shape may take place.

4.2.2. Size of Surfactant Micelles

In Figure 4.5., the extended molecular length of the surfactants is illustrated. Although the micelle form is different from the extended chain, P123 triblock copolymer is longer than the other ionic surfactants. As mentioned before, P123 surfactants form micelles whose core contains hydrophobic PPO segments while hydrophilic PEO tails are extended towards the aqueous phase. Therefore, the length of a P123 micelle is shorter than the molecular chain length of the surfactant.

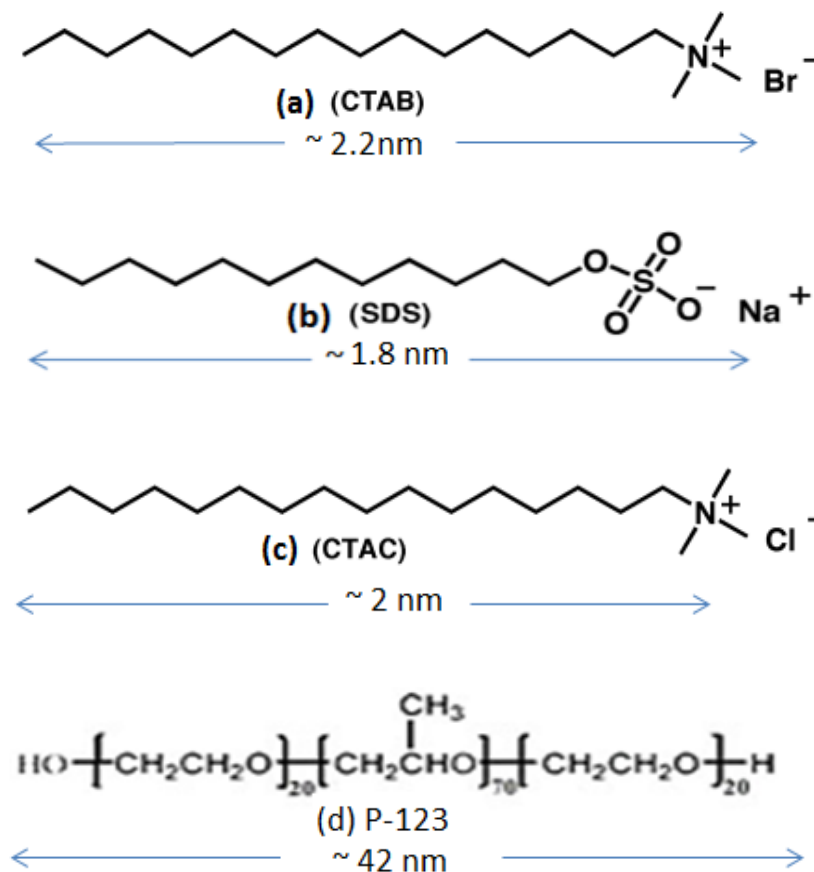


Figure 4.5. Molecular lengths of the surfactants : a) CTAB, b) SDS, c) CTAC, d) P-123 (Source: a) Wei et al., 2005; b) Zuev et al., 2007; c) Hirashima et al., 2001; d) Dutreilh-Colas et al., 2008).

For ionic surfactants, the radius of the interior region of the micelle formed by the hydrophobic groups is almost equal to the length of the extended hydrocarbon chain. The aqueous phase penetrates into the micelle beyond the hydrophilic head groups, and the first few methylene of the hydrocarbon chain bounded to the head group is present in the hydration sphere.

The micelle sizes of the selected surfactants in aqueous solution at 25 °C are shown in Figure 4.6 a-d . Under these conditions, the sizes of micelles were found by using DLS as 4.31 nm, 5.10 nm, 3.80 nm and 12.90 nm for CTAB, CTAC, SDS and P-123 surfactants, respectively. These values almost agree with the ones reported in literature (Singh et al., 2004; Goyal and Aswal, 2006; Duplatre et al., 1996; Adhikari et al., 2008).

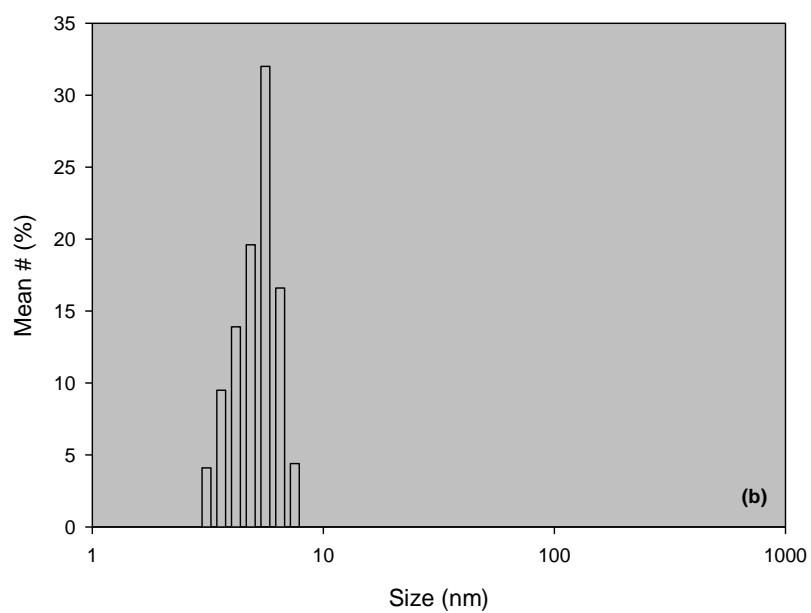
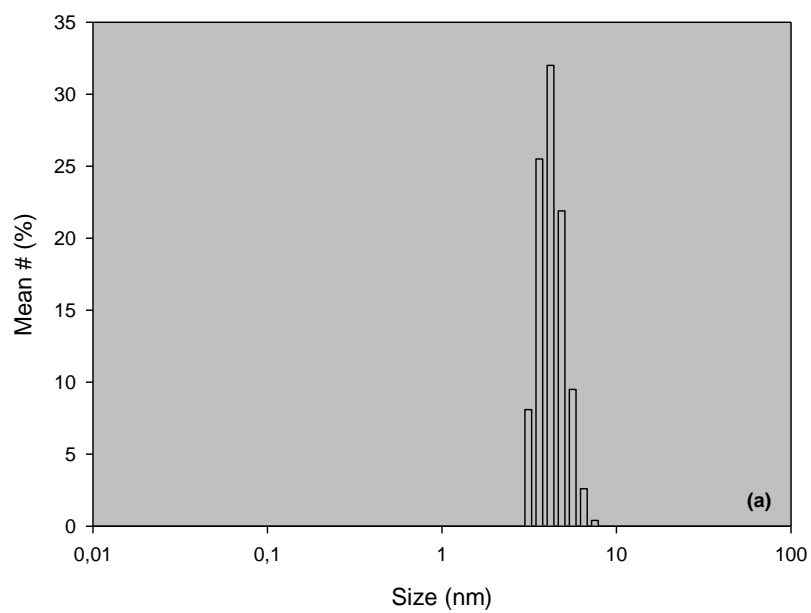


Figure 4.6. DLS measurements of the micelle solutions: a) CTAB, b) CTAC, c) SDS, and d) P-123 (Surfactant concentration: 10^{-2} M in H_2O at $25\text{ }^{\circ}C$)

(Cont. on next page)

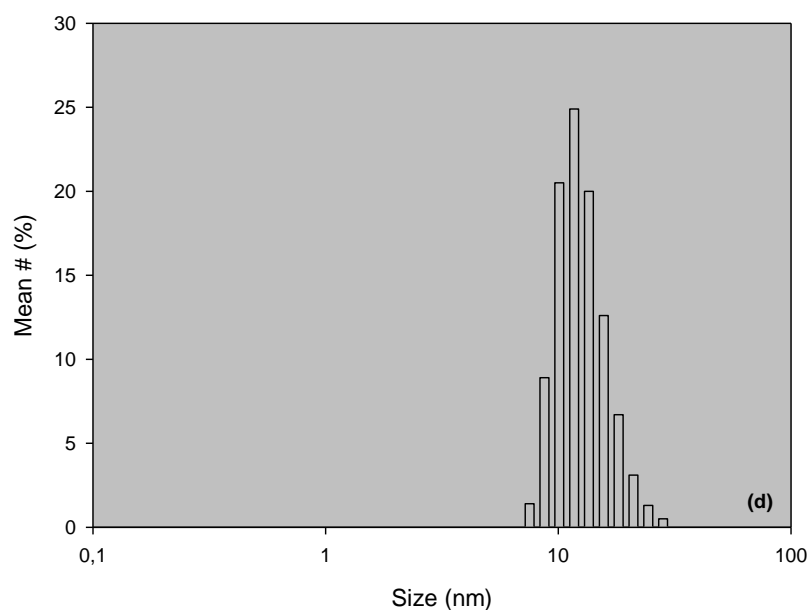
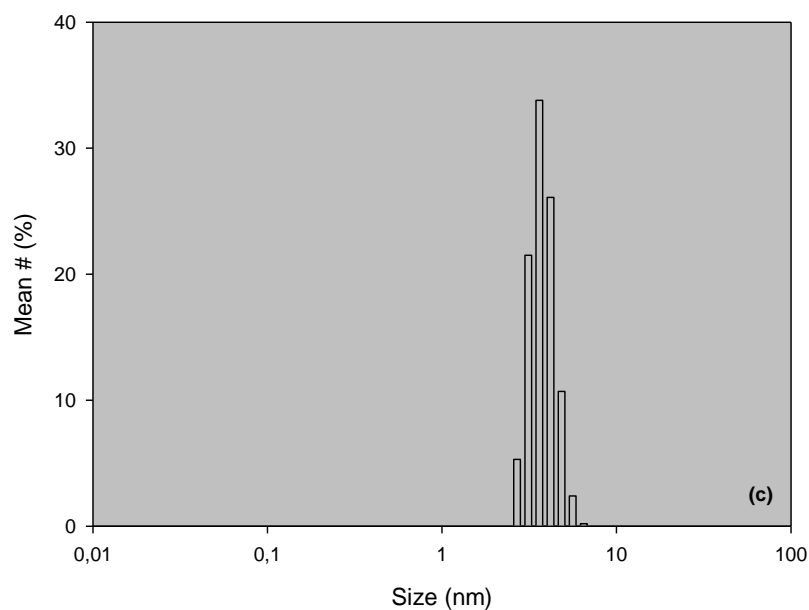


Figure 4.6. (cont.)

In Figure 4.7-10, TEM images of the selected surfactants with various concentrations in dispersion medium are shown. The ellipsoidal and spherical shape of their micelles can be easily seen from the images. Moreover, the reported values for the size of their micelles agree well with each other (Table 4.2.). Table 4.2 compares the sizes of micelles obtained from DLS measurements with other techniques.

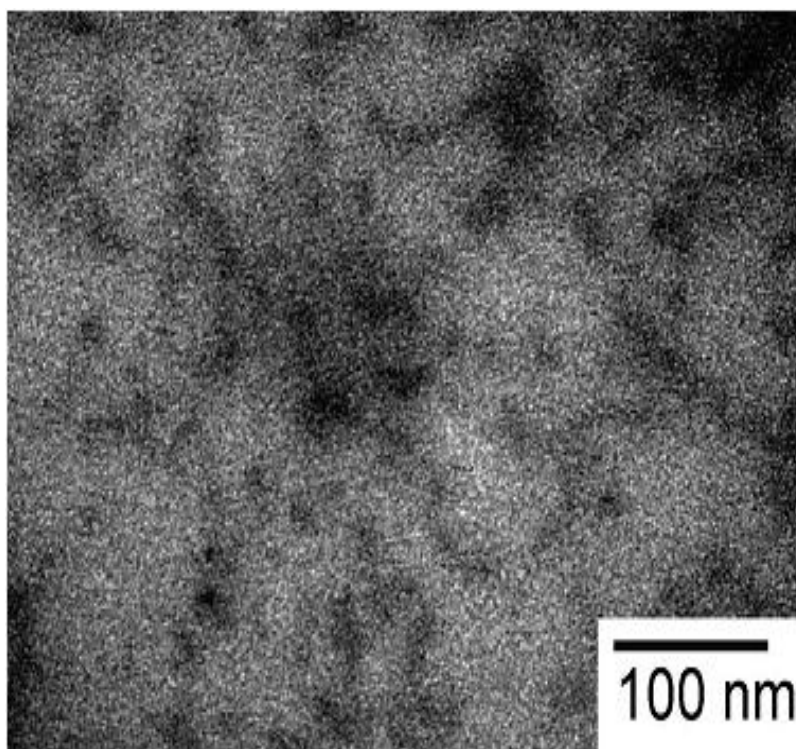


Figure 4.7. TEM image of P123 micelles (10^{-4} M)
(Source: Mandal et al., 2012)

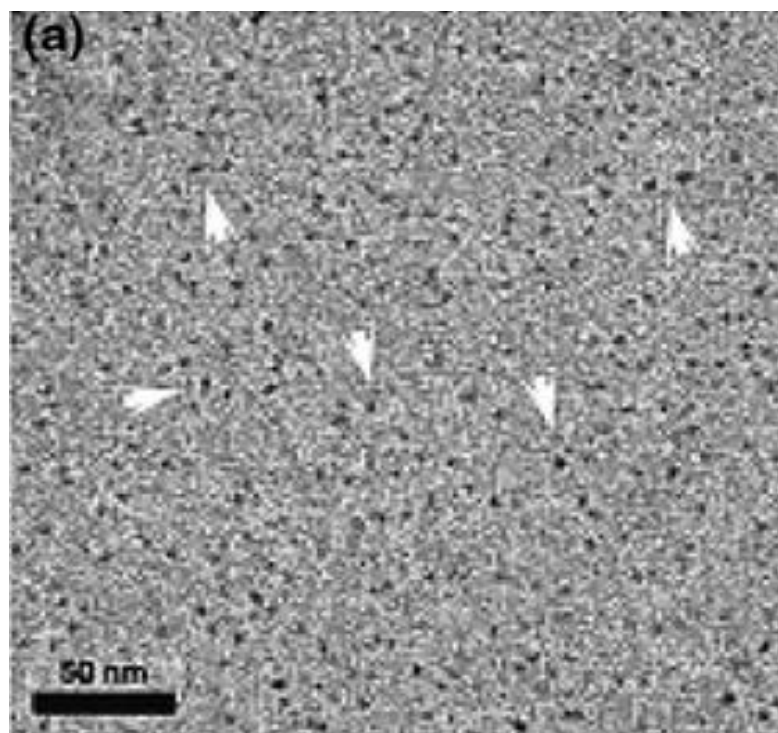


Figure 4.8. TEM image of CTAB micelles (10^{-2} M)
(Source: Kuperkar et al., 2010)

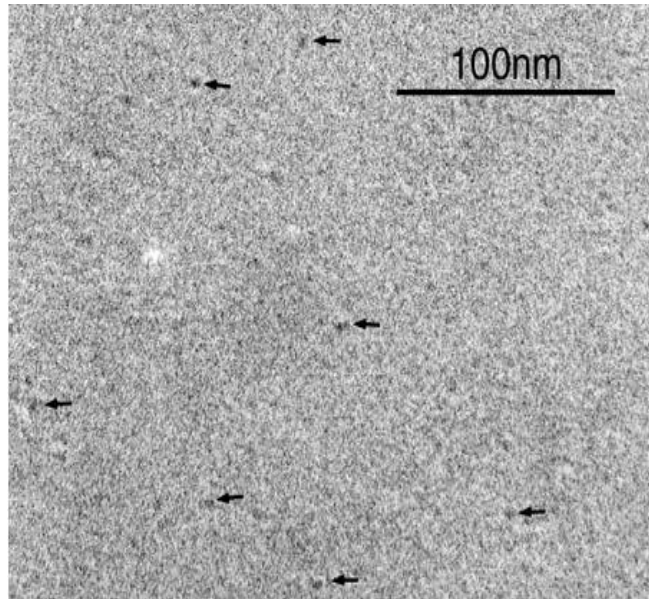


Figure 4.9. TEM image of SDS micelles (10⁻¹ M)
(Source: Hahakura et al., 2002)

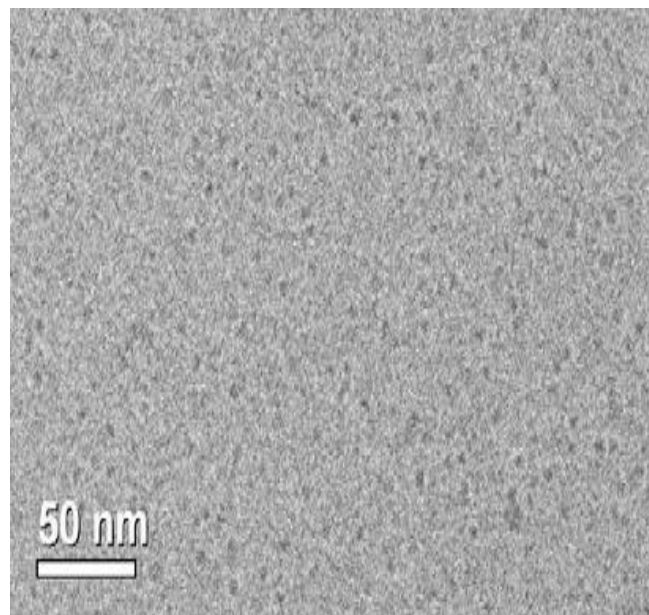


Figure 4.10. TEM images of CTAC micelles (10⁻² M)
(Source: Ge et al., 2008)

Table 4.2. Micelle size measurements by different techniques
 (Source: Singh et al., 2009; Chatterjee et al., 2005; Kuperkar et al., 2010; Mondol et al., 2012; Goyal and Aswal, 2006; Duplatre et al., 1996; Hassan et al., 2003; Adhikari et al., 2008)

Surfactant	SAXS/SANS (nm)	TEM (nm)	DLS (nm)
CTAB	6.0	6.0-8.0	6.5
CTAC	5.0	5.0	5.1
SDS	3.6	2.0	3.5-3.6
P123	18.0	20.0	18.0

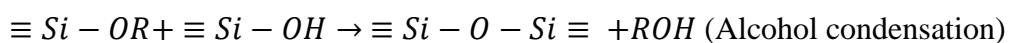
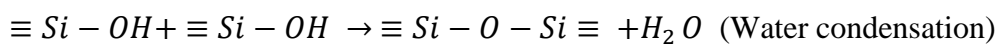
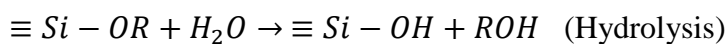
4.3. Synthesis of Silica Nanoparticles

To obtain the desired particle morphology, different types of silica nanoparticles were synthesized. These studies aimed the formation of porous silica structures in acidic or basic conditions, where ionic and nonionic surfactants were used as templates.

4.3.1. Base Catalysed Methods

In the case of base catalysed methods, by using the sol-gel phenomena and background of this type of synthesis, the formation of monodispersesilica nanoparticles were attempted. To create nanosized particles with monodispersity in both size and shape, a first well-known base catalyzed sol-gel method with novel modifications was applied, leading to the formation of BC-1 particles. The particles obtained by base catalyzed sol-gel method are monodisperse, as small as sub-100 nm in size and nonporous. On the other hand, the use of surfactants as template structures was aimed to form porous nanoparticles (BC-2). This synthesis pathway contained the use of a cationic surfactant, CTAB, as micellar template.

The reactions which take place during the synthesis of silica nanoparticles are:



where OR is an alkoxy group, most often a methoxy or ethoxy derivative. Hydrolysis under basic conditions can be defined by several steps : Nucleophilic hydroxyl ions are produced by dissociation of water in a rapid first step, the reaction of NH_3 with H_2O . Then, the hydroxyl ion attacks the silicon atom with displacement of RO^- . The rate limiting step of the complete hydrolysis of alkyl orthosilicate (i.e. TEOS) can be considered as the removal of the first alkyl group because of the electron withdrawing characteristic of the attached hydroxide group (Brinker and Scherer, 1990). The hydrolysis appears to be the first order in TEOS (van Blaaderen and Vrij, 2006).

The most widely accepted mechanism for condensation reactions include the following steps: First, the silanol which is more acidic than an alcohol, is deprotonated by RO^- and silanolate is produced. Then, the attack of silanolate on either an alkoxy silane (alcohol condensation) or a silanol molecule (water condensation) gives Si-O-Si bond.

In fact, the exact mechanism of silica formation which is called Stöber silica, is complex to understand. As mentioned above, TEOS reacts with water to form silicic acid, which then polymerizes and condenses to form spherical, monodisperse particles under suitable conditions (Lee, 2007). However, it is not clear whether the silicic acid and their derivatives directly diffuse to the surface of the growing particles or the silicic acid first nucleates into smaller particles, which then diffuse to the particle surface, resulting the aggregates because of van der Waals forces. Therefore, several models were suggested to explain the mechanism of the formation of these nanostructures. The first is the monomer addition growth model which is based on the nucleation upon exceeding the supersaturation limit and the growth of nucleus by condensation of monomeric silicic acid on the surface of nuclei (LaMer and Dinegar, 1950; Matsoukas and Gulari, 1989). This model is mainly focused on the hydrolysis and condensation rate and the solubility of silicic acid. In classical LaMer model, the monomer concentration is related to the reaction time as shown in Figure 4.11. Once the reaction starts, as the result of hydrolysis reactions, the concentration of monomer, which is hydrolyzed TEOS for this synthesis, increases with reaction time. In this model, the hydrolysis of TEOS is described as the rate determining step. It is a first order reaction in alkoxide and can be accelerated by the increase in ammonia concentration. Although the monomer concentration continues to increase and reaches at the supersaturation region by exceeding the saturated solubility ($[\text{monomer}]_{\text{solubility}}$), solid deposition does not start even at this stage. In a homogeneous nucleation system, where no nuclei or

particles are present initially, an energy barrier should be exceeded for nuclei formation. To exceed this barrier, monomer concentration should be higher than a critical value called critical supersaturation concentration or $[\text{monomer}]_{\text{nucleation}}$. When this is achieved, the nucleation process starts and monomers can either react with each other to form new nuclei or are added to the surface of existing nuclei to lead the growth of these nuclei. Due to the consumption of monomer for the nucleation and growth, the increase in the monomer concentration levels off and starts to follow a downward tendency. When the monomer concentration reduces below the critical supersaturation limit, nucleation process stops and only particle growth continues by the addition of monomers to nuclei surfaces until the saturated solubility.

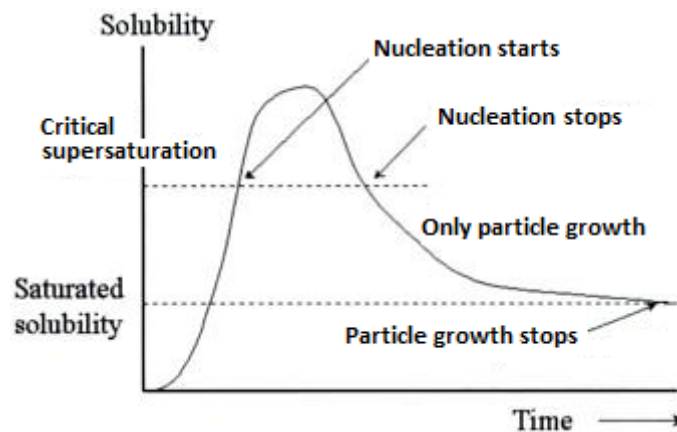


Figure 4.11. LaMer model of nucleation and particle growth
(Source: Waseda and Muramatsu, 2003)

The second model explains the nucleation and growth of Stöber particles by a controlled aggregation mechanism of small particles (Bogush and Zukoski, 1992). This model assumes that nanosized silica nuclei are created continuously during the hydrolysis and condensation of TEOS. Due to the instability of these colloidal nuclei, they coagulate and form larger particles. When their size reach above a critical limit, they become stable. Then, these relatively larger stable colloids diffuse through the solution aggregating with unstable colloids which nucleate continuously. As the colloids grow, they seek to minimize their free energy by associating with the solid particles. Thus, addition of these subsequent small nuclei to the existing particle surface of the aggregates leads to further growth. In this model, monodispersity of the final particles is obtained through size-dependent aggregation rates which means that the probability of

aggregation between the two particles of the same size decreases while the particles grow. Moreover, the size and the number of the particles depend not only on reaction kinetics but also several parameters which affect the solution stability such as ionic strength of the medium, temperature, surface charge of the particle, pH and solvent properties. Among these, the aggregation process is mainly influenced by the surface potential of the silica particles and by changing the particle interaction potential, without affecting the rates of reactions taking place in solution, monodisperse particles of different sizes can be obtained. The main inference of this approach is that the focus should be on the interaction between the particles, especially small particles, rather than the length of nucleation period. In such an aggregation model, nanosized nuclei with large interfacial areas become easily aggregated due to the high interfacial tension between the particle and solution. Therefore, small particles continue to grow to a critical size, reducing the interfacial area and the overall free energy (Stöber et al., 1968).

In addition to these approaches, Stöber silica particles may very well be first formed from nanosized subunits obeying the controlled aggregation model and then the monomer addition mechanism may be valid for the formation of final particles. Giesche (1994), Harris et al. (1990) and van Blaaderen and Vrij(2006) proposed this type of formation mechanism, depending significantly on the overall reaction conditions. Giesche (2000) suggested that this situation may be valid when the concentration of reactive silica in solution decreased and the overall reaction rate becomes much slower than that at the beginning of the reaction. As expected, a slower reaction rate favors the monomer addition mechanism at later stages.

4.3.1.1. Synthesis of BC-I Particles

BC-I particles were synthesized in ethanol solution in the absence and presence of surfactants and compounds such as CTAB, CTAC, SDS, P-123 and APTS and TEAB. Both the effect of surfactant type and concentration were tested. SEM images were used to observe the differences in size and shape of silica particles. The SEM pictures of TEAB, CTAC, CTAB, SDS, P-123 and APTS at different concentrations are presented in Figure 4.12-4.17, respectively. While Figures 4.18 and 4.19 gives the SEM pictures of all the surfactants tested together at a fixed concentration of 10^{-2} M.

These results were also summarized in Tables 4.3 and 4.4. Figure 4.20 also gives the SEM image of BC-1 particles synthesized in the absence of surfactant. As it is seen from the results that there is a significant effect of both surfactant type and concentration. Increasing surfactant concentration except P-123 increased the size of silica particles. The shape of particles on the other hand was always spherical. The dispersion of particles also changed depending on surfactant type. It seems that one of the cationic surfactants, CTAB causes an agglomeration of particles.

In this method where the medium is alcohol, the formation of silica particles are most probably in the water droplets stabilized by surfactants in alcohol. That is water and ethanol mixture form micro emulsions and water droplets dispersed in ethanol as a separate phase in the presence of surfactants. These structures may also called reverse micelles. Under the conditions of synthesis, surfactants are expected to be single monomers at all the concentrations due to dispersion medium (alcohol) and help to stabilize the water droplets. Since the effect of surfactant type and concentration on the emulsification of water in alcohol is different, their effect on the size of silica particles produced is expected to be different. This production model helps to explain the effect of surfactant type and concentration on the size and shape of silica particles. As it is seen from the results that the most effective surfactant as an emulsifier (Polat et al., 1999) P-123 (larger molecular weight), is the most effective surfactant to produce small particles.

The charge of surfactants seems to be important to affect the stability of particles produced. Anionic surfactants are expected to have no attraction for silica surfaces due to their negative surface charge. In this case, surface of particles produced will have no surfactant molecules adsorbed that sticks its hydrophobic part out. Therefore there will be no interaction between particles due to hydrophobic attraction. However, the presence of counterions (such as Na^+ in the case of SDS) may also be important at high concentrations of surfactant due to expected increase in the ionic strength of the system and compressed electrical double layer around the particle.

Thus, the concentration of counter ions may affect the aggregation rate and behaviour of the particles. As shown in Figure 4.15., the silica particles synthesized in the presence of SDS molecules have high monodispersity. This could be explained by the fact that while the ionic strength allows for the growth of particles, the surfactant molecules also provide a steric barrier for the relatively large particles and prevent their

aggregation. Although this is valid for the particles with a critical size, increasing surfactant concentration continues to cause the aggregation until the critical limit.

So, low concentrations of anionic surfactant, SDS, may have little effect on colloidal silica particles due to the weak interactions between the negatively charged silica surfaces and the negative surfactant molecules. At 10^{-5} M, the BC-1 particles do not seem to be affected by the presence of surfactants. When compared with no surfactant case, the final particle size is almost the same (160-170 nm). At 10^{-3} M, the particles become slightly larger (~210 nm) due to low surface coverage for hydrophobic interactions of particle surfaces. At 10^{-2} M, however, the effect of surfactant is significant (See SEM images). This result aligns with the proposed production model here. The result of P-123 also support the proposed model. In this case, the particle size did not change with concentration due to the lack of the interaction between the uncharged surfactant molecules and charged surface and agglomeration.

In the case of other compounds (without surface activity), such as TEAB and APTS, similar type of results were observed. The presence of these compounds changed the particlesize and dispersity. This may result from the change in the rates of nucleation and growthprocesses when they are added into the dispersion medium, in which TEOS is present, due to the differences in the hydrolysis and condensation rates of these compounds.

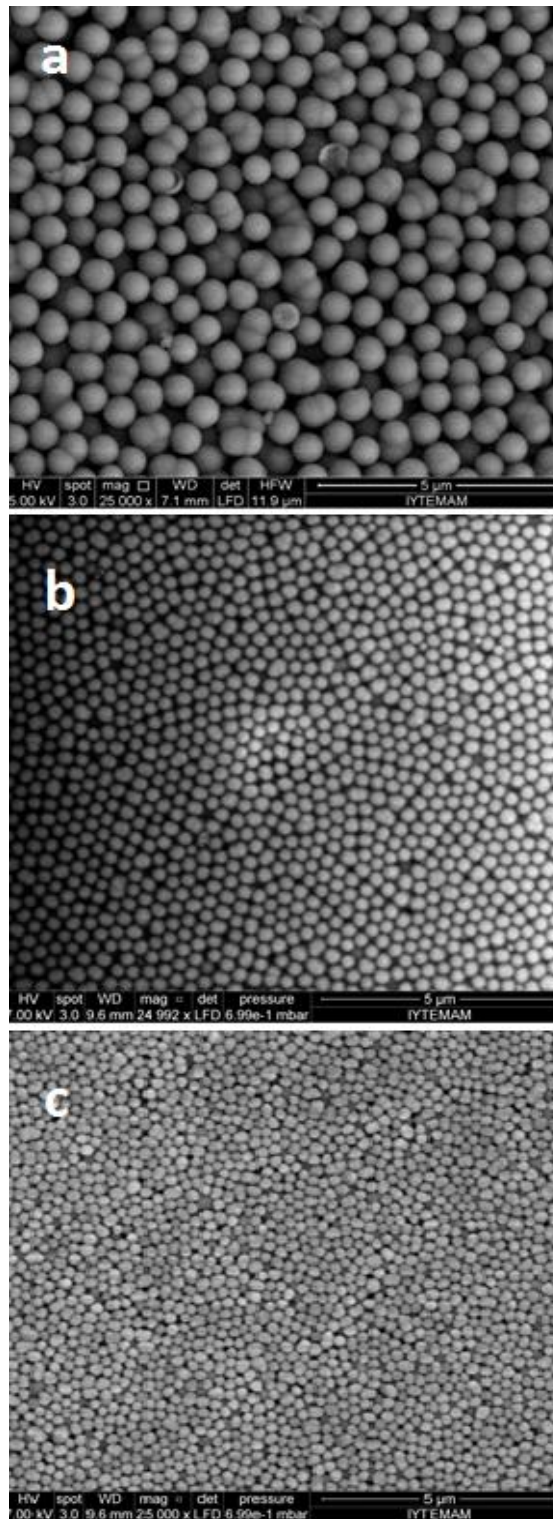


Figure 4.12. SEM images of BC-1 particles in the presence of TEAB (Concentration of TEAB : 10^{-2} M (a), 10^{-3} M (b), 10^{-5} M (c))

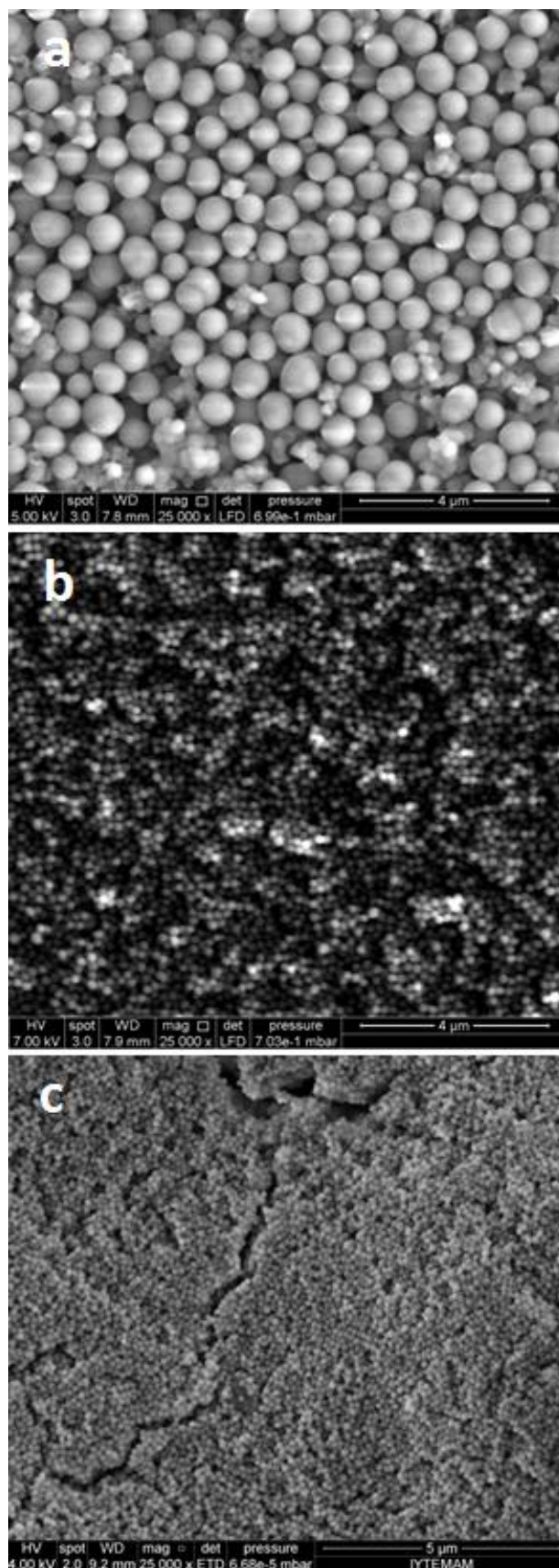


Figure 4.13. SEM images of BC-1 particles in the presence of CTAC (Concentration of CTAC : 10^{-2} M (a), 10^{-3} M (b), 10^{-5} M (c))

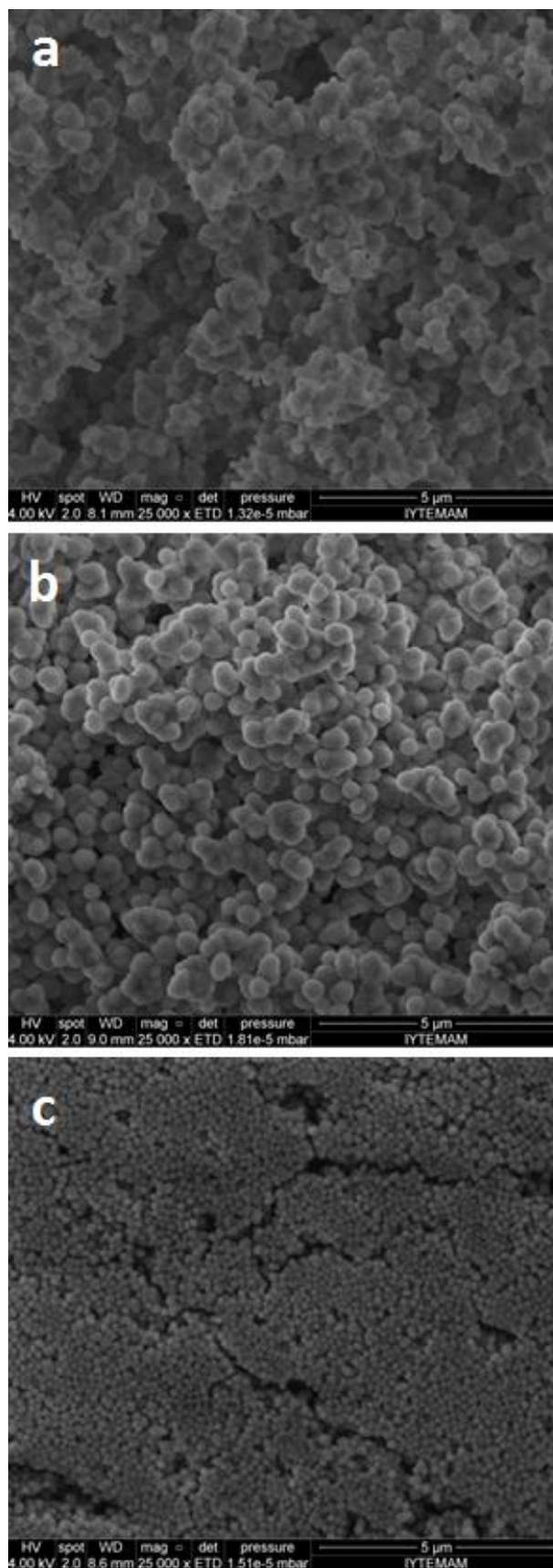


Figure 4.14. SEM images of BC-1 particles in the presence of CTAB (Concentration of CTAB : 10^{-2} M (a), 10^{-3} M (b), 10^{-5} M (c))

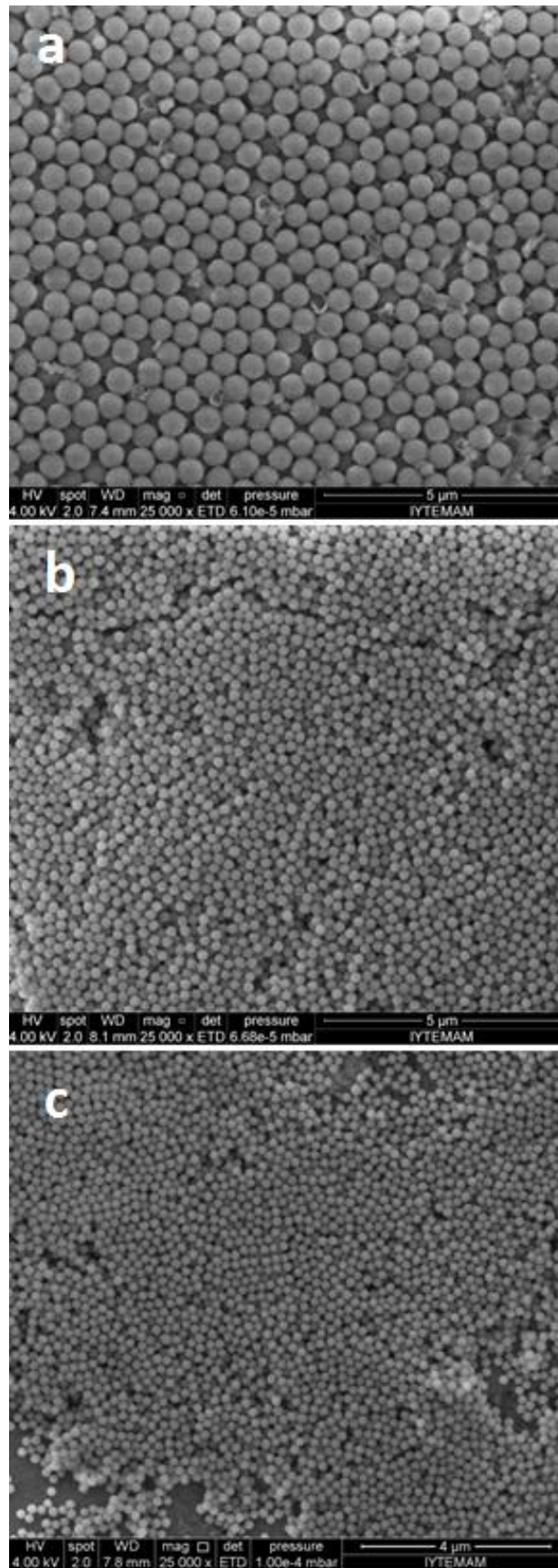


Figure 4.15. SEM images of BC-1 particles in the presence of SDS (Concentration of SDS : 10^{-2} M (a), 10^{-3} M (b), 10^{-5} M (c))

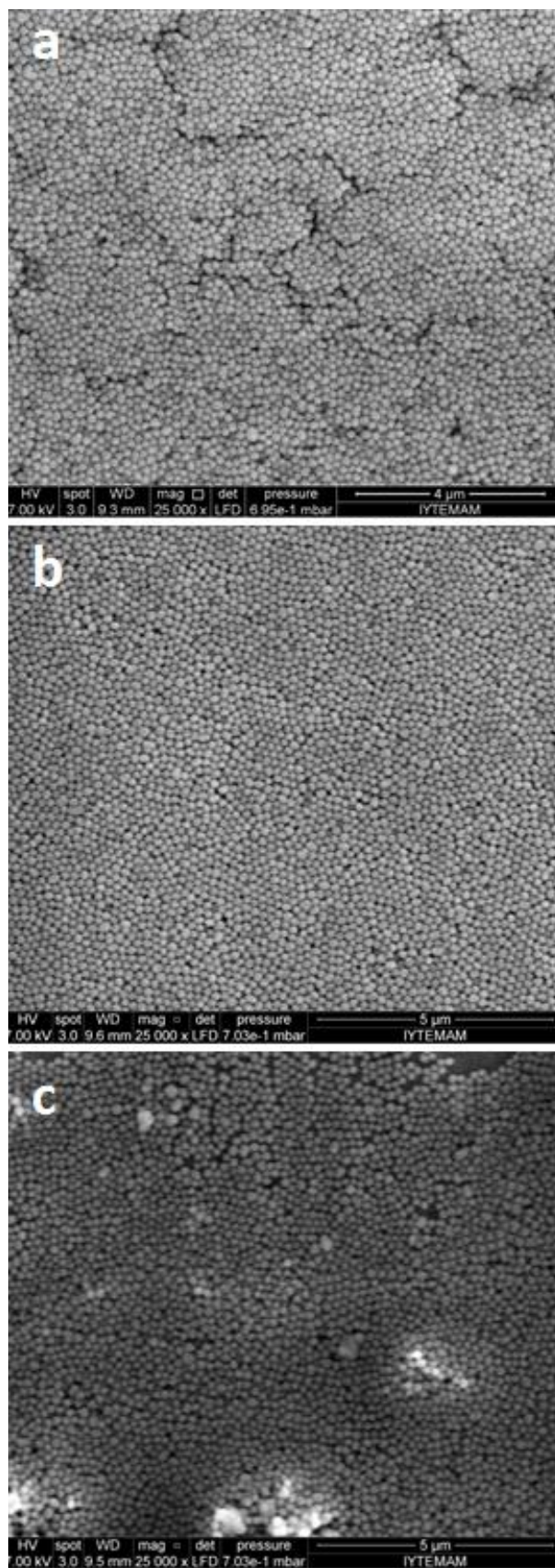


Figure 4.16. SEM images of BC-1 particles in the presence of P-123 (Concentration of P-123 : 10^{-2} M (a), 10^{-3} M (b), 10^{-5} M (c))

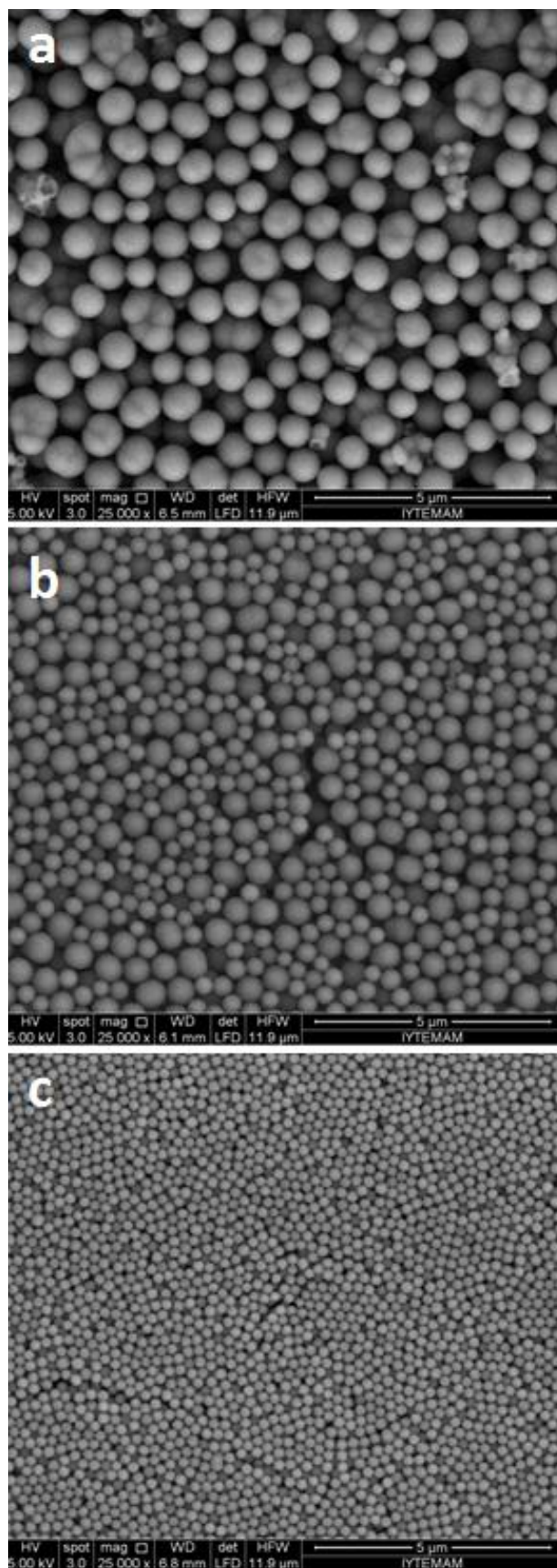


Figure 4.17. SEM images of BC-1 particles in the presence of APTS (Concentration of APTS : 10^{-2} M (a), 10^{-3} M (b), 10^{-5} M (c))

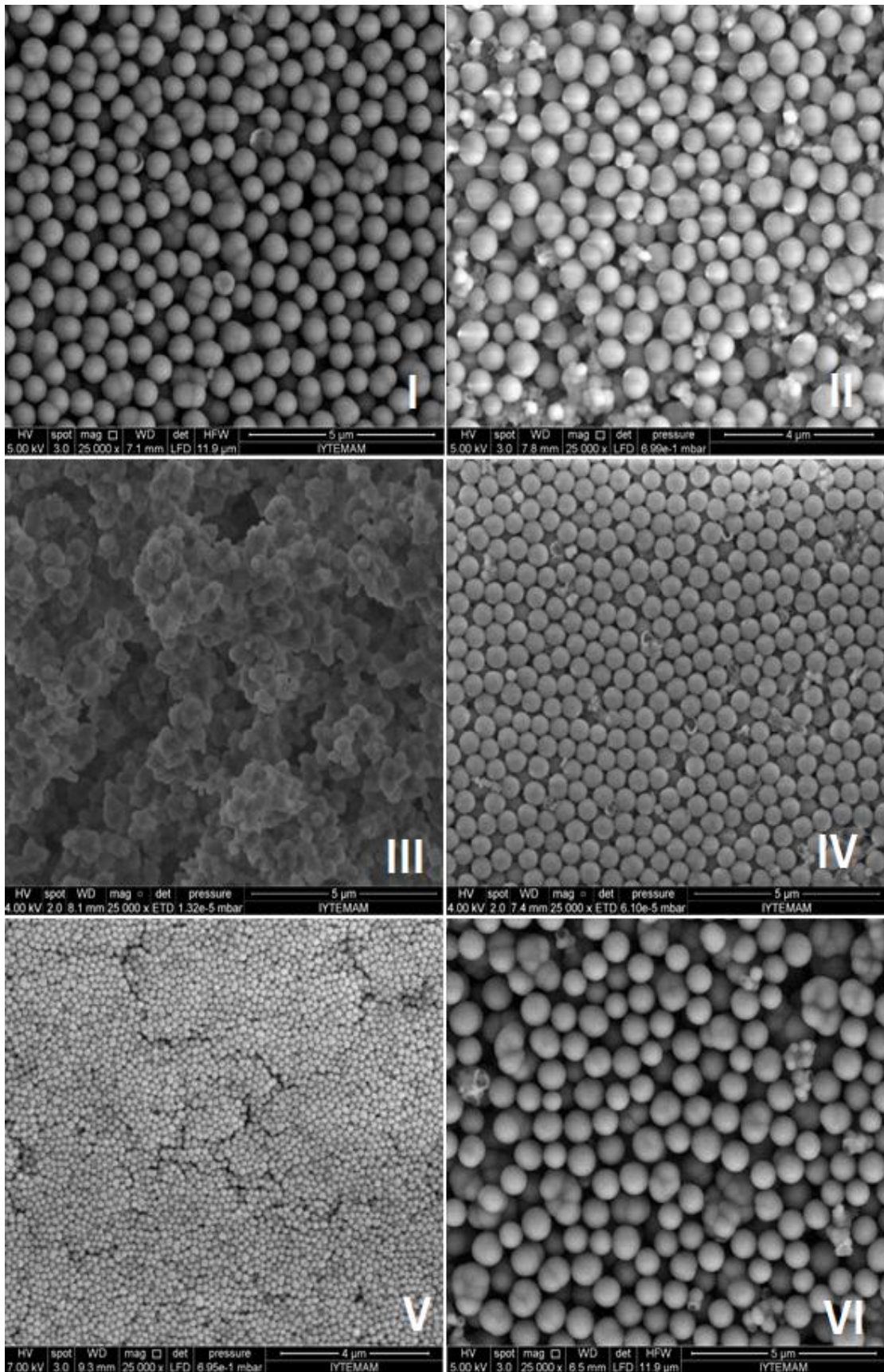


Figure 4.18. SEM images of BC-1 particles including surfactants (10^{-2} M) in dispersion medium (I: TEAB, II: CTAC, III: CTAB, IV: SDS, V: P-123, VI: APTS)

Table 4.3. Average particle sizes of BC-1 Particles (Additive Concentration: 10⁻² M) from SEM images

Surfactant	Ave. particle size (nm)	Std. Deviation (nm)
TEAB	571.08	40.00
CTAC	602.87	35.36
SDS	491.12	57.51
APTS	651.43	50.12
P-123	133.64	15.66
CTAB	- (Agglomeration)	-
None	161.05	15.46

Table 4.4. Average particle sizes of BC-1 Particles at varying additive concentrations from SEM images

Surfactant\Conc.	Average particle size obtained from SEM images (nm)		
	10 ⁻² M	10 ⁻³ M	10 ⁻⁵ M
TEAB	571.08 (40.00)	322.34 (34.27)	232.18 (21.45)
CTAC	602.87 (35.36)	125.01 (11.43)	119.83 (10.08)
SDS	491.12 (57.51)	208.22 (12.89)	174.28 (13.21)
APTS	651.43 (50.12)	402.06 (100.16)	220.57 (10.12)
P-123	133.64 (15.66)	130.25 (13.25)	126.54 (10.64)
CTAB	- (Agglomeration)	393.85 (35.18)	145.41 (16.04)

* The values in the paranthesis indicate the standard deviation in size measurements

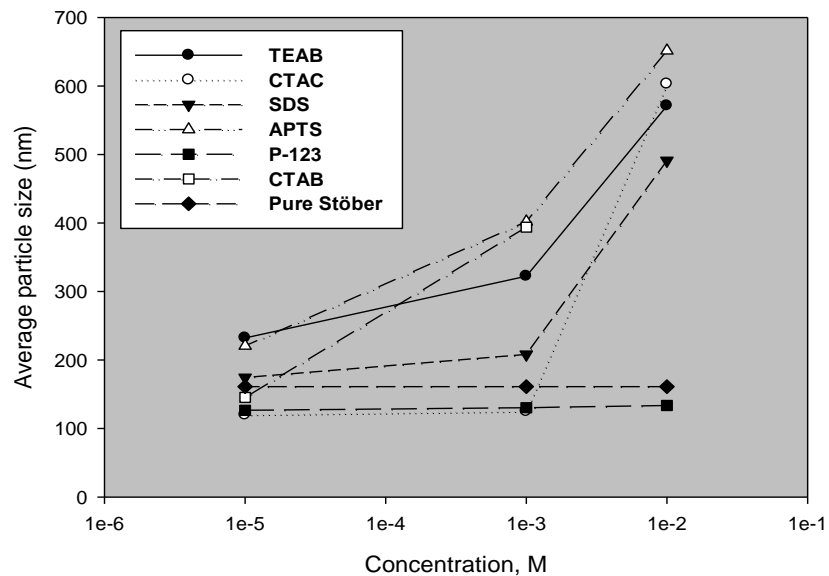


Figure 4.19. Average particle size obtained from SEM images vs surfactant concentration in dispersion medium

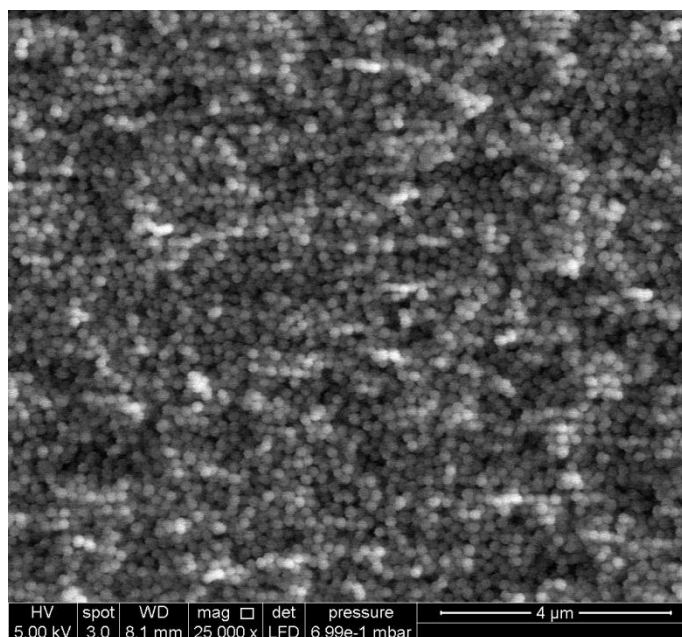


Figure 4.20. SEM image of BC-1 particle synthesized in the absence surfactant

In contrast to the effect of anionic SDS and unlike the other cationic surfactants, the colloidal silica particles showed low monodispersity in the presence of a cationic surfactant, CTAB only. In this method, the aggregation of silica nanoparticles can be attributed to the electrostatic interactions between negatively charged silica surfaces and positively charged ions of surfactants, meaning partial neutralization of the surface charge, as well as of hydrophobic interactions between the hydrocarbon tail of surfactant molecules adsorbed on silica surface. However, the differences between cationic surfactants may be due to the different counter ions that they contain. Therefore the more detailed studies on the effects of surfactants especially cationics on the production of nano silica particles should be conducted to support the hypothesis presented in this study.

FTIR analysis of the silica particles were also conducted. For pure silica particles (no surfactant in production) (Figure 4.21 b), the spectrum in the range of 3800-2500 cm^{-1} is characterized by a peak centered at 3444 cm^{-1} , which can be attributed to the O-H stretching vibration of H-bond surface hydroxyls and water. Moreover, the shoulder band at 3650 cm^{-1} may be assigned to the O-H stretching mode of isolated surface silanol groups. In the region of 2000-800 cm^{-1} , the bands related to Si-O vibrations are present. The strongest band is present at 1104 cm^{-1} , which is mainly because of the asymmetric Si-O stretching mode of Si-O-Si bridge band. In addition, the bands with

lower intensities at 944 and 799 cm^{-1} can be attributed to the stretching vibrations of surface Si-O bonds.

For BC-1 particles synthesized in the presence of CTAB (Figure 4.21 a), the O-H stretching vibration band at 3444 cm^{-1} shifted to 3429 cm^{-1} , and surface Si-O vibration bands at 944 and 799 cm^{-1} also shifted by several wavenumbers and these changes indicate strong interactions between CTA^+ ions and SiO_2 surfaces.

In order to compare pure CTAB reagent and BC-1 particles, spectra of pure CTAB was also analyzed. The asymmetric stretching mode of the headgroup $\text{CH}_3\text{-(N}^+)$ is at 3017 cm^{-1} while at 2959 cm^{-1} , the asymmetric stretching mode of the CTAB terminal CH_3 group is present. However, in the case of BC-1, the peak at 3017 cm^{-1} disappeared, and the 2959 cm^{-1} band shifted to 2965 cm^{-1} (Figure 4.22). In the 1550-1400 cm^{-1} region of the same spectrum (Figure 4.23) the $\text{CH}_3\text{-(N}^+)$ asymmetric deformation mode at 1487 and 1473 cm^{-1} for pure CTAB shifted to 1490 and 1478 cm^{-1} for BC-1. These changes in spectrum demonstrate the strong interactions between the headgroups of CTAB and silica surface.

Zeta potential measurements also indicate the coagulation of BC-1 particles when CTAB was used as an additive. At 10^{-2} M CTAB, zeta potential value became zero, implying that the surface charge of silica was completely screened by the hydrophobic tail of CTAB. Therefore, the coagulation of these nanoparticles occurred.

The effect of ions was also observed under different salt concentrations. As expected, high concentration of ions leads to the agglomeration of particles due to the reduced repulsive interactions between particle surfaces. Thus, it promotes the particle growth and aggregation.

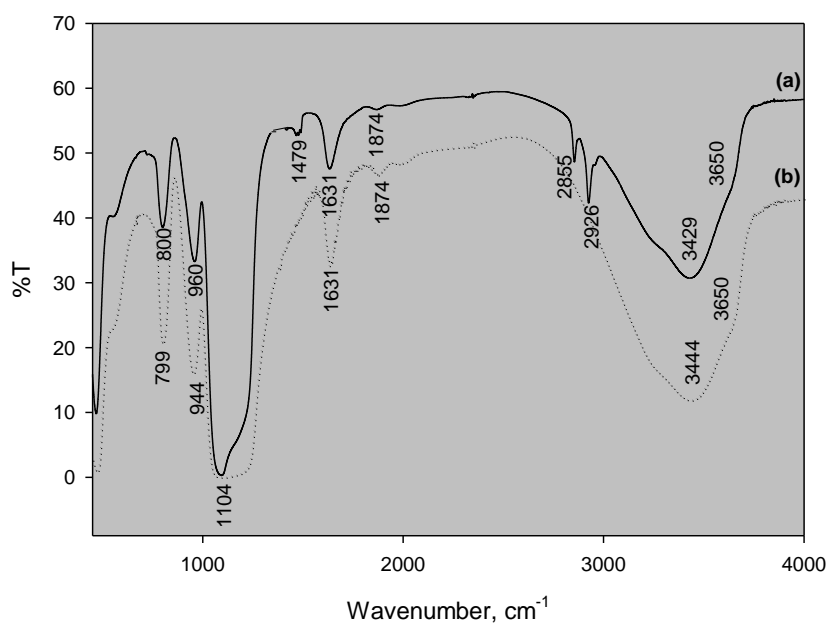


Figure 4.21. FTIR spectra of (a) BC-1 particles, (b) pure silica particles

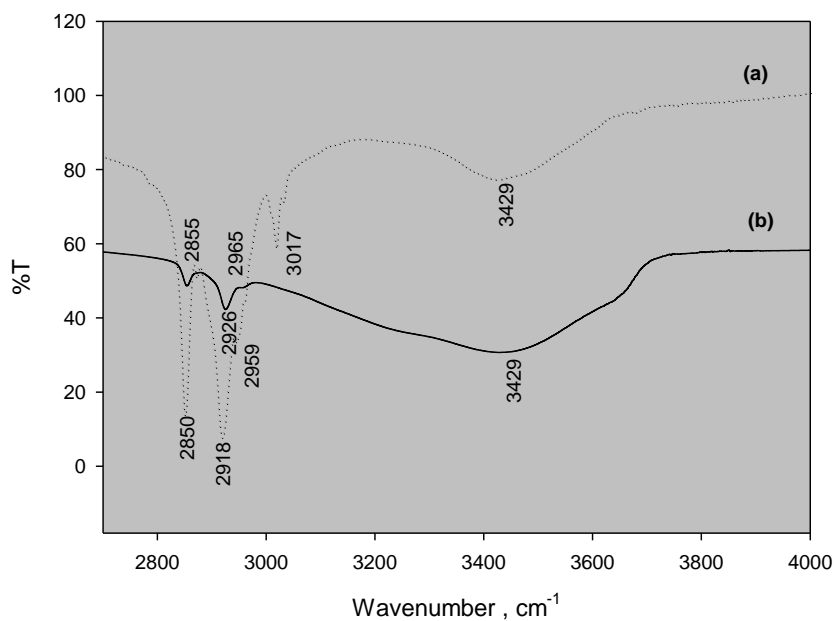


Figure 4.22. Expanded FTIR spectra of (a) pure CTAB reagent, (b) BC-1 particles at high frequencies

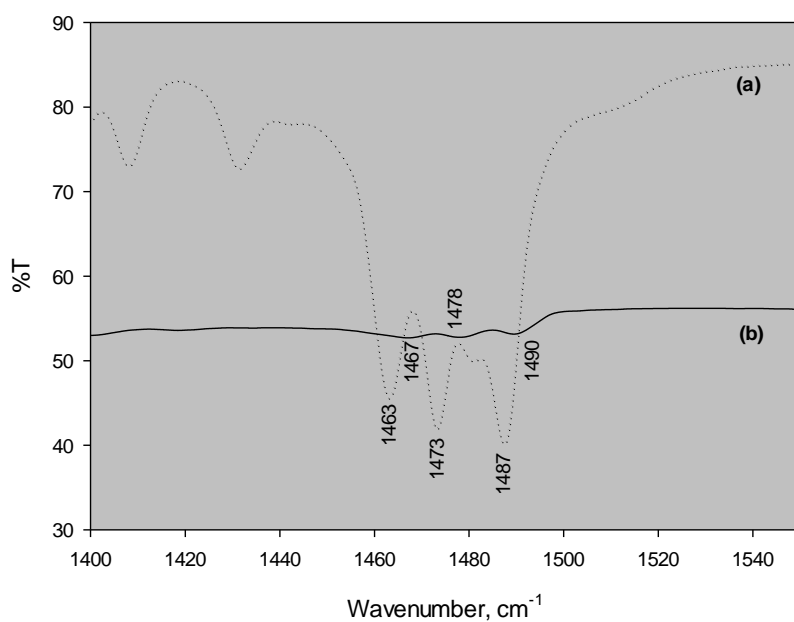


Figure 4.23. Expanded FTIR spectra of (a) pure CTAB reagent, (b) BC-1 particles at low frequencies

4.3.1.2. Synthesis of BC-2 Particles

These type of materials are called MCM-41. There have been several models which were suggested to explain the formation of MCM-41 type materials. Generally, these models are based on the formation of silica structure arised from the solubilized inorganic precursors in the presence of a cationic surfactant. The surfactant, which possess a hydrophilic head group and a hydrophobic tail, self-organizes to minimize the contact between its incomtable ends and the models focuses on how the silica precursor interacts with these surfactant molecules.

Mobile researchers proposed a “liquid crystal templating” (LCT) mechanism, which suggests two pathways in formation of silica mesostructures: 1) The liquid crystal phase exists before the addition of silica precursor and the silica precursor which occupies the space between the preexisting hexagonal liquid crystal phases deposites on the micellar rods, 2) The hexagonal arrangement of the surfactants is provided by the addition of silica precursor. In both cases, the negatively charged inorganic silicate species due to the high pH of the medium interact with the positively charged

ammonium head group of CTAB, leading to the condensation into a solid framework (Beck et al., 1992).

Based on LCT mechanism, other possible models were proposed. Chen et al. (1993) reported that the MCM-41 structures started to form with the deposition of monolayers silicate precursor onto the isolated micellar rods. Condensation of the silicates then took place to form the MCM-41 mesostructure. Another approach proposed the direct assembly of surfactant molecules into the hexagonal liquid crystal phase after the addition of silicate species. In this model, the silicates, organized into layers, were located between the micellar rods. The silicate layers were then puckered and collapsed around the micellar rods and were transformed into the MCM-41 structure (Steel et al., 1994). Monnier et al. (1993) and Stucky et al. (1994) suggested that MCM-41 could be synthesized from a lamellar phase. They proposed that the silica/micelle assemblies were initially layered and formed due to the electrostatic attraction between the anionic silicate species and cationic CTAB head groups. Then, the condensation of silicate makes the charge density decrease. The transformation of the lamellar mesophase into hexagonal structure was obtained from the curvature between the layers to maintain the charge density balance with the cationic head groups.

During the formation of MCM-41 nanoparticles, several experimental conditions such as the reaction temperature and surfactant concentration have significant effects on the particle size and shape. To observe these effects, the synthesis was performed at either constant temperature with variable surfactant concentrations or constant surfactant concentration at different temperatures.

The effect of the temperature on the particle morphology was observed only at 0.01 M CTAB in dispersion medium. As the temperature increased from 25°C to 45 °C, the size of particles decreased (Figure 4.24.). However, the size of particles which were synthesized at 35°C and 45°C were similar to each other. Similar observations were also observed at the other concentrations. These results are not presented here. Although the temperature has no influence on the surface characteristics at 0.05 M CTAB, average pore size increases with the increase in temperature at 0.01 M. The reason may be the fact that the higher temperature causes more free and flexible movements of the surfactant tails which can result in a larger molecular volume for the surfactant and provide the formation of larger pores after calcination. However, such a change in morphology may be expected to occur at the higher temperatures than 45 °C.

The concentration effect is more dominant than the temperature on the particle size and shape. As shown in Figure 4.25, at high concentration (0.05 M), rod-like BC-2 particles were obtained. The average particle size of these particles were about 450 nm. When the surfactant concentration was reduced, both the size and shape of BC-2 nanoparticles changed significantly. At lower concentrations (0.01 and 0.001 M), the particles transformed into spherical structures with an average size of ~200 nm. The possible reason of the change in particle shape as the surfactant concentration varies may be the transition of micelles from cylindrical to spherical structure around which the silica growth occurs. The same relation between the surfactant concentration and the particle size/shape was also observed in the case of other temperatures. Moreover, when CTAB concentration is 0.001 M, smaller silica spheres were obtained. The average particle sizes of BC-2 particles are illustrated in Table 4.5.

TEM images were obtained for these samples to observe the size and order of the pores. As shown in Figure 4.26-27, silica particles have mesopores in hexagonally ordered structure. Both the size and shape of BC-II particles can be also clearly seen, as indicated by the SEM images. The ordered mesoporous structure is maintained while the surfactant concentration in reaction medium changes. The pore sizes obtained from TEM images agree well with the values obtained from nitrogen sorption analysis.

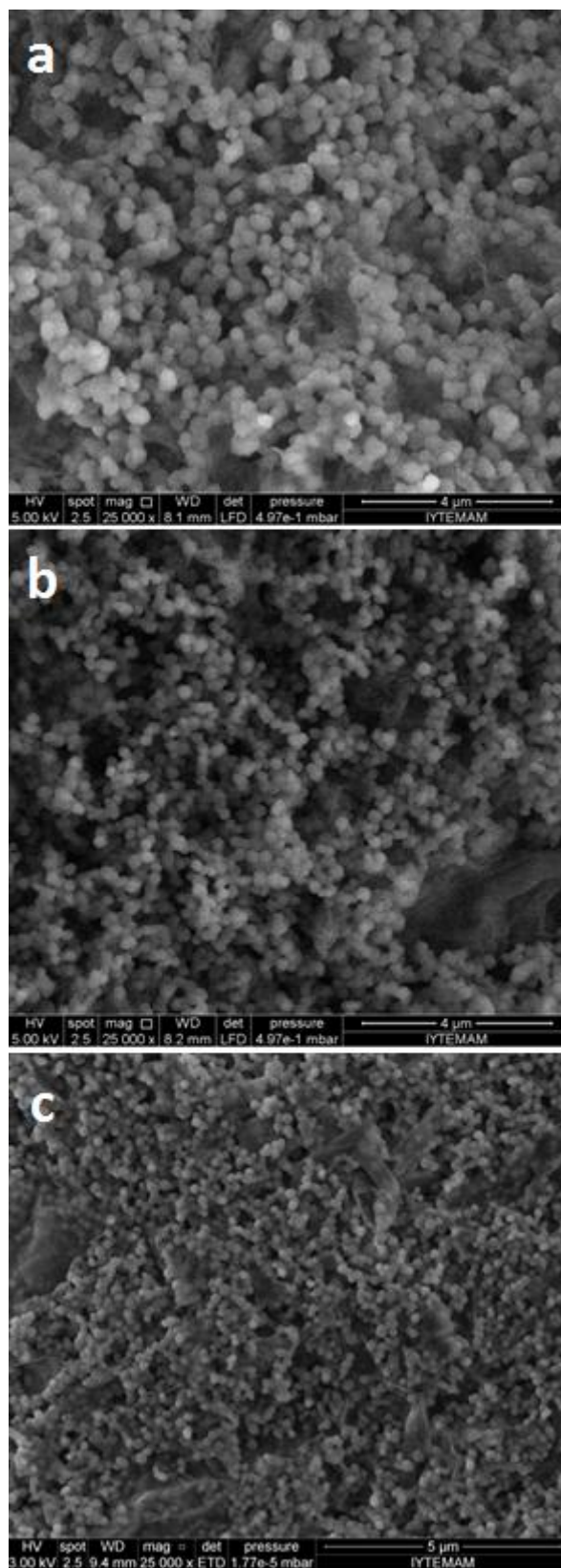


Figure 4.24. SEM images of BC-2 particles including 0.01 M CTAB (Synthesis temperature: 25 °C (a), 35 °C (b), 45 °C (c))

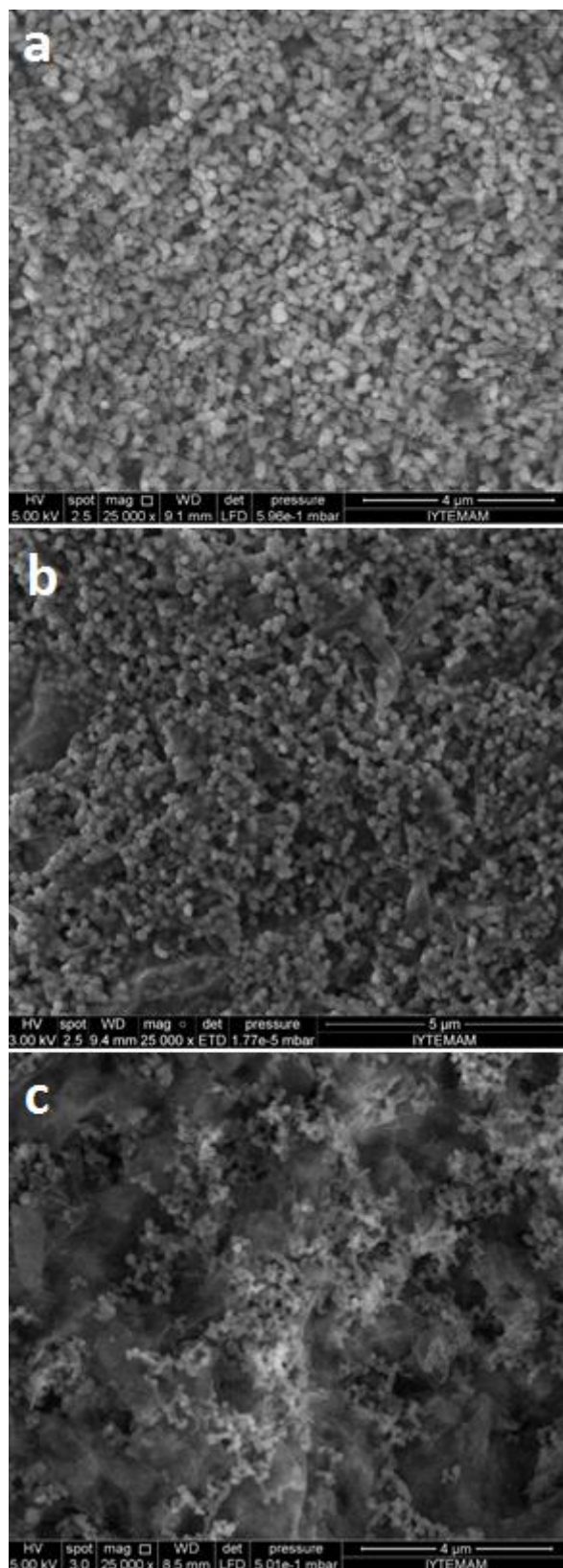


Figure 4.25. SEM images of BC-2 particles synthesized at 45 °C (CTAB concentrations: 0.05 M (a), 0.01 M (b), 0.001 M (c))

Table 4.5. Average particle sizes (nm) of BC-2 particles obtained by SEM images

CTAB concentration	Temperatures		
	25 °C	35 °C	45 °C
0.05 M	390 (20)	400 (30)	450 (45)
0.01 M	370 (60)	260 (40)	200 (30)
0.001 M	210 (30)	160 (20)	170 (30)

* The values in the paranthesis indicate the standard deviation of the measurements

Table 4.6. Nitrogen Sorption Measurements of BC-2 (0.05 M CTAB)

Temp.	BET Surface Area (m ² /g)	Pore volume (cm ³ /g) ^a	Pore width (4V/A) (nm) ^b
25 °C	1093,4	0.87	2.72
35 °C	1041.19	0.80	2.73
45 °C	981.43	0.79	2.79

^aSpecific pore volume was calculated via BJH adsorption cumulative volume of pores

^bAverage pore width was calculated from N₂ adsorption branch using BJH method

Table 4.7. Nitrogen Sorption Measurements of BC-2 (0.01 M CTAB)

Temp.	BET Surface Area (m ² /g)	Pore volume (cm ³ /g) ^a	Pore width (4V/A) (nm) ^b
25 °C	1038.5	0.84	2.70
35 °C	869.56	0.80	3.23
45 °C	673.45	0.78	3.56

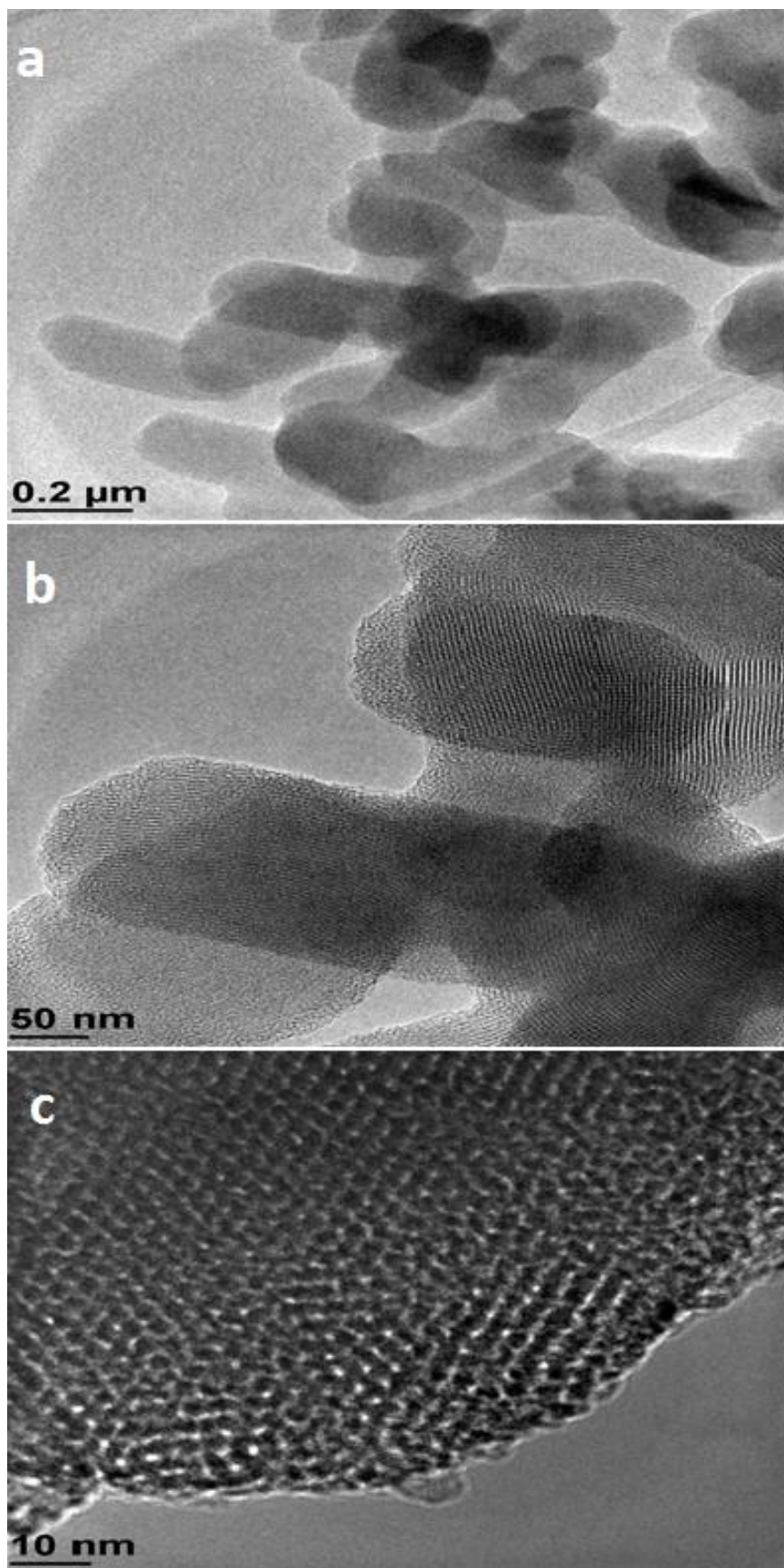


Figure 4.26. TEM images of BC-2 particles (0.05 M CTAB) with different magnifications

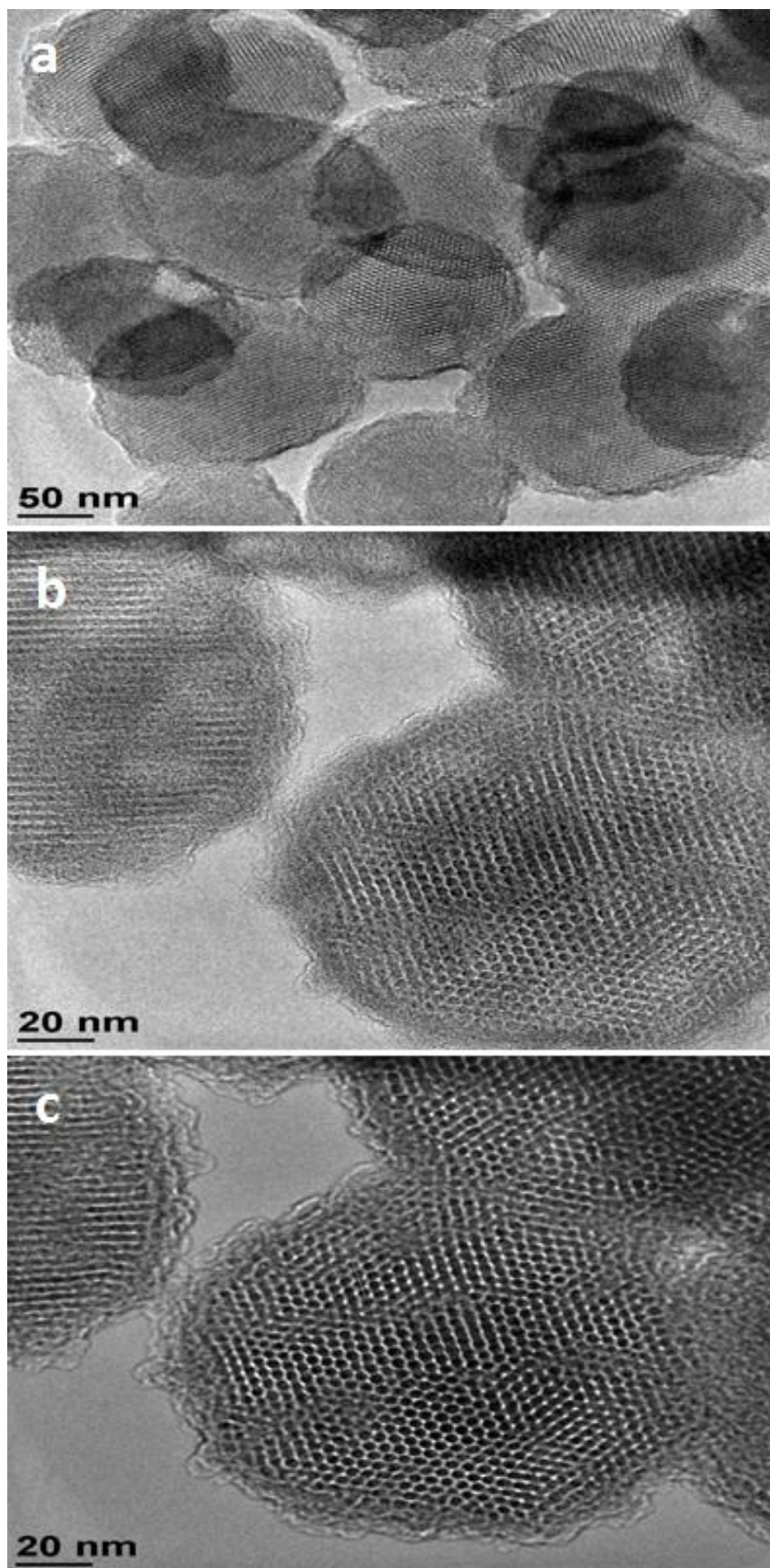


Figure 4.27. TEM images of BC-2 particles (0.01 M CTAB) with different magnifications

4.3.2. Acid Catalyzed Methods

The formation mechanism of AC particles can be assumed to be similar to the synthesis of BC-2 particles. As mentioned before, there are two main pathways followed in the formation of these nanostructures: Liquid crystal templating and cooperative assembly mechanisms. In the former pathway, P123 micelles which are spherical at first become elongated when the silica precursor is added. Then, the micelles arrange themselves in a hexagonal order as the silica walls are built around them. As a result of the following calcination step, the surfactants are removed and mesoporous silica forms. The latter mechanism includes: 1) coating of the P123 micelles with silica and decrement in zeta potential, 2) formation of the liquid-like particles by aggregation of silica coated micelles, and 3) solidification of the liquid-like particles and transformation into the final mesoporous silica (Beck et al., 1992; Mesa et al., 2008).

The transition of micelle shapes from spherical to cylindrical is essential in the synthesis of P123 templated mesoporous silica particles. Because the temperature and reagent concentrations are kept constant during the synthesis, this transition occurs upon the addition of TEOS into the reaction medium. Ethanol has an important role in this shape transformation. It is a by-product of TEOS reactions and the PPO blocks are soluble in ethanol. As ethanol goes into the hydrophobic core of the micelles, the core volume begins to expand, causing an increase in critical packing parameter. Thus, the P123 micelles transform into cylindrical structures (Johansson, 2010).

To adjust the surface characteristics of silica particles, hydrothermal treatment upon the formation of silica structures is performed. Due to the temperature dependence of P123, the treatment of the as-synthesized particles in water at high temperature may enhance the pore size, pore wall thickness and surface area. After the formation of the hexagonal structure, the PEO chains are trapped into the silica, leading to the micropores in the final particles. As the temperature increases, PEO chains become more hydrophobic. These chains then retract from the silica walls and face into the more hydrophobic part of the micelles which is the core of the micelles. This results in an increase in pore size and decrease in microporosity and surface area. Moreover, the hydrothermal treatment enhances the silica walls against the shrinkage during calcination (Galarneau et al., 2001).

The formation of AC particles was examined under several variable experimental parameters such as the amount of TEOS, the presence of additives (KCl and glycerol), the presence of co-surfactants, the reaction time, the stirring time and the hydrothermal treatment at the end of the synthesis. All of these parameters affect the structure of the final particles.

The shape of AC type materials is usually rod-like and they have an average particle size higher than 1 μm in length. In this study, the synthesized AC particles were also longer than 1 μm at first, which was proved by SEM images. Then, different conditions were emphasized in order to reduce the particle size to the nanometer scale. The average particle sizes obtained from SEM images were displayed in Table 4.8.

First, the effect of the amount of TEOS was investigated. To observe this effect, 0.01, 0.0075 and 0.005 mol (\sim 0.33 M, 0.25 M and 0.17 M, respectively) TEOS was added into the solution as silica source. As shown in Figure 4.28, silica structures can be formed until the amount of TEOS was reduced to 0.005 mol in dispersion medium. At this point, no rod-like silica particles were observed. On the other hand, the decreasing amount of TEOS caused the decrease in the length of AC particles. This may be attributed to the change in surfactant/TEOS ratio.

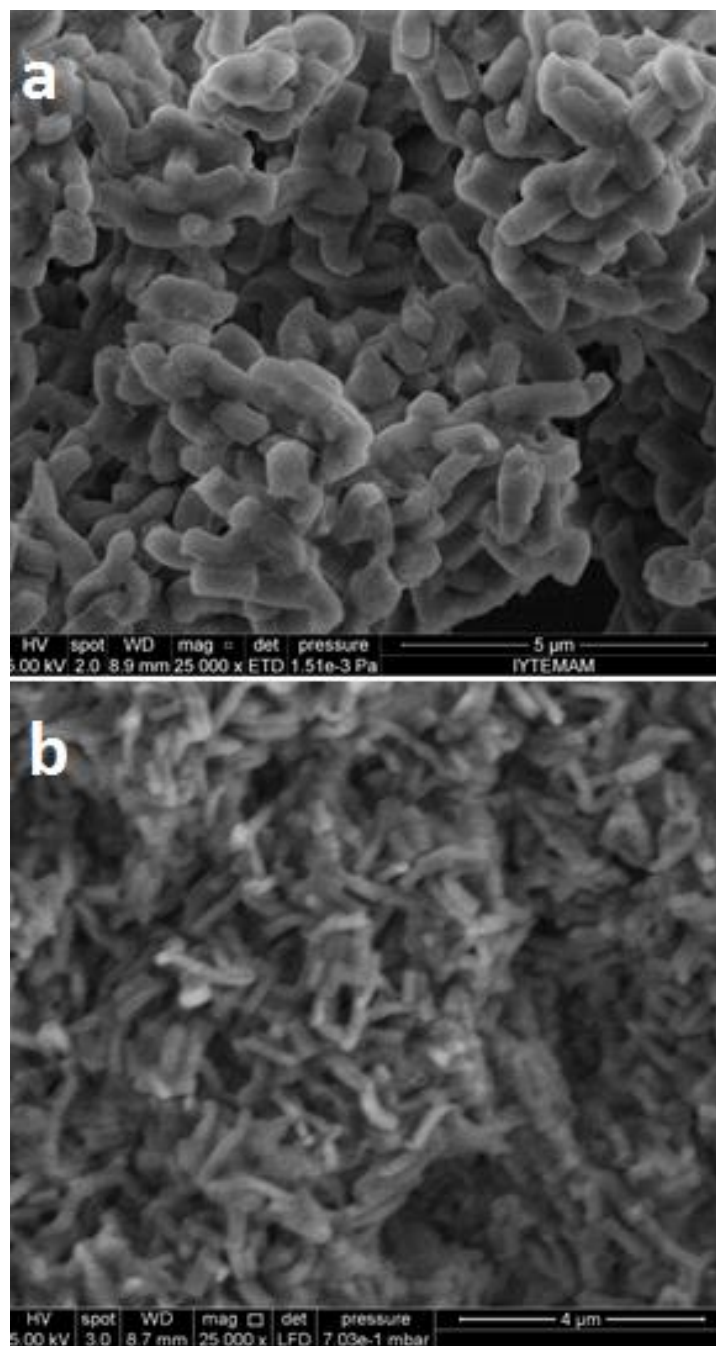


Figure 4.28. SEM images of AC particles synthesized with variable TEOS concentrations (AC-1-24-24 (a), AC-2-24-24 (b))

The presence of additives also had influence on the particle size and shape. Glycerol with the same amount of P123 and 0.1 M KCl dissolved in solution were used to synthesize the ordered porous nanoparticles. Their presence in reaction medium has been reported to reduce the particle size (Wang et al.,2009; Wan et al., 2009). As shown in Figure 4.29, while AC-4-24-24 particles showed a homogeneous distribution in size and shape, the presence of glycerol caused the formation of particles with various size

and shapes due to the agglomeration. Moreover, the length of the synthesized AC-4-24-24 was almost 800 nm, but the agglomerated AC-3-24-24 silica particles were in the range of micron sizes.

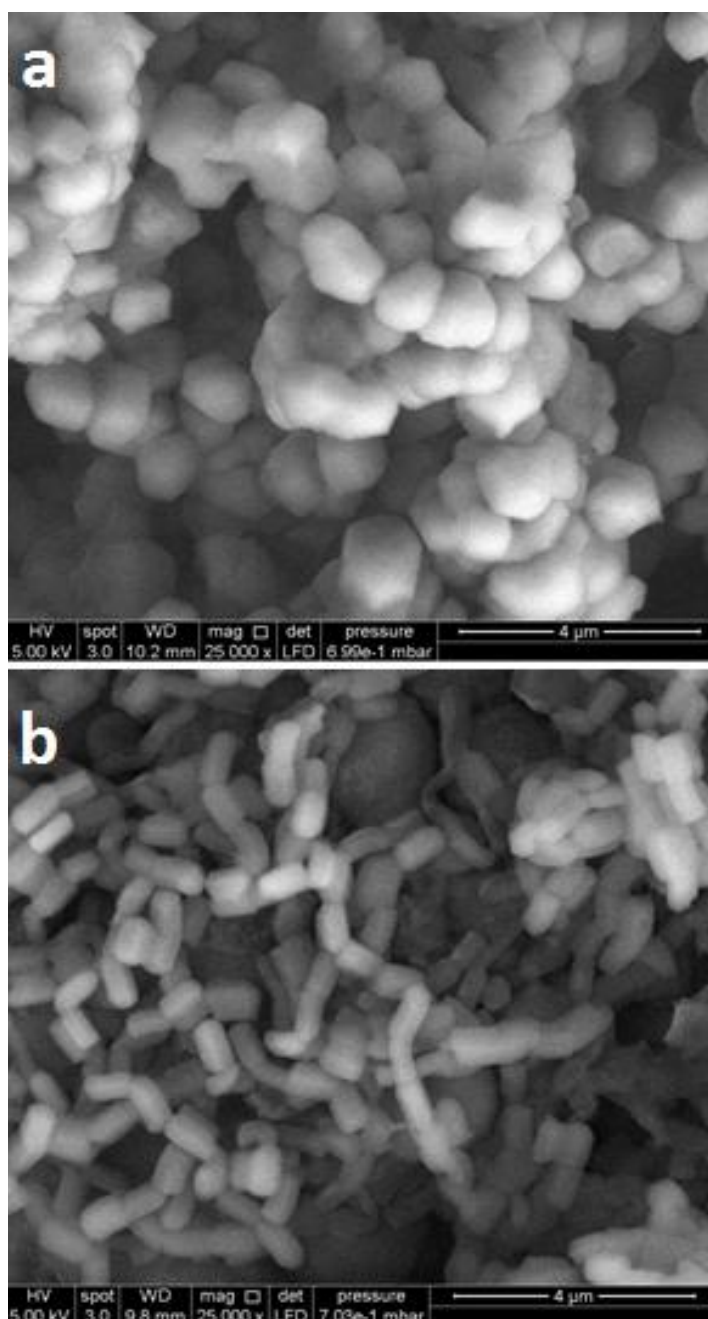


Figure 4.29. SEM images of AC particles a) AC-3-24-24 and b) AC-4-24-24

The effect of co-surfactants in the synthesis of AC nanoparticles was also examined by using cationic CTAB and anionic SDS as the additive compounds. The

SEM images proved that the particles' homogeneity was lost in the presence of surfactant mixtures (Figure 4.30.). In the case of CTAB, very big agglomerates formed instead of submicron sized silica particles. Although the silica particles became agglomerated in the presence of SDS, the particle size did not increase as observed in the case of CTAB.

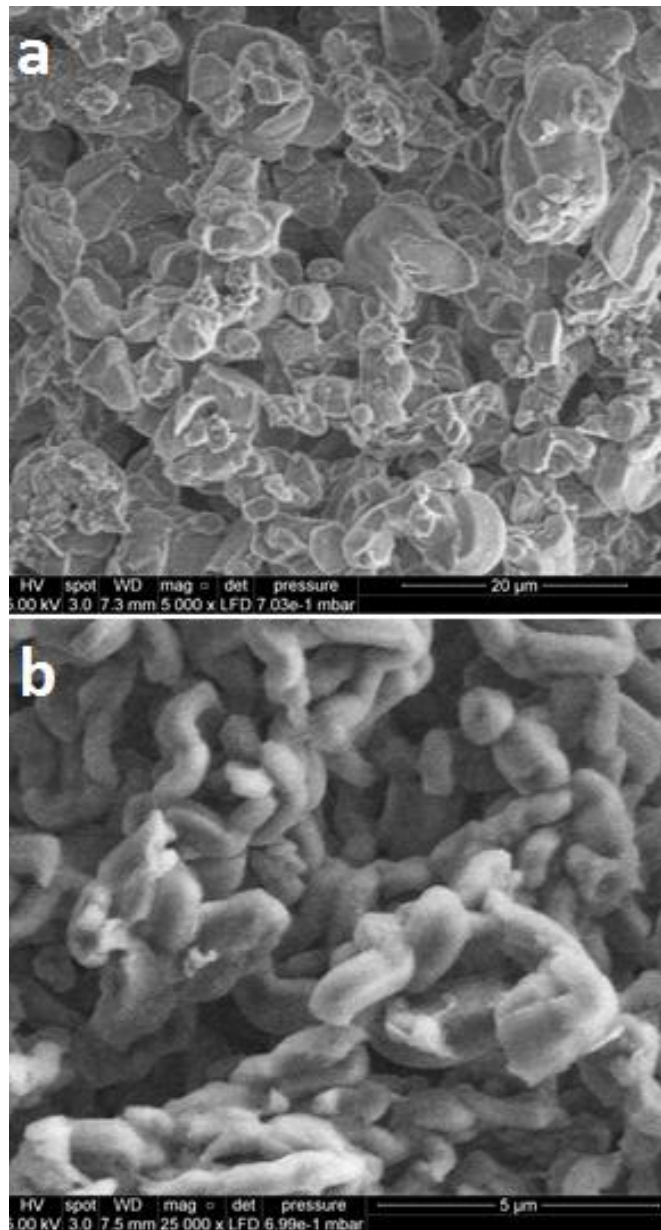


Figure 4.30. SEM images of AC particles synthesized in the presence of a) 0.0058 M CTAB and b) 0.0058 M SDS

Another interesting inference in this study was the effect of reaction and stirring time on the particle size and shape. The reaction time was reduced from 24 h to 6 and 3 h while the stirring times upon TEOS addition were 5 min and 24 h. According to the SEM analysis, the reaction time had no significant influence on the average particle size while the change in the stirring time affected the particle size. As shown in Figure 4.31 and Figure 4.32, 5 min of stirring after the TEOS addition caused a decrease in the average particle size of AC-3-24-24 and an increase in size of AC-2-24-24.

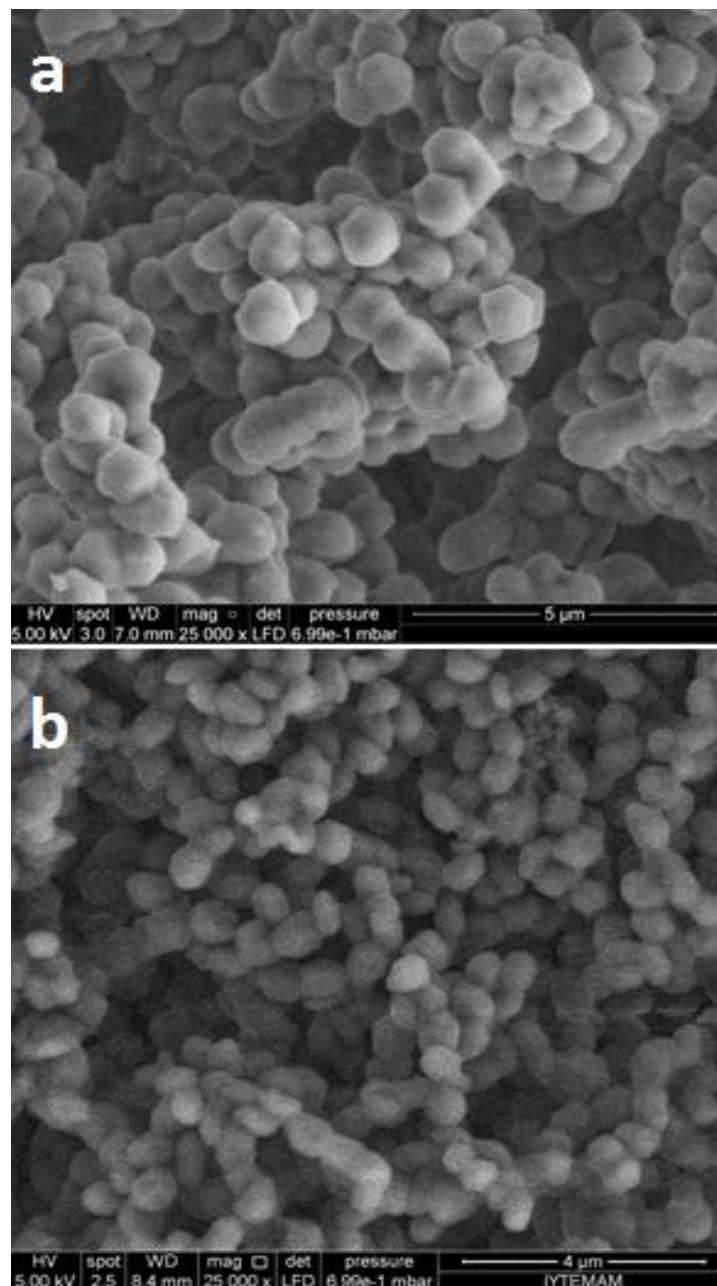


Figure 4.31. SEM images of AC particles a) AC-3-24-24 b) AC-3-24-5

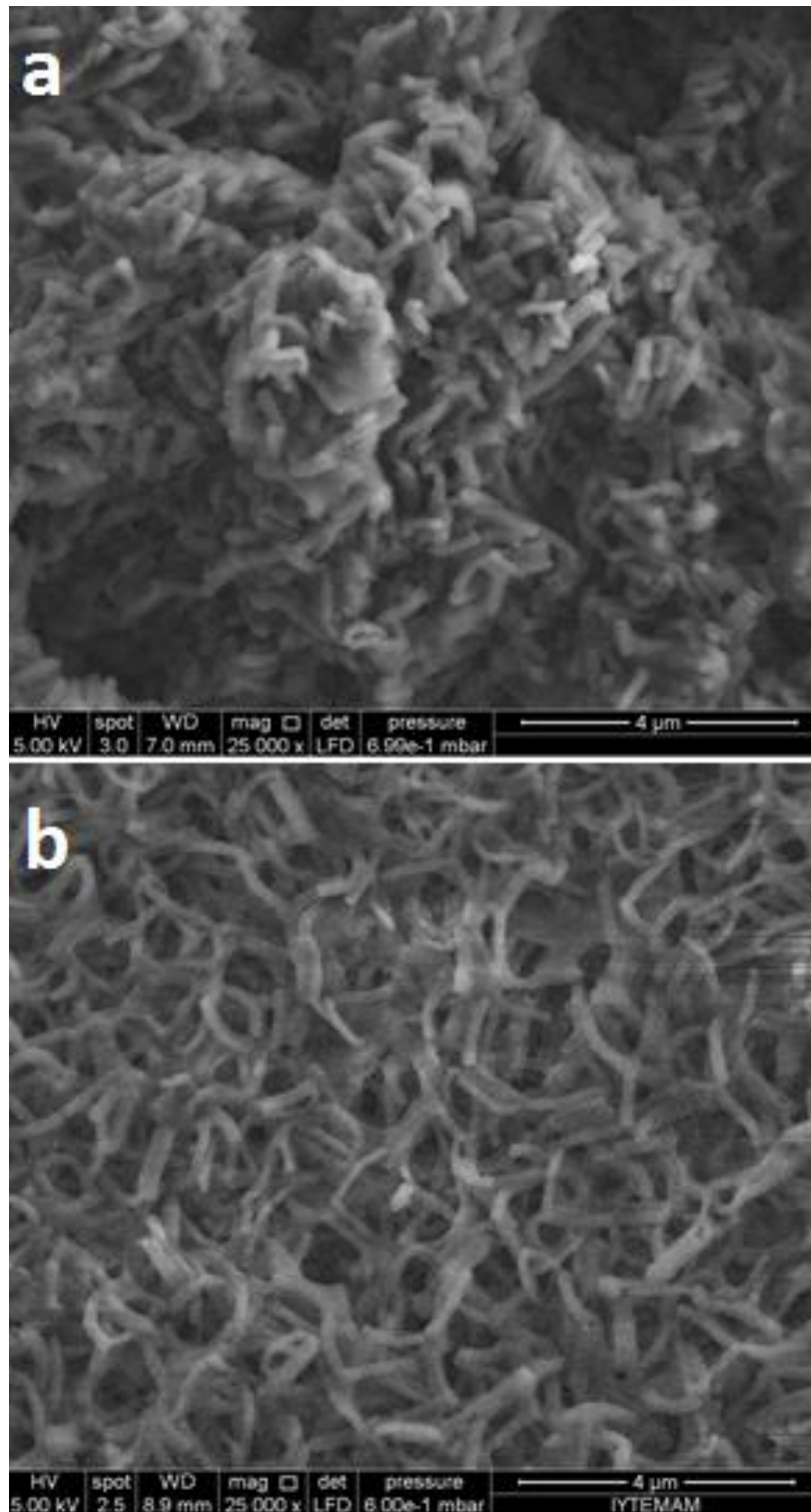


Figure 4.32. SEM images of AC particles a) AC-2-24-24 b) AC-2-24-5

Figure 4.33 indicates a type IV isotherm which is typical for the mesoporous materials. According to the nitrogen sorption measurements (Table 4.9.), the hydrothermal treatment enhanced the surface properties of AC particles. When the hydrothermally treated and untreated AC particles were compared, the treated ones had

larger pore size, specific pore volume and higher surface area. Another result was that the increasing TEOS/P123 ratio led to the pore characteristics such as larger pore size and specific pore volume and lower surface area. Moreover, AC-3-6-5 particles indicated the formation of porous structure. Although their surface properties were more improved than AC* particles, their pore volume was not as large as that of AC structures.

Table 4.8. Average particle sizes (nm) of AC particles obtained from SEM images

Sample	Reaction time (h)					HT*
	24		6		3	
	Stirring time					
	24 h	5 min	6 h	5 min	3 h	
AC-1	> 1000	> 1000	> 1000	~ 800	-	> 1000
AC-2	540	> 700	600	> 700	590	~ 640
AC-3	~ 1000	~ 800	-	~ 750	-	> 1000
AC-4	900	860	-		750	820

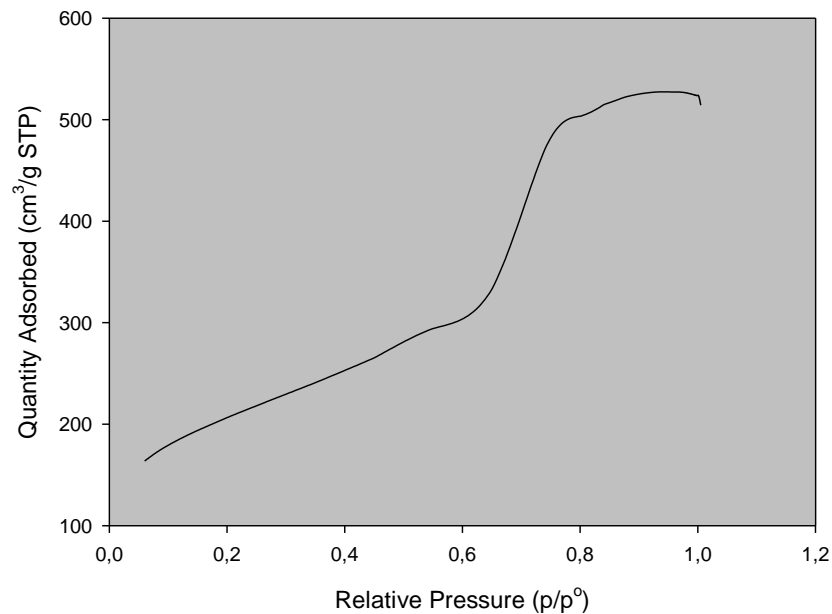


Figure 4.33. Nitrogen Adsorption Isotherm of AC type particles

Table 4.9. Nitrogen sorption measurements of the selected AC particles

Sample	BET Surface Area (m ² /g)	Pore volume (cm ³ /g) ^a	t-plot micropore volume (cm ³ /g)	Pore width (4V/A) (nm) ^b
AC-1	654.67	0.90	0.09	5.05
AC-1-24-24*	422.23	0.30	0.06	2.80
AC-2	711.31	0.81	0.05	4.56
AC-2-24-24*	418.76	0.31	0.06	2.95
AC-3-6-5	614.63	0.58	0.11	3.78
AC-3-24-24*	428.68	0.27	0.11	2.55

TEM analysis proved the formation of the hexagonally ordered mesoporous silica nanoparticles (Figure 4.34-35). The average size of the pores was approximately 5 nm. This result aligns with the nitrogen sorption measurements.

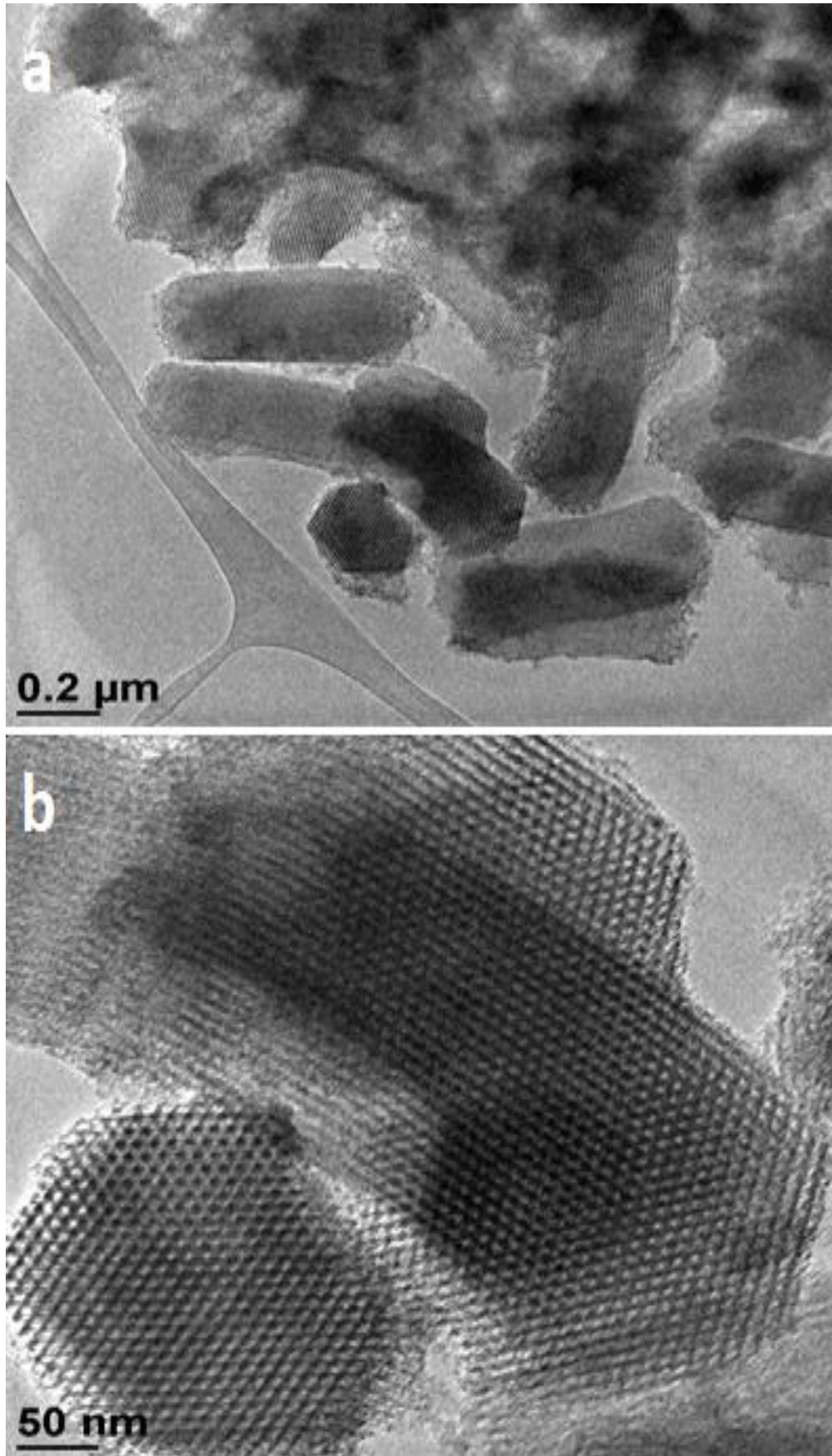


Figure 4.34. TEM images of AC-2-24-24 particles

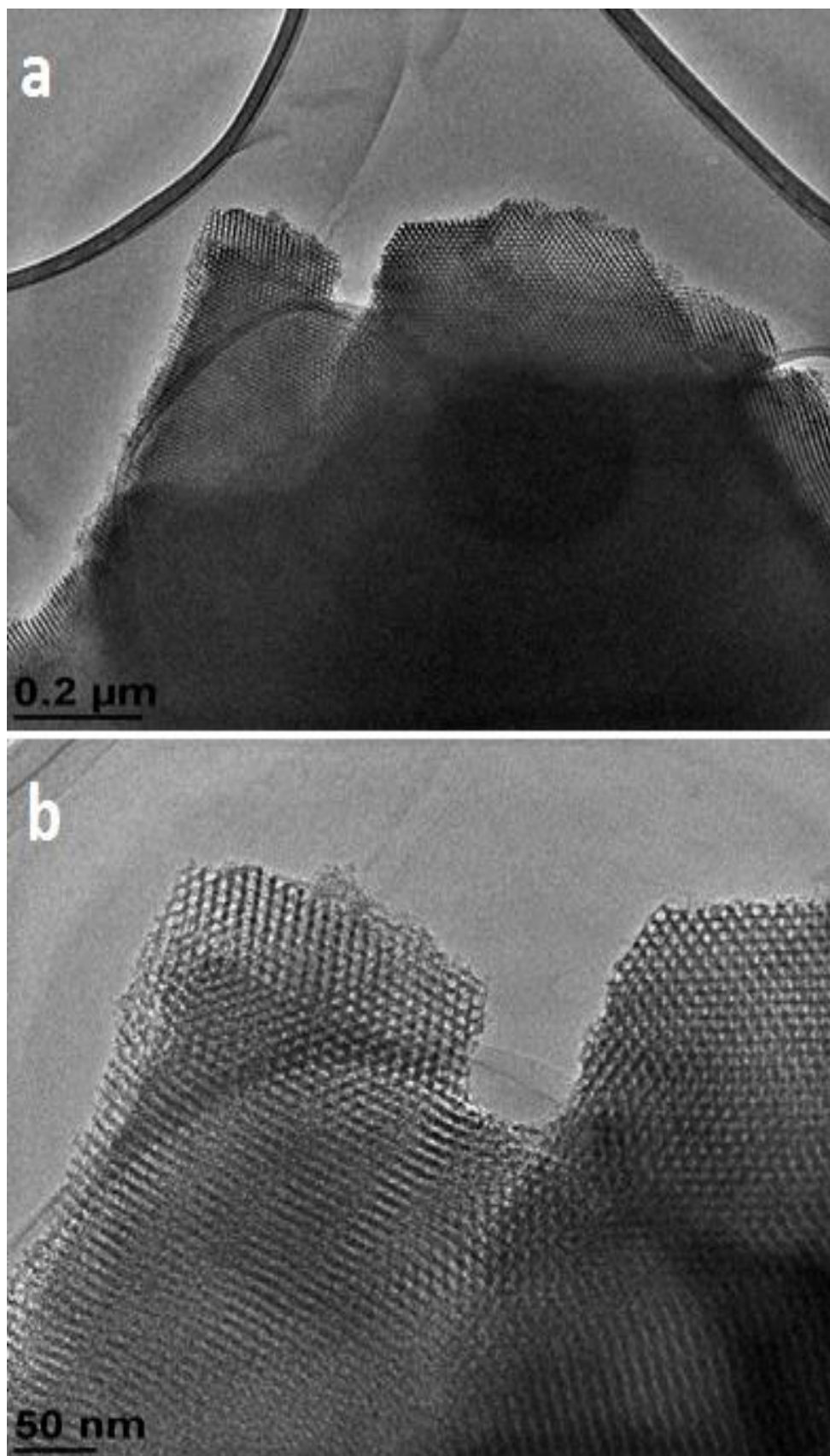


Figure 4.35. TEM images of AC-1-24-24 particles

4.4. Carbon Coating of the Silica Nanoparticles

BC-2 particles were chosen to be covered by carbon to obtain mesoporous silica nanoparticles with hydrophobic surfaces. SEM, SEM-EDX and TEM analysis showed that BC-2 particles can keep their size and shape after the carbonization process (Figure 4.36). EDX analysis shown in Figure 4.37 indicates that the particles contained both silica and carbon compounds. However, the pores of the particles are not clearly open (Figure 4.38).

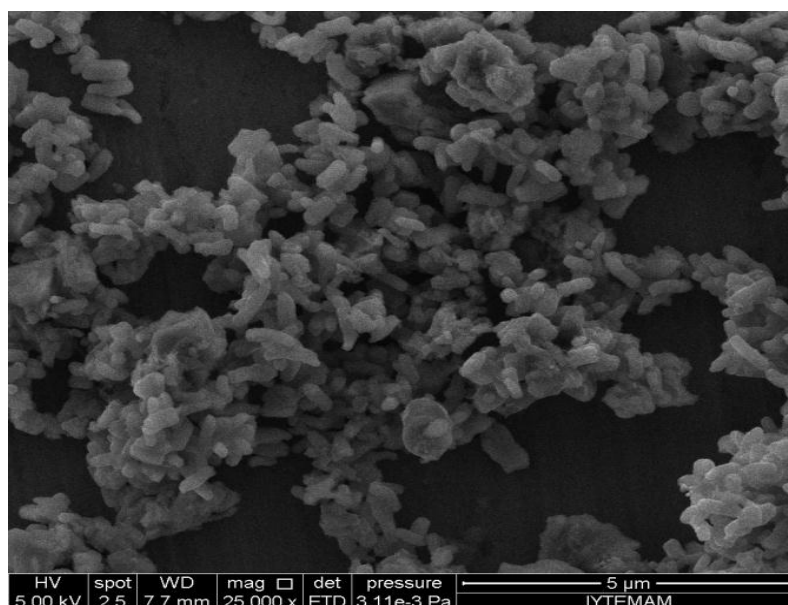


Figure 4.36. SEM images of carbonized CBC-2

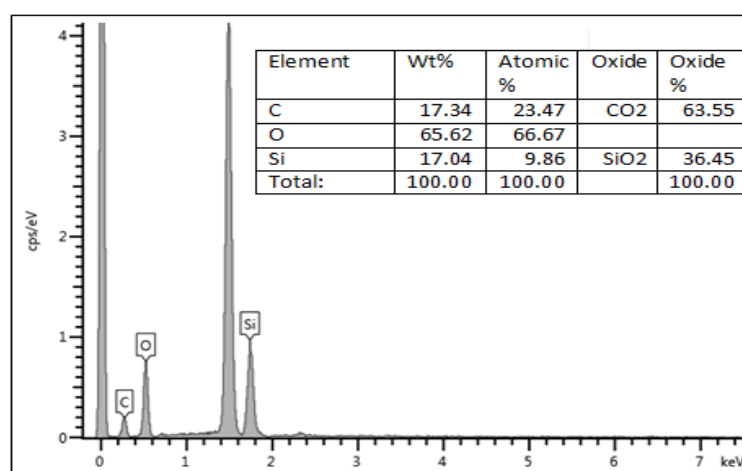


Figure 4.37. EDX analysis of carbonized CBC-2 particles

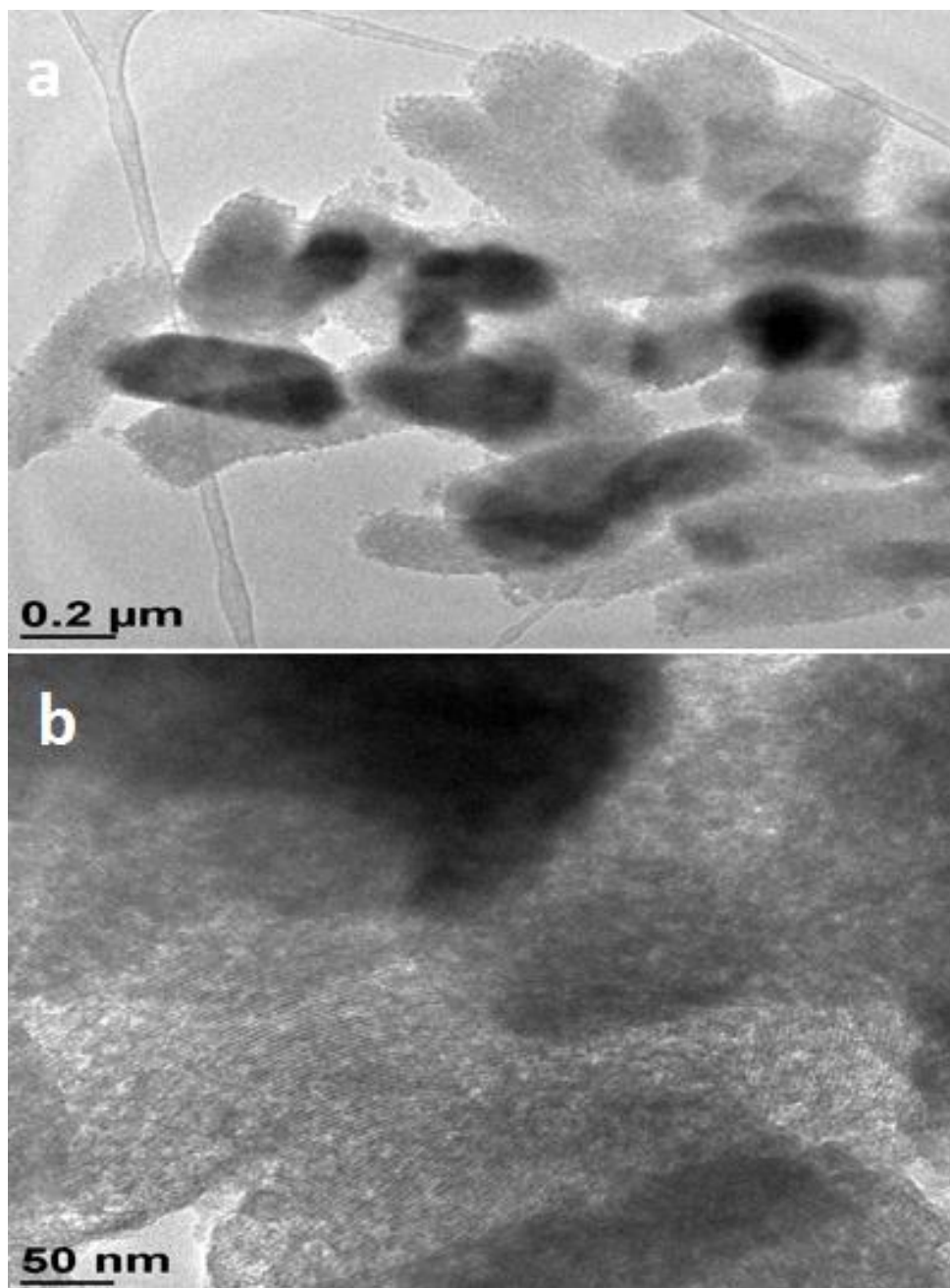


Figure 4.38. TEM images of carbonized CBC-1 particles

Since the carbonization process of silica surfaces affected the porosity due to the carbon filling into the pores, the pores of silica were filled with calcium carbonate before the carbonization step. After carbon covering process, the silica particles were treated with HCL to remove calcium carbonate to open pores. Therefore, the porous structure can be kept after the pyrolysis process. In Figure 4.39, SEM images indicated that the size and shape of BC-2 particles on which calcium carbonate was precipitated were almost the same as pure BC-2 particles. In Figure 4.40, EDX analysis also proved

the presence of calcium carbonate on silica. Moreover, TEM analysis (Figure 4.41) showed that the average pore size of mesoporous silica particles slightly decreased below 3 nm after carbon coverage. However, the pore order and mesoporosity can be obtained.

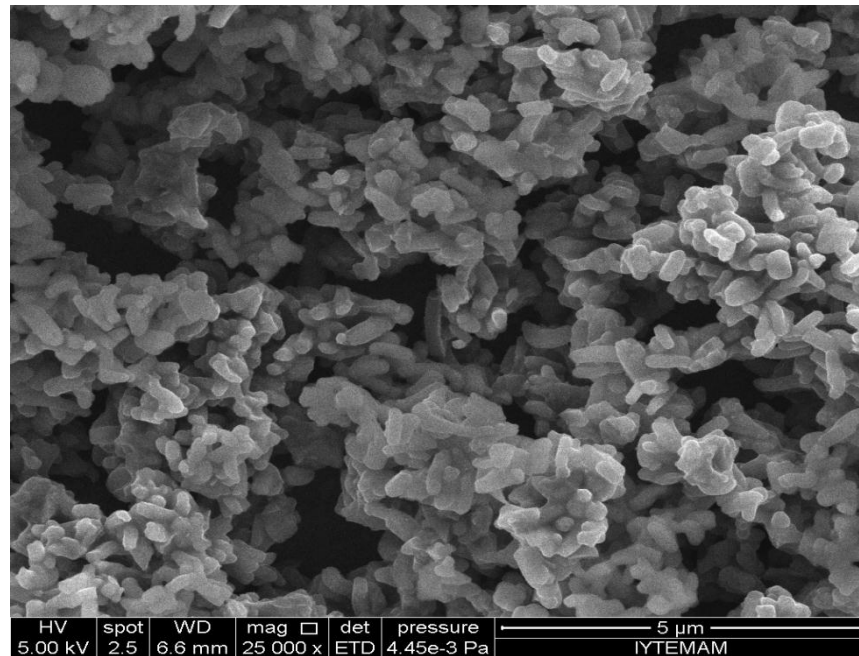


Figure 4.39. SEM image of BC-2 particles on which calcium carbonate was precipitated

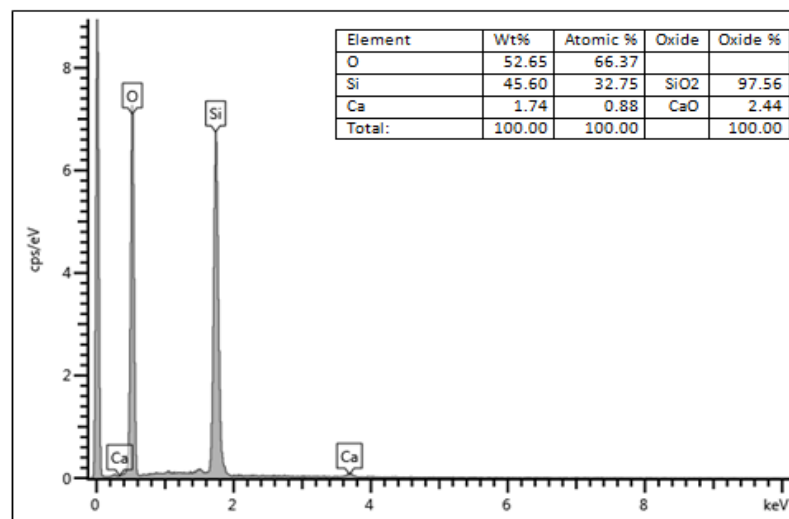


Figure 4.40. EDX analysis of BC-2 particles on which calcium carbonate was precipitated

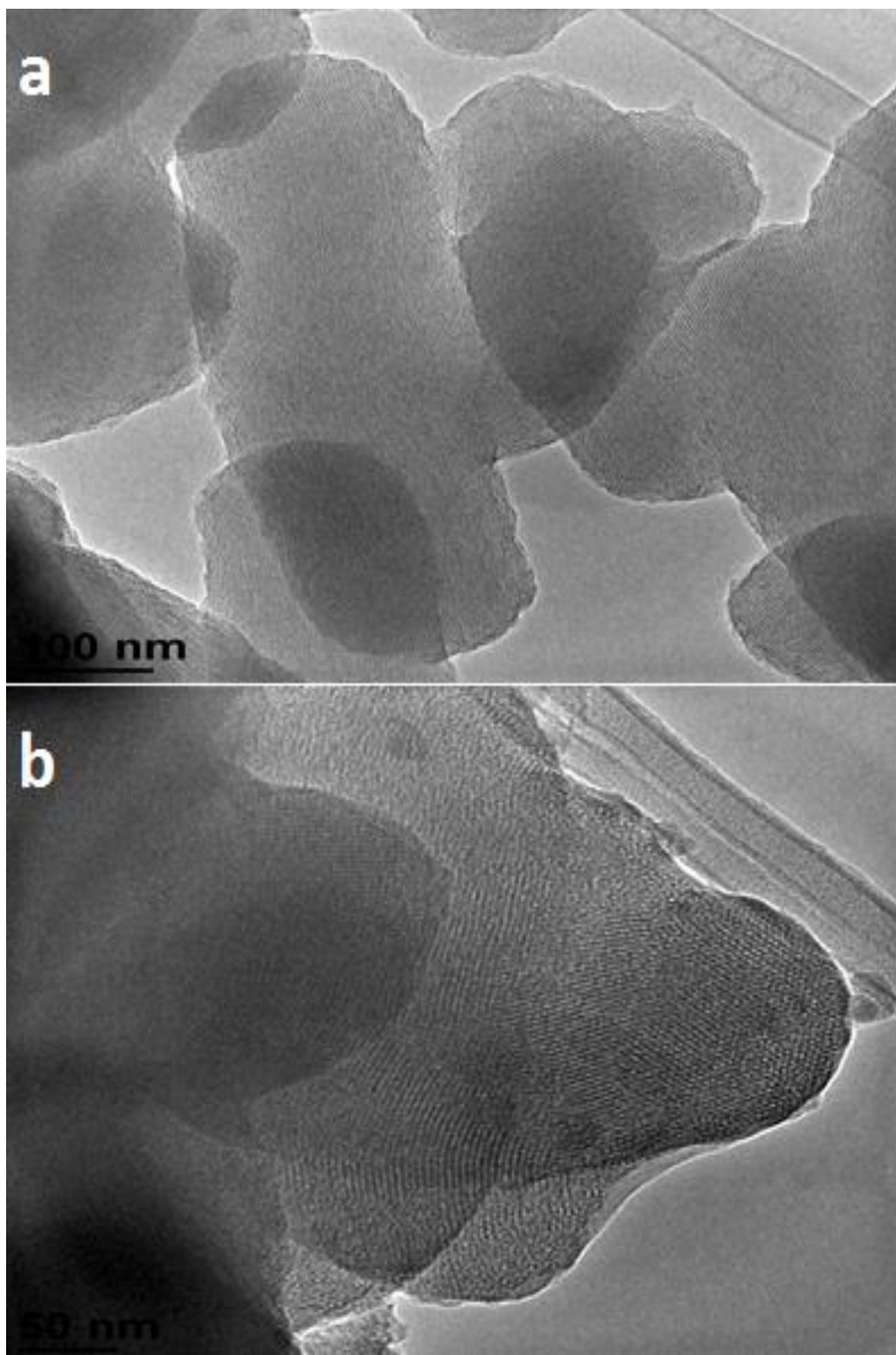


Figure 4.41. TEM images of carbonized CBC-2 particles

CHAPTER 5

CONCLUSIONS

This study is aimed at synthesizing silica particles with distinct physico-chemical properties at the outer (particle) and inner (pores) surfaces with potential use in controlled drug transport and release. That is to have nanosized particles with low energy (hydrophobic) perimeters which function as non-reacting transporters for targeted delivery along with high energy (hydrophilic) sites inside the pores to achieve controlled release. Surfactants were used in combination with both based and acid catalysed methods to achieve silica particles with desired structural properties. Then these particles were carbonized to obtain low energy surfaces. The materials synthesised were characterized using SEM, XRD, FTIR, XRF, AFM, TGA, BET surface area and pore size distribution, size and zeta potential measurements.

The effect of surfactants were found to be different depending on the type of methods used. In ethanol-water mixture, the formation of silica nanoparticles was thought to take place in the water droplets stabilized by surfactants, whose type and concentration determined the size of the particles by affecting a) the emulsification process and b) the interactions (silica-silica and silica-surfactant molecules) involved during production process. Increasing surfactant concentration except P-123 increased the size of silica particles. The shape of particles however was always spherical. The dispersion of particles also changed depending on surfactant type. While higher concentration (0.01 M) of cationic surfactants led to the aggregation of the particles and an increase in polydispersity, monodisperse structures could be obtained in the presence of anionic surfactant and at low surfactant concentrations (10^{-3} - 10^{-5} M).

In the case of based catalysed silica production in water, however, surfactant micelles were used as templates to produce pores. In this case the effect of surfactant type and concentration was attributed to their effect on the CMC, micelle shape and size. It was found that while rod-like particles (~400 nm in length) were obtained at 0.05 M CTAB, spherical particles (~200 nm) were synthesized at lower concentrations (0.01 M).

Acid catalysed silica production was again in water medium and surfactant micelles were used as template materials to produce pores and the effect of surfactant type and concentration was attributed to their effect on the CMC, micelle shape and size. Therefore the properties of silica particles was found to change depending on conditions. Here the rod-like (600-800 nm in length) and cubic (800-1000 nm) shape nanoparticles were produced.

The mesoporous silica nanoparticles synthesized under basic conditions had a surface area of $\sim 1000 \text{ m}^2/\text{g}$ and average pore size of $\sim 3 \text{ nm}$, while acid catalyzed silica particles exhibited lower surface area of $\sim 700 \text{ m}^2/\text{g}$ and larger pore size of $\sim 5 \text{ nm}$. These differences were most probably depend on the different surfactant type and hydrothermal treatment used in the acid catalyzed synthesis.

To have silica particles with low energy (hydrophobic) perimeters, carbonization of mesoporous silica nanoparticles produced in the presence of calcium carbonate (that is used to fill the pores) was performed. It was observed that the resulting materials are still porous in ordered structure and hydrophobic in perimeters.

REFERENCES

- Adamson A.W., Gast A.P., 1997, *Physical Chemistry of Surfaces*, New York, Wiley
- Adhikari, A., Dey S., Mandal U., 2008, "Solvation Dynamics in Ionic Liquid Swollen P123 Triblock Copolymer Micelle: A Femtosecond Excitation Wavelength Dependence Study", *J. Phys. Chem. B*, Vol. 112, pp. 6350–6357
- Alexandridis P., Holzwarth J.F., Hatton T.A., 1994, "Micellization of Poly(ethylene oxide)-Poly(propylene oxide)-Poly(ethylene oxide) Triblock Copolymers in Aqueous Solutions: Thermodynamics of Copolymer Association", *Macromolecules*, Vol. 27, pp. 2414-2425
- Alexandridis P., Athanassiou A., Fukuda S., Hatton T.A., 1994, "Surface activity of poly(ethylene oxide)-block-poly(propylene oxide)-block-poly(ethylene oxide) copolymers", *Langmuir*, Vol. 10, pp. 2604–2612
- Anderson M.T., Martin J.E., Odinek J.G., Newcomer P.P., 1998, "Effect of Methanol Concentration on CTAB Micellization and on the Formation of Surfactant-Templated Silica (STS)", *Chemical Materials*, Vol. 10, pp. 1490-1500
- Andersson J., Rosenholm J., Areva S., Linden M., 2004, "Influences of Material Characteristics on Ibuprofen Drug Loading and Release Profiles from Ordered Micro- and Mesoporous Silica Matrices", *Chemical Materials*, Vol. 16, pp. 4160–4167
- Arruebo M., Fernández-Pacheco R., Ibarra M.R., Santamaría J., 2007, "Magnetic nanoparticles for drug delivery", *Nanotoday*, Vol. 2, pp. 22-32
- Asiyanbola B., Soboyejo W., 2008, "For the Surgeon: An Introduction to Nanotechnology", *Journal of Surgical Education*, Vol. 65, pp. 155-161
- Babu K.M.V., 2007, *The Development of a Novel Controlled Release Drug Delivery System*, PHD Thesis, University of Waikato, Hamilton
- Balas F., Manzano M., Colilla M., Vallet-Regi M., 2008, "L-TRP adsorption into silica mesoporous materials to promote bone formation", *Acta Biomaterials*, Vol. 4, pp. 514–22
- Beck J.S., Vartuli J.C., Roth W.J., Leonowicz M.E., 1992, "A new family of mesoporous molecular sieves prepared with liquid crystal templates", *Journal of the American Chemical Society*, Vol. 114, pp. 10834-10843
- Beck J.S., Vartuli J.C., Kennedy G.J., Kresge C.T., 1994, "Molecular or Supramolecular Templating: Defining the Role of Surfactant Chemistry in the Formation of Microporous and Mesoporous Molecular Sieves", *Chemical Materials*, Vol. 6, pp. 1816-1821

- Bogush G.H., Zukoski C.F., 1992, "Uniform silica particle precipitation: an aggregative growth model", *Journal of Colloid Interface Science*, Vol. 142, pp. 19-34
- Brinker C.J., Scherer G.W., 1990, *Sol-gel science the Physics and Chemistry of Sol-gel processing*, San Diego, Academic Press
- Chatterjee S., Nandi S., Bhattacharya S.C., 2005, "Fluorescence resonance energy transfer from Fluorescein to Safranin T in solutions and in micellar medium", *Journal of Photochemistry and Photobiology A: Chemistry*, Vol. 173, pp. 221–227
- Chen C.-Y., Burkett S.L., Li H.-X., Davis M.E., 1993, "Studies on mesoporous materials II. Synthesis mechanism of MCM-41", *Microporous Materials*, Vol. 2, pp. 27-34
- Cho K., Wang X., Nie S., 2008, "Therapeutic Nanoparticles for Drug Delivery in Cancer", *Clinical Cancer Research*, Vol. 14, pp. 1310-1316
- Cooper S.M., Cruden B.A., Meyyappan M., 2004, "Gas transport characteristics through a carbon nanotubule", *Nano Letters*, Vol. 4, pp. 377–381
- De Jong, W.H., Borm, P.J.A., 2008, "Drug delivery and nanoparticles: Applications and hazards", *International Journal of Nanomedicine*, Vol. 3, pp. 133–149
- Doadrio A.L., Sousa E.M.B., Doadrio J.C., Pariente J.P., Izquierdo-Barba I., Vallet-Regi M., 2004, "Mesoporous SBA-15 HPLC evaluation for controlled gentamicin drug delivery", *Journal of Control Release*, Vol. 97, pp. 125–132
- Doadrio J.C., Sousa E.M.B., Izquierdo-Barba I., Doadrio A.L., 2006, "Functionalization of mesoporous materials with long alkyl chains as a strategy for controlling drug delivery pattern", *Journal of Material Chemistry*, Vol. 16, pp. 462–466
- Donaldson K., Stone V., Tran C.L., Kreyling W., Borm P.J.A., 2004, "Nanotoxicology", *Occupational and Environmental Medicine*, Vol. 61, pp. 727-728
- Duplatre G., Marques M.F.F., Miguel M.D.G., 1996, "Size of Sodium Dodecyl Sulfate Micelles in Aqueous Solutions as Studied by Positron Annihilation Lifetime Spectroscopy", *J. Phys. Chem.*, Vol.100, pp. 16608-16612
- Dutreilh-Colas M., Yan M., Labrot P., 2008, "AFM evidence of perpendicular orientation of cylindrical craters on hybrid silica thin film templated by triblock copolymer", *Surface Science*, Vol. 602, pp. 829-833
- Feng P.Y., Bu X.H., Stucky G.D. Pine D.J., 2000, "Monolithic Mesoporous Silica Templated by Microemulsion Liquid Crystals", *Journal of American Chemical Society*, Vol. 122, pp. 994-995

- Fontell K., 1990, "Cubic phases in surfactant-like lipid systems", *Colloid and Polymer Science*, Vol. 268, pp. 264–285
- Galarneau A., Cambon H., Di Renzo F., Fajula F., 2001, "True Microporosity and Surface Area of Mesoporous SBA-15 Silicas as a Function of Synthesis Temperature", *Langmuir*, Vol. 17, pp. 8328-8335
- Gaumet M., Vargas A., Gurny R., Delie F., 2007, "Nanoparticles for drug delivery: The need for precision in reporting particle size parameters", *European Journal of Pharmaceutics and Biopharmaceutics*, Vol. 69, pp. 1-9
- Ge W., Kesselman E., Talmon Y., 2008, "Effects of chemical structures of parahalobenzoates on micelle nanostructure, drag reduction and rheological behaviors of dilute CTAC solutions", *J. Non-Newtonian Fluid Mech.* Vol. 154 pp. 1–12
- Giesche H., 1994, "Synthesis of Monodispersed Silica Powders I. Particle Properties and Reaction Kinetics", *Journal of the European Ceramic Society*, Vol. 14, pp. 189-204
- Giesche H., 2000, "Hydrolysis of silicon alkoxides in homogeneous solutions", *Fine particles synthesis, characterization, and mechanisms of growth*, Chapter 2.1, pp. 126-146
- Gokulakrishnan N., Kania N., Léger B., Lancelot C., Grosso D., Monflier E., 2011, "An ordered hydrophobic P6mm mesoporous carbon with graphitic pore walls and its application in aqueous catalysis", *Carbon*, Vol. 49, pp. 1290–1298
- Gomez-Serrano V., Gonzalez-Garcia C.M., Gonzalez-Martin M.L., 2001, "Nitrogen adsorption isotherms on carbonaceous materials. Comparison of BET and Langmuir surface areas", *Powder Technology*, Vol. 116, pp. 103-108
- Gonzalez-Lopez J., Sandez-Macho I., Concheiro A., 2010, "Poloxamines and Poloxamers as Polymeric Micellar Carriers for Simvastatin: Interactions at the Air Water Interface and in Bulk Solution", *Journal of Physical Chemistry*, Vol. 114, pp. 1181–1189
- Goyal P.S., Aswal V.K., 2006, "Combined SANS and SAXS in Studies of Nanoparticles", *Indian Journal of Pure & Applied Physics*, Vol. 44, pp. 724-728
- Hahakura S., Isoda S., Ogawa T., 2002, "Formation of ultrafine platinum particles in an aqueous solution with a surfactant", *Journal of Crystal Growth*, Vol. 237–239, pp. 1942–1945
- Harris M.T., Brunson R.R., Byers C.H., 1990, "The Base-catalyzed hydrolysis and condensation reactions of dilute and concentrated TEOS solutions", *Journal of Non-Crystalline Solids*, Vol. 121, pp. 397-403

- Hassan P.A., Fritz G. Kaler E.W., 2003, "Small angle neutron scattering study of sodium dodecyl sulfate micellar growth driven by addition of a hydrotropic salt", *Journal of Colloid and Interface Science*, Vol. 257, pp.154–162
- Hecht E., Hoffmann H., 1994, "Interaction of ABA block copolymers with ionic surfactants in aqueous solutions", *Langmuir*, Vol. 10, pp. 86–91
- Hirashima H., Imai H., Balek V., 2001, "Preparation of mesoporous TiO₂ gels and their characterization", *Journal of Non-Crystalline Solids*, Vol. 285, pp. 96-100
- Horcajada P., Ramila A., Perez-Pariente J., Vallet-Regi M., 2004, "Influence of pore size of MCM-41 matrices on drug delivery rate", *Microporous and Mesoporous Materials*, Vol. 68, pp. 105–109
- Horjacada P., Ramila A., Ferey G., Vallet-Regi M., 2006, "Influence of superficial organic modification of MCM-41 matrices on drug delivery rate", *Solid State Sciences*, Vol. 8, pp. 1243-1249
- Hu Z.H., Srinivasan M.P., Ni Y.M., 2000, "Preparation of Mesoporous High-Surface-Area Activated Carbon" *Adv. Mater.*, Vol. 12, pp.62-65
- Huang C.W., Hsu C.H., Kuo P.L., Hsieh C.T., Teng H., 2011, "Mesoporous carbon spheres grafted with carbon nanofibers for high-rate electric double layer capacitors", *Carbon*, Vol. 49 pp. 895–903
- Huo Q., Margolese D.I., Feng P., Gier T.E., Stucky G.D., 1994, "Generalized Syntheses of Periodic Surfactant/Inorganic Composite Materials", *Nature*, Vol. 368, pp. 317-321.
- Ibrahim I.A.M., Zikry A.A.F., Sharaf M.A., 2010, "Preparation of spherical silica nanoparticles: Stober silica", *Journal of American Science*, Vol. 6, pp. 985-989.
- Izquierdo-Barba I., Martinez A., Doadrio A.L., Perez-Pariente J., 2005, "Release evaluation of drugs from ordered three-dimensional silica structures", *European Journal of Pharmaceutical Sciences*, Vol. 26, pp. 365–373
- Jian G., Ying R., Wei G., 2009, "Molecular Dynamics Simulation of Effect of Salt on the Compromise of Hydrophilic and Hydrophobic Interactions in Sodium Dodecyl Sulfate Micelle Solutions", *Chinese Journal of Chemical Engineering*, Vol. 17, pp. 654-660
- Johansson E.M., 2010, Controlling the Pore Size and Morphology of Mesoporous Silica, Licentiate Thesis No. 1451, Linköping University, Linköping
- Jun S., Joo S.H., Ryoo R., Kruk M., Jaroniec M., Liu Z., 2000, "Synthesis of New, Nanoporous Carbon with Hexagonally Ordered Mesostructure", *Journal of American Chemical Society*, Vol. 122, pp. 10712

- Kabanov A.V., Nazarova I.R., Astafieva I.V., 1995, "Micelle Formation and Solubilization of Fluorescent Probes in Poly(oxyethylene-b-oxypropylene-b-oxyethylene) Solutions", *Macromolecules*, Vol. 28, pp. 2303-2314
- Kaneda M., Tsubakiyama T., Carlsson A., Sakamoto Y., 2002, "Structural Study of Mesoporous MCM-48 and Carbon Networks Synthesized in the Spaces of MCM-48 by Electron Crystallography", *Journal of Physical Chemistry B*, Vol. 106, pp. 1256-1266
- Kim J., Lee J., Hyeon T., 2004, "Direct synthesis of uniform mesoporous carbons from the carbonization of as-synthesized silica/triblock copolymer nanocomposites", *Carbon*, Vol. 42, pp. 2711-2719
- Kim K.T., Meeuwissen S.A., Nolte R.J.M., van Hest J.C.M., 2010, "Smart nanocontainers and nanoreactors", *Nanoscale*, Vol. 2, pp. 844-858
- Kim S.S., Pauli T.R., Pinnavaia T.J., 2000, "Non-ionic surfactant assembly of ordered, very large pore molecular sieve silicas from water soluble silicates", *Chemical Communications*, pp. 1661-1662
- Kim S., Pinnavaia T.J., 2001, "A low cost route to hexagonal mesostructured carbon molecular sieves", *Chemical Communications*, pp. 2418-2419
- Kleitz F., Choi S.H., Ryoo R., 2003, "Cubic *Ia3d* large mesoporous silica: synthesis and replication to platinum nanowires, carbon nanorods and carbon nanotubes", *Chemical Communications*, Vol. 17, pp. 2136-2137.
- Knox J.H., Unger K.K., Mueller H., 1983, "Prospects for Carbon as Packing Material in High-Performance Liquid Chromatography", *Journal of Liquid Chromatography*, Vol. 6, pp. 1-36
- Knox J.H., Kaur B., Millward G.R., 1986, "Structure and performance of porous graphitic carbon in liquid chromatography", *Journal of Chromatography*, Vol. 352, pp. 3-25
- Kowalewski T., Tsarevsky N.V., Matyjaszewski K., 2002, "Nanostructured Carbon Arrays from Block Copolymers of Polyacrylonitrile", *J. Am. Chem. Soc.*, Vol. 124, pp. 10632-10633
- Kozlov M.Y., Melik-Nubarov N.S., Batrakov E.V., 2000, "Relationship between Pluronic Block Copolymer Structure, Critical Micellization Concentration and Partitioning Coefficients of Low Molecular Mass Solutes", *Macromolecules*, Vol. 33, pp. 3305-3313
- Kruk M., Jaroniec M., Kim T.W., Ryoo R., 2003, "Synthesis and Characterization of Hexagonally Ordered Carbon Nanopipes", *Chemical Materials*, Vol. 15, pp. 2815-2823

- Kuperkar K., Abezgauz L., Prasad K., 2010, "Formation and Growth of Micelles in dilute Aqueous CTAB Solutions in the Presence of NaNO₃ and NaClO₃", *Journal of Surfactant and Detergents*, Vol. 13, pp. 293–303
- Kyotani T., 2000, "Control of pore structure in carbon", *Carbon*, Vol. 38, pp. 269-286.
- LaMer V.K., Dinegar R.H., 1950, "Theory, Production and Mechanism of Formation of Monodispersed Hydrosols", *Journal of American Chemical Society*, Vol. 72, pp. 4847-4854
- Lee M.H., 2007, *Microstructure and Microrheology of colloidal gels*, PHD thesis, University of Delaware, Delaware
- Liang C.D., Hong K.L., Guiochon G.A., Mays J.W., Dai S., 2004, "Synthesis of a Large-Scale Highly Ordered Porous Carbon Film by Self-Assembly of Block Copolymers", *Angewandte Chemie*, Vol. 43, pp. 5785-5789
- Liang C., Li Z., Dai S., 2008, "Mesoporous Carbon Materials: Synthesis and Modification" *Angewandte Chemie International Edition*, Vol. 47, pp. 3696-3717
- Liu X., Tian B., Yu C., 2002, "Room-Temperature Synthesis in Acidic Media of Large-Pore Three-Dimensional Bicontinuous Mesoporous Silica with Ia3d Symmetry", *Angewandte Chemie International Edition*, Vol. 41, pp. 3876-3878
- Lu A.H., Schuth F., 2006, "Nanocasting: A Versatile Strategy for Creating Nanostructured Porous Materials", *Advanced Materials*, Vol. 18, pp. 1793-1805
- Macakova L., Blomberg E., Claesson P.M., 2007, "Effect of Adsorbed Layer Surface Roughness on the QCM-D Response: Focus on Trapped Water", *Langmuir*, Vol. 23, pp. 12436-12444
- Mainardes, R.M., Silva L.P., 2004, "Drug delivery systems: Past, present, and future." *Current Drug Targets*, Vol. 5, pp. 449–455
- Mandal S., Ghatak C., Rao, V.G., 2012, "Pluronic Micellar Aggregates Loaded with Gold Nanoparticles (Au NPs) and Fluorescent Dyes: A Study of Controlled Nanometal Surface Energy Transfer", *J. Phys. Chem. C*, Vol. 116, pp. 5585–5597
- Manzano M., Aina V., Areato C.O., Balas F., 2007, "Studies on MCM-41 mesoporous silica for drug delivery: Effect of particle morphology and amine functionalization", *Chemical Engineering Journal*, Vol. 137, pp. 30-37.
- Marzouqa D.M., Zughul M.B., Taha M.O., Hodali H.A., 2011, "Effect of particle morphology and pore size on the release kinetics of ephedrine from mesoporous MCM-41 materials", *Journal of Porous Materials*, Vol., pp. 1-9

- Matsoukas T. Gulari E., 1989, "Monomer-Addition Growth with a Slow Initiation Step: A Growth Model for Silica Particles from Alkoxides", *Journal of Colloid Interface Science*, Vol.132, pp. 13-21
- Mesa M., Sierra L., Guth J.-L., 2008, "Contribution to the study of the formation mechanism of mesoporous SBA-15 and SBA-16 type silica particles in aqueous acid solutions", *Microporous and Mesoporous Materials*, Vol. 112, pp. 338–350
- Mishra B., Patel B.B., Tiwari S., 2009, "Colloidal nanocarriers: a review on formulation technology, types and applications toward targeted drug delivery", *Nanomedicine: Nanotechnology, Biology, and Medicine*, Vol. 6, pp. 9-24.
- Mondol T., Batabyal S., Pal S.K., 2012, "Interaction of an Antituberculosis Drug with Nano-sized Cationic Micelle: Förster Resonance Energy Transfer from Dansyl to Rifampicin in the Microenvironment", *Photochemistry and Photobiology*, Vol. 88, pp. 328–335
- Monnier A., Schüth F., Huo Q., Kumar D., Margolese D., Maxwell R.S., Stucky G.D., Krishnamurty M., Petroff P., Firouzi A., Janicke M., Chmelka B.F., 1993, "Cooperative Formation of Inorganic-Organic Interfaces in the Synthesis of Silicate Mesostructures", *Science*, Vol. 261, pp. 1299-1303
- Mukerjee P., Mysels K.J., 1971, *Critical Micelle Concentration of Aqueous Surfactant Systems*, Washington D.C,US. Government Printing Office
- Munoz B., Ramila A., Perez-Pariente J., Diaz I., Vallet-Regi M., 2003, "MCM-41 Organic Modification as Drug Delivery Rate Regulator", *Chemical Materials*, Vol. 15, pp. 500-503
- Nomura T., Asai Y., Murahashi N., 2000, "Formation of Spherical Micelles by the Novel Platelet Activating Factor Receptor Antagonist, E5880", *Chem. Pharm. Bull.* Vol. 48, pp. 947-950
- Ochekpe N.A., Olorunfemi P.O., Ngwuluka N.C., 2009, "Nanotechnology and Drug Delivery Part 2: Nanostructures for Drug Delivery", *Tropical Journal of Pharmaceutical Research*, Vol. 8, pp. 275-287
- Oya A., Yoshida S., Alcanizmonge J., Linaressolano A., 1995, "Formation of mesopores in phenolic resin-derived carbon fiber by catalytic activation using cobalt", *Carbon*, Vol. 33, pp. 1085-1090
- Ozaki J., Endo N., Ohizumi W., Igarashi K., Nakahara M., Oya A., 1997, "Novel preparation method for the production of mesoporous carbon fiber from a polymer blend", *Carbon*, Vol. 35, pp. 1031-1033
- Pekala R.W., 1989, "Organic aerogels from the polycondensation of resorcinol with formaldehyde", *Journal of Materials Science*, Vol. 24, pp. 3221-3227
- Polat H., Polat M., Chander S., 1999, "Kinetics of Dispersion of Oil in the Absence and Presence of Block Co-polymers", *Journal of AIChE*, Vol. 45, pp. 1866-1874

- Qu F., Zhu G., Huang S., Li S., Sun J., Zhang D., Qiu S., 2006, "Controlled release of Captopril by regulating the pore size and morphology of ordered mesoporous silica", *Microporous and Mesoporous Materials*, Vol. 92, pp. 1–9
- Redhead H.M., Davis S.S., Illum L., 2001, "Drug delivery in poly(lactide-co-glycolide) nanoparticles surface modified with poloxamer 407 and poloxamine 908: in vitro characterisation and in vivo evaluation", *Journal of Controlled Release*, Vol. 70, pp. 353–363
- Rosen M.J., 2004, *Surfactants and Interfacial Phenomena*, New Jersey, Wiley
- Ryoo R., Joo S.H., Jun S., 1999, "Synthesis of Highly Ordered Carbon Molecular Sieves via Template-Mediated Structural Transformation", *Journal of Physical Chemistry B*, Vol. 103, pp. 7743-7746
- Sahoo S.K., Labhassetwar V., 2003, "Nanotech approaches to drugdelivery and imaging", *DDT*, Vol. 8, pp. 1112-1120
- Sahu K., Ghosh S., Mondal S.K., 2006, "Ultrafast fluorescence resonance energy transfer in a micelle", *Journal of Chemical Physics*, Vol. 125, pp. 044714-044714-8
- Sakai T., Kurosawa H., Okada T., 2011, "Vesicle formation in mixture of a PEO-PPO-PEO block copolymer (Pluronic P123) and a nonionic surfactant (Span 65) in water", *Colloids and Surfaces A: Physicochemical Engineering Aspects*, Vol. 389, pp. 82–89
- Santini J.T., Richards A.C., Scheidt R., Cima M.J. Langer R., 2000, "Microchips as Controlled Drug-Delivery Devices", *Angewandte Chemie International Edition*, Vol. 39, pp. 2396-2407
- Schüth F., Singh K.S.W., Wietkamp J., 2002, *Handbook of porous solids volume 4*, Weinheim, Wiley-VCH
- Singh M., Ford C., Agarwal V., 2004, "Structural Evolution in Cationic Micelles upon Incorporation of a Polar Organic Dopant", *Langmuir*, Vol. 20, pp. 9931-9937
- Singh R., Lillard Jr. J.W., 2009, "Nanoparticle-based targeted drug delivery", *Experimental and Molecular Pathology*, Vol. 86, pp. 215-223
- Slowing I., Trewyn B.G., Giri S., Lin V. S.-Y., 2007, "Mesoporous Silica Nanoparticles for Drug Delivery and Biosensing Applications", *Advanced Functional Materials*, Vol. 17, pp. 1225-1236
- Song S.W., Hidajat K., KawiS., 2005, "Functionalized SBA-15 Materials as Carriers for Controlled Drug Delivery: Influence of Surface Properties on Matrix–Drug Interactions", *Langmuir*, Vol. 21, pp. 9568–9575

- Steel A., Carr S.W., Anderson M.W., 1994, "¹⁴N NMR Study of Surfactant Mesophases in the Synthesis of Mesoporous Silicates", *J. Chem. Soc.Chem. Commun.*, pp. 1571–1572
- Stöber W., Fink A., 1968, "Controlled Growth of Monodisperse Silico Spheres in the Micron Size Range", *Journal of Colloid and Interface Science*, Vol. 26, pp. 62–69
- Stucky G.D., Monnier A., Schüth F., Huo Q., 1994, "Molecular and Atomic Arrays in Nano-and Mesoporous Materials Synthesis", *Mol. Cryst. Liq. Cryst.*, Vol. 240, pp. 187–200
- Szymczyk K., Janczuk B., 2007, "The adsorption at solution–air interface and volumetric properties of mixtures of cationic and nonionic surfactants", *Colloids and Surfaces A: Physicochemical Engineering Aspects*, Vol. 293, pp. 39–50
- Tamai H., Kakii T., Hirota Y., Kumamoto T., Yasuda H., 1996, "Synthesis of Extremely Large Mesoporous Activated Carbon and Its Unique Adsorption for Giant Molecules", *Chemical Materials*, Vol. 8, pp. 454–462
- Tamon H., Ishizaka H., Yamamoto T., Suzuki T., 1999, "Preparation of mesoporous carbon by freeze drying", *Carbon*, Vol. 37, pp. 2049–2055
- Tanaka S., Nishiyama N., Egashira Y., Ueyama K., 2005, "Synthesis of ordered mesoporous carbons with channel structure from an organic–organic nanocomposite", *Chemical Communications*, pp. 2125–2127
- Tanev P. T., Pinnavaia T.J., 1995, "A Neutral Templating Route to Mesoporous Molecular Sieves", *Science*, Vol. 267, pp. 865–867
- Tanford, C., 1980, *The Hydrophobic Effect*, New York, Wiley
- Tofani L., Feis A., Snoke R.E., 2004, "Spectroscopic and Interfacial Properties of Myoglobin/Surfactant Complexes", *Biophysical Journal*, Vol. 87, pp. 1186–1195
- Torchilin V.P., 2007, "Micellar Nanocarriers: Pharmaceutical Perspectives", *Pharmaceutical Research*, Vol. 24, pp. 1–16
- Tunçay M., Göktürk S., 1997, "Effect of Ethanol on the Partition Coefficient Of Cyclohexylacetate Between Bulk and Cetyltrimethylammonium Bromide Micellar Pseudophases", *Spectroscopy Letters*, Vol. 30, pp. 825–834
- Turova T.Y., Turevskaya E.P., Kessler V.G., Yanovskaya M.I., 2002, *The Chemistry of Metal Alkoxides*, New York, Kluwer Academic Publishers
- Vallet-Regi M., Balas F., Arcos D., 2007, "Mesoporous Materials for Drug Delivery", *Angewandte Chemie International Edition*, Vol. 46, pp. 7548–7558

- Vallet-Regí M., Doadrio J.C., Doadrio A.L., Izquierdo-Barba I., Pérez-Pariente J., 2004, "Hexagonal ordered mesoporous material as a matrix for the controlled release of amoxicillin", *Solid State Ionics*, Vol. 172, pp. 435–439
- Vallet-Regí M., Ramila A., del Real, R.P., Perez-Pariente J., 2001, "A New Property of MCM-41: Drug Delivery System", *Chemical Materials*, Vol. 13, pp. 308–311
- Van Blaaderen A., VrijA., 1994, "Synthesis and Characterization of Colloidal Model Particles Made from Organoalkoxysilanes", *The Colloid Chemistry of Silica*, Chapter 4, pp 84–111
- Veronese F.M., Pasut G., 2005, "PEGylation, Successful Approach to Drug Delivery", *Drug Discovery Today*, Vol. 10, pp. 1451-1458
- Vix-Guterl C., Boulard S., Parmentier J., Werckmann J., Patarin J., 2002, "Formation of Ordered Mesoporous Carbon Material from a Silica Template by a One-Step Chemical Vapour Infiltration Process", *Chemical Letters*, Vol. 10, pp. 1062-1063.
- Vix-Guterl C., Frackowiak E., Jurewicz K., Friebe M., Parmentier J., Béguin F., 2005, "Electrochemical energy storage in ordered porous carbon materials", *Carbon*, Vol. 43, pp. 1293–1302
- Wan H., Liu L., Li C. 2009, "Facile synthesis of mesoporous SBA-15 silica spheres and its application for high-performance liquid chromatography", *Journal of Colloid and Interface Science*, Vol. 337, pp. 420–426
- Wan Y., Zhao D.Y., 2007, "On the Controllable Soft-Templating Approach to Mesoporous Silicates", *Chem. Rev.*, Vol. 107, pp. 2821-2860
- Wang Y., Zhang F. Wang Y., 2009, "Synthesis of length controllable mesoporous SBA-15 rods", *Materials Chemistry and Physics*, Vol. 115, pp. 649–655
- Waseda Y., Muramatsu A., 2004, *Morphology control of materials and nanoparticles*, Berlin, Springer
- Wei G., Wang L., Zhou H., 2005, "Electrostatic assembly of CTAB-capped silver nanoparticles along predefined λ -DNA template", *Applied Surface Science*, Vol. 252, pp. 1189–1196
- Westermarck S., 2000, *Use of Mercury porosimetry and nitrogen adsorption in characterization of the pore structure of mannitol and microcrystalline cellulose granules and tablets*, Academic Dissertation, University of Helsinki, Helsinki.
- Winsor P.A., 1968, *Chem. Rev.* Vol. 68, pp. 1-40
- Xu J., Yudasaka M., Kouraba S., 2008, "Single wall carbon nanohorn as a drug carrier for controlled release", *Chemical Physical Letters*, Vol. 461, pp. 189-192

- Yang B., Guo C., Chen S., 2006, "Effect of Acid on the Aggregation of Poly(ethylene oxide) Poly(propylene oxide) Poly(ethylene oxide) Block Copolymers", *Journal of Physical Chemistry B*, Vol. 110, pp. 68-74
- Yang Y., Sayari A., 2005, "SBA-15 templated-ordered mesoporous carbon: effect of SBA-15 microporosity", *Studies in Surface Science and Catalysis*, Vol. 156, pp. 543-550
- Yokoyama M., 2005, "Drug targeting with nano-sized carrier systems", *Journal of Artificial Organs*, Vol. 8, pp. 77-84
- Zeng W., Qian X.F., Zhang Y.B., Yin J., Zhu Z.K., 2005, "Organic modified mesoporous MCM-41 through solvothermal process as drug delivery system" *Mater. Res. Bull.*, Vol. 40, pp. 766-772
- Zhao D., Huo Q., Feng J., 1998, "Nonionic Triblock and Star Diblock Copolymer and Oligomeric Surfactant Syntheses of Highly Ordered, Hydrothermally Stable, Mesoporous Silica Structures", *J. Am. Chem. Soc.*, Vol. 120, pp. 6024-6036
- Zhao D., Huo Q., Feng J., 1999, "Novel Mesoporous Silicates with Two-Dimensional Mesostructure Direction Using Rigid Bolaform Surfactants", *Chem. Mater.*, Vol. 11, pp. 2668-2672
- Zhao D.Y., Feng J.L., Huo Q.S., Melosh N., Fredrickson G.H., Chmelka B.F., Stucky G.D., 1998, "Triblock Copolymer Syntheses of Mesoporous Silica with Periodic 50 to 300 Angstrom Pores", *Science*, Vol. 279, pp. 548-552
- Zhao P., Wang L., Suna C., Jiang T., Zhang J., 2012, "Uniform mesoporous carbon as a carrier for poorly water soluble drug and its cytotoxicity study", *European Journal of Pharmaceutics and Biopharmaceutics*, Vol. 80, pp. 535-543
- Zhu Y.F., Shi J.L., Chen H.R., She, W.H., 2005, "A facile method to synthesize novel hollow mesoporous silica spheres and advanced storage property", *Microporous and Mesoporous Materials*, Vol. 84, pp. 218-222
- Zhua S., Chen C., Chen Z., Liu X., 2011, "Thermo-responsive polymer-functionalized mesoporous carbon for controlled drug release", *Materials Chemistry and Physics*, Vol. 126, pp. 357-363
- Zuev Y.F., Kurbanov R.Kh., Idiyatullin B.Z., 2007, "Sodium dodecyl sulfate self-diffusion in premicellar and low-concentrated micellar solutions in the presence of a background electrolyte", *Colloid Journal*, Vol. 69, pp. 444-449